(19)

The Effect of Molecular Orientation on the Wear of Ultra-High Molecular Weight Polyethylene

by

Natasha Anna Chang

B.A.,Dartmouth College (1996)
B.E.,Thayer School of Engineering, Dartmouth College (1996)

Submitted to the Department of Mechanical Engineering
in partial fulfillment of the requirements for the degree of

Master of Science in Mechanical Engineering

at the

MASSACHUSETTS INSTITUTE OF TECHNOLOGY

June 1998

Author .....
Department of Mechanical Engineering
May 8, 1998

Certified by .....
Myron Spector
Senior Lecturer
Thesis Supervisor

Accepted by .....
Ain Sonin
Chairman, Department Committee on Graduate Students

The Effect of Molecular Orientation on the Wear of Ultra-High Molecular Weight Polyethylene

by

Natasha Anna Chang

Submitted to the Department of Mechanical Engineering
on May 8, 1998, in partial fulfillment of the
requirements for the degree of
Master of Science in Mechanical Engineering

Abstract

A study of the friction and wear properties of isotropic, fiber reinforced and molecularly oriented ultra-high molecular weight polyethylene (UHMWPE) was conducted on a reciprocating wear tester. The tests were carried out with a Co-Cr cylinder sliding against a flat sample of UHMWPE in bovine serum at 1.5 Hz for over a million cycles. In the fiber reinforced material, layers of woven UHMWPE fibers were embedded in a UHMWPE matrix. Molecularly oriented UHMWPE was produced by channel die compression of standard UHMWPE. The fiber reinforced samples were tested in one configuration and 3 different degrees of consolidation. The less consolidated samples failed catastrophically, and the more consolidated sample had a wear rate of 2×10^{-7}mm^3/Nm, comparable with that of the unreinforced, standard UHMWPE. The channel die oriented samples were tested in various configurations and degrees of anisotropy. They all showed similar wear behavior as the standard, with a wear rate of approximately 1×10^{-7}mm^3/Nm. The average frictional values of all the samples ranged from 0.08 to 0.11.

Thesis Supervisor: Myron Spector
Title: Senior Lecturer

Acknowledgments

First and foremost I would like to thank my parents, for all the sacrifices they made so that I could have the opportunity to study in the States. I would also like to thank my brother, Jonathan, and my Dartmouth College chums, Juan and his sister Fiorella Leon, Roy Cheung, Ha Oac, Phuong Hang, for maintaining my sanity.

Special thanks to Prof. Francis Kennedy at Dartmouth College for introducing and preparing me to work in the field of Tribology, and for giving me such a complete and through view of mechanical engineering.

I would like to thank Yot Boontongkong for being a good friend, both showing and helping me with the mass production of samples, and anything in his lab that might accidentally go boom. William Mosi Jones for spending a great deal of time helping me prepare samples for the SEM and then scanning them. Vedran Knezevic for being a gentleman and lending me some of his time for SEM work. Fred Cote for always having an answer to How do you make...?

Prof. Trumper and the fellows of the Precision Motion Control Lab who were kind enough to include me in their lab outings, lending me some of their time when I needed a hand, and allowing me to use their equipment. In particular I would like to thank Steve Ludwick and David Ma for answering all my random questions. Special thanks for David Ma for introducing me to the joy of Latex, now I have truly been through the MIT experience.

I would also like to thank the members of the Tribology Lab, my coworkers throughout these two years.

Last, but not least, I would like to thank my advisors Dr. Myron Spector, and Dr. Anuj Bellare for their guidance and support. I would particularly like to thank Dr. Myron Spector for allowing me a great deal of latitude in the pursuit of this project, and letting me assume more administrative responsibilities; thus giving me a better perspective of the academic world.

I would also like to acknowledge the financial support provided by the Veterans Administration.

Contents

List of Figures

List of Tables

Chapter 1

Introduction

1.1 Motivation

The use of ultra-high molecular weight polyethylene (UHMWPE) in total joint replacement prosthesis was introduced in the 1960s. Initially, polytetrafluoroethylene (PTFE) was used as a bearing material because of its low friction coefficient against a metal counterface but, unfortunately it exhibited unacceptably high wear rate. Therefore, it was replaced by UHMWPE, a material that proved to have a lower wear rate. UHMWPE has been the bearing material of choice since the late 1960s. The success of total joint replacement prostheses has led to its increasing use in younger patients who place higher demands on the artificial joint. Consequently, the long term wear performance of the materials used in the prosthesis has become an important issue in the longevity of the joint.

The wear of UHMWPE could result in the failure of the joint in two ways. Most importantly, wear debris elicits a foreign body response in which macrophages engulfing the polymer particles release inflammatory agents that cause the resorption of bone tissue, resulting in loosening of the prosthesis. Also, gross wear through of the UHMWPE component could result in metal to metal contact. Thus, it is compelling to lower the wear rate of the UHMWPE bearing, and still maintain its low friction coefficient and high biocompatibility in bulk form [1, 2, 3, 4].

There have been very few attempts at the post-processing molecular modification

of UHMWPE to better meet the needs of total joint replacements in general, or to specifically address the different failure patterns observed for the different designs of total joint replacements [1]. Thus, it is important to study whether there is a relationship between molecular structure and the wear rate of UHMWPE that could be used to this effect.

1.2 Background

1.2.1 Characterization and Types of Wear

There are several different wear mechanisms, [5], and those that are though to dominate in the case of UHMWPE sliding against a Co-Cr counterface are:

•Abrasive wear which generally produces a surface topography characterized by long grooves in the sliding direction where the particles are either removed or form mounds on the sides of the grooves as a result of plastic deformation and rupture at the micron and sub-micron scale. There are two different kinds of abrasive wear, two body and three body.

-Two body abrasive wear occurs when a hard rough surface slides against a softer surface (in this case Co-Cr sliding against UHMWPE). The rate of this kind of wear is very much dependent on the surface roughness of the harder material and its relative hardness compared to the material it is sliding against. In total joint replacements this form of wear is lowered by highly polishing the Co-Cr contact surface.

-Three body abrasive wear occurs when hard particles are introduced between the two sliding surfaces abrading them. Generally the hard abrading particles will become embedded in the softer material and plow into its sliding pair. In the clinical situation, this occurs when bone cement particles or metallic particles from the surface of the implant find their way in between the two sliding pairs in total joint replacements.

• Adhesive wear takes place when the contacting surfaces adhere due to the attractive forces between the atoms of the two surfaces. If this adhesive attractive force is stronger than the cohesive force holding the particle onto its original surface, there

will be a removal of a small particle. This kind of wear is indicative of higher frictional forces and is generally more prevalent between similar materials (*i.e.*, metal against metal, and not metal against plastic).

• Delamination wear was introduced in 1973 by Nam Suh [6, 7] and addresses cases of reciprocating wear, *i.e.*, where there is repetitive loading, and frictional heating does not play a role. Therefore, the contacting surfaces have a chance to smooth out and become more conformal. Subsequent failure generally occurs because of subsurface fatigue. The general sequence of events for delamination wear is as follows:

-The two sliding surfaces come into contact, asperity with asperity. The asperity of the softer material are deformed and some are fractured through repetitive loading, eventually resulting in a relative smooth surface. Consequently there is no longer an asperity to asperity contact, but an asperity to plane contact.

-Accumulation of plastic shear deformation from repetitive loading takes place on the softer material due to the traction of the hard asperity.

-Crack nucleation takes place below the surface. The depth of these cracks is dependent on two factors with opposing effects. The hydrostatic compressive forces beneath the contact asperity that hinder the crack growth, and the plastic shearing that promote it. Also hard inclusions or voids will act to aid crack nucleation.

-These cracks propagate parallel to the surface joining with neighboring ones until they finally shear to the surface, creating long and thin debris sheets.

Of these three forms of wear the two that cause most concern in total knee arthroplasty are abrasive wear and delamination wear. Two body abrasive wear can generally be reduced by using a highly polished counterface. Three body abrasive wear, which is generally due to cement and metallic particles being trapped between the two sliding surfaces, can be reduced by using a harder counterface (for instance, using a ceramic instead of a metal) and also by limiting the use of fixing cement, or fixing the prosthesis with a different method. Consequently as long as the metallic femoral condyle remains smooth, delamination wear becomes an important factor in determining the life of the polyethylene bearing.

Delamination wear is generally associated with the fatigue of the subsurface region of the material. In the case of the UHMWPE tibial component of the total knee replacement prosthesis this issue is more difficult to address since it is a problem directly associated with the material and not easily solved by small changes in the design of the prosthesis. The replacement bearing would not only have to perform better in terms of wear but it would also have to maintain the other characteristics that make UHMWPE the current material of choice for orthopedic use, such as low friction coefficient and high biocompatibility. The solution could be found by either implementing a completely new material, or by modifying the UHMWPE currently used.

The characterization of wear is generally done in first approximation with the aid of Archard's wear equation. It states that the wear rate is proportional to the contact load, W, and inversely proportional to the surface hardness, H.

$$w = K\frac{W}{H} \tag{1.1}$$

The constant of proportionality, K, is a dimensionless wear coefficient that depends on the tribological system and is obtained empirically. For practical applications a dimensional wear coefficient, k, is used because for most materials it is generally difficult to obtain the hardness of the uppermost layer. This dimensional wear coefficient is defined as $k = K/H$, and it is a function of the wear volume (mm^3) per unit of sliding distance (m) and normal load (N) [5]. For the purpose of this thesis we calculated the dimensional coefficient of wear, k.

1.2.2 Wear of Total Joint Replacement Prosthesis

The study of wear in total joint replacement has taken two major routes, *in vivo* and *in vitro*. *In vivo* the focus has been mainly in characterizing the form of wear that caused the prosthesis to fail by studying the two sliding surfaces, specifically, the UHMWPE bearing; and the size and shape of the wear debris accumulated in the periprosthetic tissue. *In vitro*, attempts to create an accelerated simulation of the

form of wear found *in vivo* have been made. Also, studies to determine how varying different testing parameters affects the wear of UHMWPE have been conducted.

From the *in vivo* studies it has been found that most prosthesis failures necessitating revision were due to osteolysis that caused prosthetic loosening [1, 2]. Studies have linked initiation of osteolysis to the macrophage reaction to the wear debris of the UHMWPE bearing [2, 3, 4]. The examination of the UHMWPE surface of these failed joints at revision surgeries has revealed large craters, which produced large numbers of wear particles. Initially it was believed that these were due primarily to abrasive wear from the hard acrylic particles ("bone cement"), because the area surrounding the crater was generally scratched and the cement particles could be found embedded in the polyethylene. These findings did not reconcile with the cases where there was no evidence that abrasion was taking place, *i.e.*, the area surrounding the crater was smooth or cement was not used to fix the implant. The alternative explanation to this form of wear was that the repetitive loading and high stresses caused the polyethylene surface to both fatigue and/or deform. The cyclic loading of the surface caused cracking and delamination wear. In a few studies, the rate of delamination wear was found to be dependent on a)fusion defects present because of low temperature forming, and b)heat treatment of the surface. In the surfaces that were heat treated there was a transition between the heat treated zone, with lower crystallinity, and the nontreated polyethylene at 1mm below the surface. This transition point occurred at the depth where the highest stress was located, and was believed to aid in the delamination wear process [1, 8, 9]. Wear, due to surface deformation occurs as the indentor causes a pileup of the UHMWPE ahead of it. As it slides the polyethylene is subjected to some cold flow that creates a fold on the surface. Eventually, after repetitive loading, the fold is thinned and torn off the surface [10].

In recent years there has been an awareness that the gamma radiation used for the sterilization of UHMWPE parts predisposed the polymer to oxidation at the depth where the subsurface strain tends to accumulate, and likely explains many of the early failures of the components that display gross delamination [11, 12]. More recent methods of sterilization employ gamma radiation in a vacuum or in an inert atmosphere, in

some cases followed by heat treatment to stabilize free radicals. These gamma radiation treatments introduce cross-linking into the polymer chains and thereby alter the material properties. Other orthopedic manufacturers have implemented non-ionizing methods of sterilization, in particular ethylene oxide gas sterilization. This method has no effect on the polymer structure. For the purpose of this thesis we have chosen to use the unsterilized polymer in its extruded rod form as the standard.

The problem associated with third body abrasive wear can be limited by the judicious use of cement or the implementation of highly adherent coatings for non-cemented prostheses. In the case of nonconformal contact it could be addressed by better designs that simulate the movement of the knee joint, where contact stresses are lower and better distributed [13, 14]. Fatigue failure due to excessive wear debris of the polyethylene is an issue that can only be improved by improving the material itself, and to do this, the wear behavior of polyethylene has been studied extensively *in vitro*.

For proper *in vitro* studies it is imperative that the wear test simulates certain conditions to which the UHMWPE bearing is subjected in the body. Moreover, this needs to be achieved on a reasonable time scale. This implies accelerated testing. Studies by Fisher, *et al.* [15], and Barret, *et al.* [16], showed that unless there was sufficient frictional heating for localized melting to take place sliding velocity does not have as strong an effect on wear as other parameters, such as, environment and counterface roughness.

Counterface roughness was found to have a strong impact on determining the predominant wear mechanism, and the amount of wear debris produced [16, 17, 18]. Specifically, a three fold increase in the counterface roughness (Ra) caused a forty fold increase in wear [17]. But whether abrasive wear or delamination wear was dominant depended on whether the material removal was fast enough that it did not allow the accumulation of plastic strain in the subsurface, specifically at approximately 40μm below the sliding surface [17, 18, 19]. It was also found that when sliding in an environment with bovine serum (*i.e.*, no transfer film is formed) the smoother the counterface, the lower the abrasive wear. Cooper, *et al.* [17], found that in general if

you start with a highly polished counterface (mirror finish) its roughness at the end of the test was approximately of Ra of 0.03μm.

Studies that compare the *in vivo* and *in vitro* wear, show that similar wear mechanisms are active but that their relative emphasis is different. Also, *in vitro* studies have shown that the worst wear scenario is when there is a nonconformal sliding contact with cyclic loading. Cases where there is just cyclic loading cause minimal surface damage, generally just an indentation. Rolling contact exhibited less wear than sliding because of the absence of shear stresses. In general, the *in vitro* studies have shown that 10 million cycles produce an equivalent surface damage as seen in an implant with five years of usage [20, 21, 22].

In summary a main cause of the wear of the bearing when sliding against a smooth counterface is related to surface deformation and subsurface failure due to fatigue. This is particularly true in the total knee replacement prosthesis, where primarily there is a unidirectional reciprocating sliding contact between the tibia and the femoral component, *i.e.*, the tibiofemoral contact.

1.2.3 Oriented Polymers

A previous study by Boontongkong [23] has shown that UHMWPE, like high density polyethylene (HDPE), can be crystallographically and molecularly oriented by using a channel die to induce plane strain compression. It was suggested that UHMWPE assumes a fibrillar like structure and that the lamella take on a chevron morphology; moreover the lamella, voids, and molecules are somewhat oriented in the flow direction. This type of texturing was believed to begin to take place within a compression ratio of 1.4 and to be accentuated with higher compression ratios.

In other work, Sung and Suh [24], showed that uniaxially oriented fiber reinforced polymeric composites, such as oriented graphite fiber-epoxy and kevlar fiber-epoxy, exhibited lower wear rates when the fibers were oriented perpendicular to the sliding surface. This was mainly due to the fact that the fibers arrested the crack propagation parallel to the surface (delamination wear). The cracks in this case occurred in the form of debonding of the fiber from the matrix up to a certain depth, and for further

crack growth the fibers had to be worn down. A more recent study by Suh, *et al.* [25], of a UHMWPE homocomposite, *i.e.*, a UHMWPE matrix with UHMWPE fibers as a reinforcing agent, showed similar results. When the fibers were uniaxially oriented normal to the sliding surface the mass loss due to wear in dry reciprocating sliding conditions was an order of magnitude lower than the standard isotropic UHMWPE. These previous investigations formed the basis of the rationale in this thesis to study the effects of molecular orientation of polyethylene chains on the wear properties of the polymer.

1.3 Problem Statement

The hypothesis is that the long term reciprocating sliding wear of UHMWPE can be lowered by arresting the crack growth parallel to the surface that lead to delamination wear. Also, abrasive wear might be lowered by reducing the depth of penetration of the hard asperities of the Co-Cr counterface in the UHMWPE surface. Two forms of textured UHMWPE and the standard isotropic UHMWPE that is used currently were studied and compared. One form was produced by using a molecularly oriented sample generated using channel die compression. In this case it was hypothesized that the surface orthogonal to the flow direction would exhibit lower wear than the surface orthogonal to the constrained or loaded direction. It was postulated that the lamella, molecules and voids that are parallel to the flow direction (and thus perpendicular to the sliding surface) would both arrest, the crack growth that leads to delamination wear, and the abrasive wear since the harder lamella would wear slower, like in the UHMWPE fibers in Suh, *et al.* [25].

The other oriented sample that was tested was a biaxially oriented UHMWPE fiber reinforced UHMWPE composite, in which the bonding of the fiber and the matrix was expected to be better than the composite used by Sung and Suh [24] and Suh, *et al.* [25].

Chapter 2

Materials

2.1 Raw Material Description

2.1.1 The Standard and Compressed UHMWPE

The standard UHMWPE was obtained from Westlake Plastic (Lenni, PA). It was a circular ram extruded circular rod of three inches in diameter. The resin was manufactured by Hoechst Celanese Corporation, Holstalen GUR 4150HP. The molecular weight was six million, with 53% crystallinity and a density of 0.932g/cc, equation 2.1.

$$\rho = 0.53(1.000g/cc) + 0.47(0.855g/cc) = 0.932g/cc \tag{2.1}$$

where 1.000g/cc is the density of the crystal, and 0.855g/cc is the density of the amorphous phase. The melt flow index was essentially zero [23].

As noted previously, nonsterilized, as received, UHMWPE was used as the standard control. The rational behind this was that one sterilization method that has been used is ethylene oxide gas, that is known not to affect the polymer.

Based on information in the literature [26, 27] on low density polyethylene and experimental stress-strain data collected by Boontonkong [23] the mechanical properties of the UHMWPE were determined. For the case of low density polyethylene (LDPE) the value of the bulk modulus, E, ranges from 55.1-172MPa, and the maximum yield strength, $\sigma_{y_{max}}$, ranges from 15.2-78.6MPa. The experimental data collected from

Boontongkong [23] showed values within the range given above. The maximum yield strength was found to be approximately 15MPa. The bulk modulus was calculated by taking the initial slope of a stress-strain curve obtained from the plane strain compression of the UHMWPE, equation 2.2, and was found to be approximately 145MPa.

$$E = \frac{\sigma}{\epsilon} = \frac{7.372MPa}{0.0508} = 145MPa \tag{2.2}$$

These values were the ones used in the Hertzian contact stress calculations in a later section. Due to the difficulty in obtaining Poisson's ratio experimentally, it was assumed that the value for UHMWPE was similar to that of low density polyethylene. The value for Poisson's ratio, ν, found in the literature for LDPE was 0.38 [27].

2.1.2 Fiber Reinforced UHMWPE

The fiber reinforced polyethylene was provided by Dr. Yachin Cohen of the Technion-Israel Institute of Technology, and its described in [28]. It was comprised of layers of UHMWPE fabric in a UHMWPE matrix. The fibers of the fabric were Spectra 1000, Allied Corp. Ltd., and the matrix was Hostalen GUR4113, Hoechst. The external surface of the sample was melted and allowed to recrystallized in an unoriented form. The thickness of the unoriented layer and the degree of consolidation of the bulk of the sample were controlled during processing.

The mechanical properties of the material were also reported in the study cited, [28], table 2.1. Dr. Cohen, *et al.*, study also suggested, that the limiting factor for the mechanical properties measured was the cohesive properties of the matrix, and not due to failure at the fiber/matrix interface.

For the purpose of this thesis three different types of samples were tested, MP-56 and MP-58 having a fibrous bulk structure but unoriented polyethylene surface, and MP-60 that was highly consolidated both on the surface and the bulk. The samples had a void content of over 10%, resulting in an expected absorption of more water than the standard or compressed sample.

Test	Value
Shear Strength	20-25 MPa
Unidirectional laminate longitudinal tensile strength	1.3-1.5 GPa
Unidirectional laminate transversal tensile strength	21-25 MPa[a]
Unidirectional unstreched laminate transverse elongation of failure	$\approx 70\%$[b]
Elongation at break of composite made from completely stretched laminates (in all directions)	0.6-1.2 %

[a] For the completely stretched sample at 25°C
[b] For the unstretched sample at 25°C

Table 2.1: Mechanical Properties of Fiber Reinforced UHMWPE.

The process of producing polymer fibers normally orients the molecular chains. Therefore, for the purpose of this thesis the fiber reinforced material will also be referred to as "fiber oriented" UHMWPE.

2.1.3 The Co-Cr Counterface

The cylindrical counterface was a Co-Cr alloy, American Society of Testing Materials (ASTM) F-75, as typically used in orthopedic applications. The Rockwell C hardness was measured for all four cylinders used, their average values were found to be 32, 32, 33, 38. From the literature [29] it was found that the bulk modulus, E, was 172GPa. the surface finish of the metal counterface is discussed in section 3.4, Counterface Roughness.

2.2 Recrystallization of Standard UHMWPE

The samples to be oriented through compression were first recrystallized so that their initial texturization was isotropic. They were heat-treated at temperatures between $160 - 170$°C for an hour, and then were allowed to cool slowly in the oven for a period of approximately three hours until they reached room temperature.

2.3 Channel Die Compression

Following the procedure established by Boontongkong [23], the samples were compressed in a channel die originally built by Lin and Argon [30]. The degree of compression is referred to as the compression ratio, λ, and it is defined as the ratio of the initial height and the final height of the sample at the end of the compression. The channel die, as shown in fig. 2-1, has a channel of width 10.5mm and length of 76.2mm. The load was applied though a plunger with a slip fit into the channel. The whole set up was maintained at 80°C with the aid of two heating slabs placed along the length of the channel die.

The recrystallized samples were machined to fit snugly in the channel. The channel was lubricated with Dow-Corning high temperature bearing grease (medium consistency) to minimize friction between the channel, and the plunger or sample. The recrystallized samples were heated and maintained at 80°C and then compressed at a fixed engineering strain rate of 0.0025 per second. Once the desired compression ratio was reached, the plunger was stopped but the load was maintained. The setup was allowed to cool to room temperature, so that upon removal the sample would not strain recover as much as at the compression temperature. Once at room temperature, the sample was removed from the channel die and cleaned with isopropyl alcohol to remove the grease. The sample was then placed in a holder that fixed both the loaded direction and the constrained direction. Subsequently it was heat treated for 2 days at 90°C to remove residual strains. The samples tested had a compression ratio of 1.7 and 2.75.

In previous studies the molecular structure of the channel die material was characterized, [23, 31]. It is believed that the texture of the compressed samples was different depending upon compression ratio. In both the samples with compression ratio of 1.7 and 2.75 the molecular chains of the amorphous phase were prominently oriented along the flow direction. This features becomes more pronounced the higher the compression ratio. The crystalline lamella, which are like thin wafers, structure of the two compression ratio used were very different. For the samples with 1.7 compres-

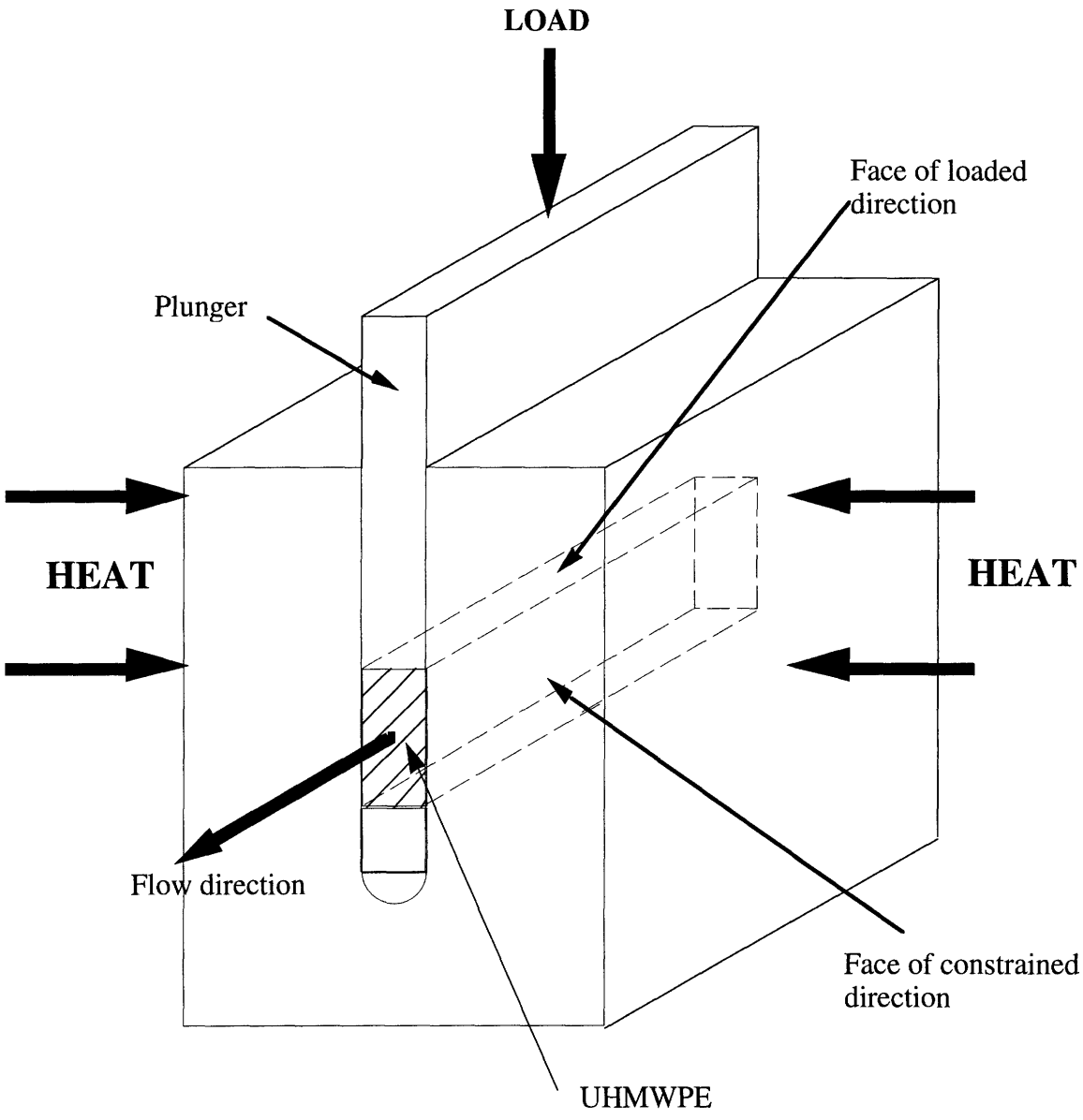

Figure 2-1: Channel Die.

sion ratio, many of the lamella surfaces had rotated parallel to the loading plane. In the higher compression ratio, 2.75, the dominant feature was kinked lamellae stacks that were formed from the lamellae whose normal were originally parallel to the constrained direction and the flow direction. An earlier study on HDPE by Song, *et al.* [32], gives an indirect supporting evidence of this type of morphology.

2.4 Lubricant

The wear of UHMWPE is different depending upon the environment in which it is taking place. In the case where there is dry sliding, or the lubricant being used is either water or saline solution, several authors [33, 34, 35, 36, 37] report the formation of a transfer film and large flake like particles of up to millimeters across and on average of 2μm in size. Preliminary testing in saline solution confirm these observation, 10 samples were tested with varying sliding distances ranging from 2.5 to 22.5km. In cases where the lubricant used has protein molecules in it, such as bovine serum, studies [35, 36, 37] have shown that no transfer film or a nonuniform transfer film was formed. These studies also show that the wear particles are submicron in size and of more spheroid or fibrillar form. There are no reports of transfer film or large wear particle formation in clinical studies of total joint replacement prosthesis. Thus, it has been concluded by Wang, *et al.* [37], that the use of bovine serum as a lubricant in laboratory wear test replicates the wear mechanism seen *in vivo* better than the use of water lubrication. Bovine serum supplied by Sigma-Aldrich and was the lubricant used for the wear test in this thesis.

Bovine serum denatures rapidly because of bacterial growth at room temperature. Following Lee and Pienkowski, [38], procedure to arrest this process, the bovine serum was mixed with a 1% by volume aqueous solution of sodium azide in the following proportion, two parts serum, one part sodium azide solution. The water used to prepare the solution was triple filtered at 0.2μm distilled water. Both the water and the sodium azide was supplied by E. Merk Science. During the wear test the bovine serum had to be changed every four days, following the European standard for room

temperature test [39], because of the denaturing of the serum believed to be due to frictional heating at the contact point.

Chapter 3

Methods

3.1 The Wear Tester, General Description

The wear tester is of a sliding cylinder on flat geometry. It was built specifically to simulate the sliding that occurs between the tibial plateau and the metallic femoral condyle in a nonconformal total knee replacement prosthesis, fig. 3-1 and 3-2.

The tester consist of three channels with pneumatic cylinders that applied a load corresponding that of an individual, between 889.6-934.08N (200-210lb.). In two of the channels there are strain gages between the pneumatic piston and the counterface to measure normal and frictional forces. The samples were placed in a holder with lubricant (water, bovine serum, etc.) which rested on a carriage. The carriage slid back and forth with a frequency of 1.5Hz, and amplitude of 2.858cm (1.125in).

During the course of this thesis the existing strain gages were wired so as to obtain both tangential and normal forces acting on the sample. The gages were then calibrated to obtain the relationship between the output voltage and the load applied. For the wear testing the output was measured with a data acquisition system. This process is explained in detail in section 3.5.

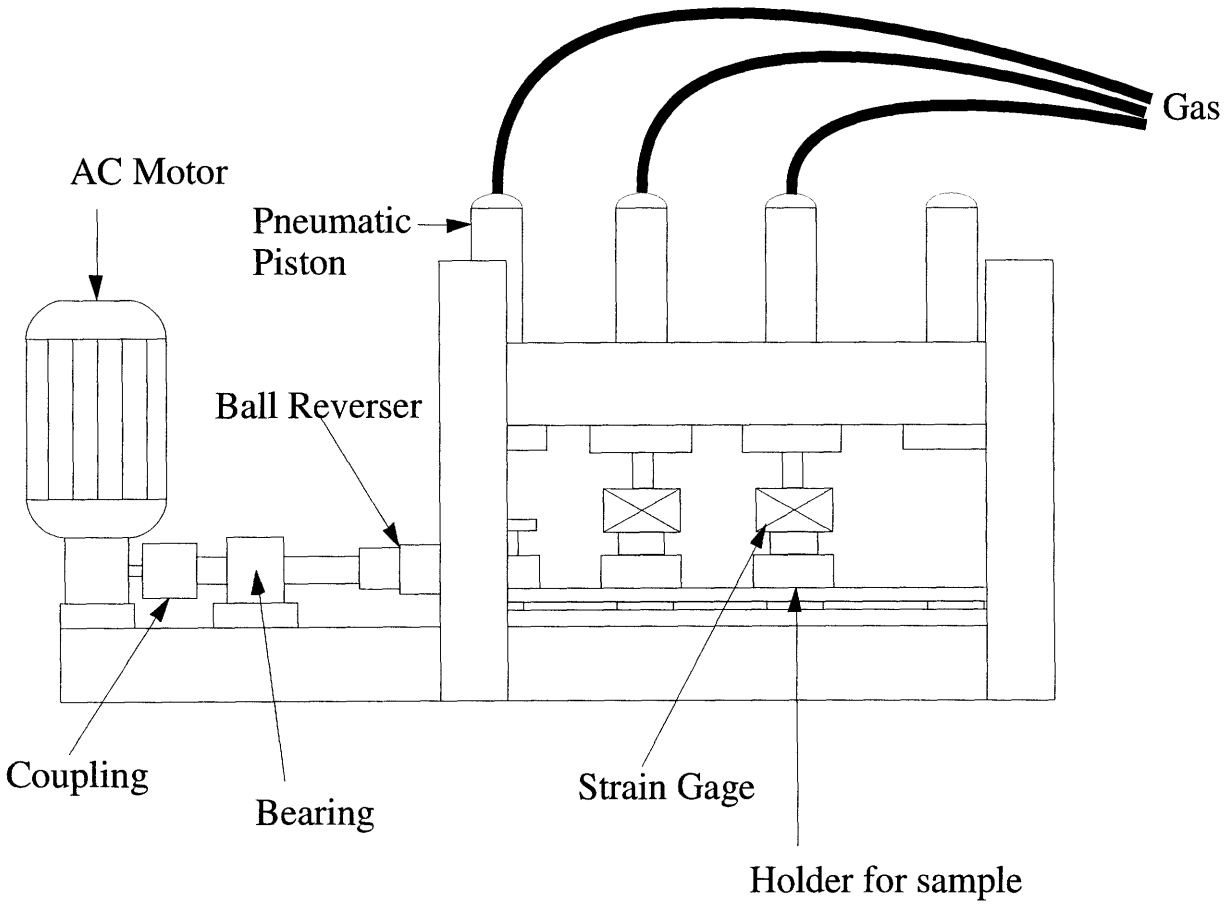

Figure 3-1: General view of the wear tester.

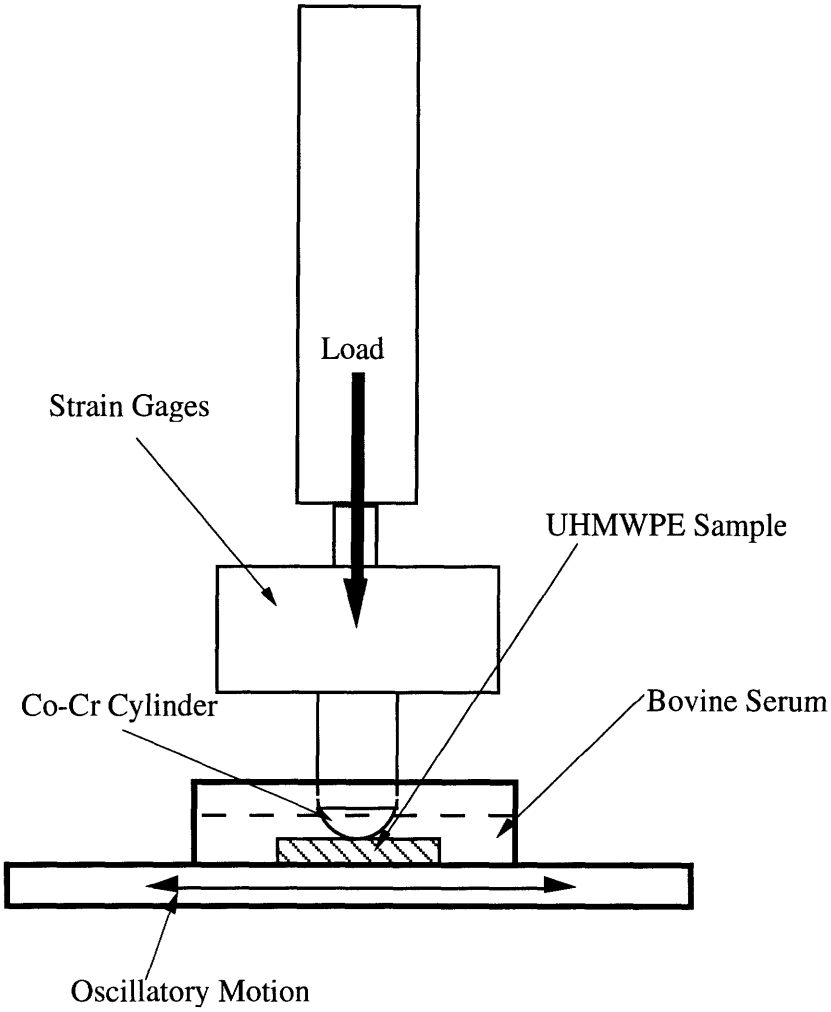

Sliding speed: 3.375in/sec=0.0857m/sec
Wear Track: 1.125in=2.858cm
Normal Load approximately 889.6-934.08N (200-210lb.)
Oscillatory Motion: 1.5Hz.
Lubricant: Bovine Serum
Cylinder Diameter: 1.125in=2.858cm
Cylinder Width: b = 0.625in = 1.59cm

Figure 3-2: View of one channel of the wear tester.

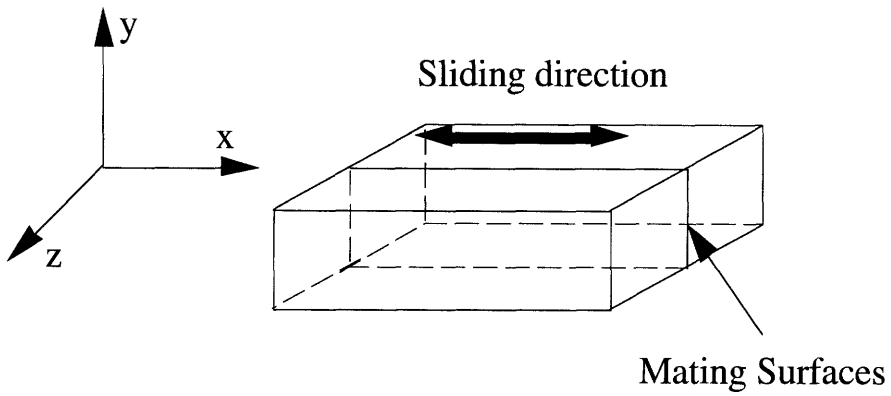

Figure 3-3: Sample for wear test.

3.2 Testing Geometry

The nonconformal contact between the UHMWPE bearing and the Co-Cr counterface of the wear tester was a line contact. This simulated a worst case scenario and was selected as it was expected to accelerate the wear process. The minimum sample size required was 2x3.5x1cm, The samples produced from the plane strain channel die compression were 1.05x1x7.6cm, which was not large enough. If the narrower sample was used, the cylinder would have had to have been scaled down to maintain a similar line contact geometry. Otherwise, the validity of the test would have been compromised because edge effects could have played an important role in the wear process.

Assuming that the UHMWPE behaves like an elastic material, and using Hertzian contact stress analysis, we found that the maximum contact stress for a 889.6N load was 14.55MPa for the original setup. A scaled down version with the same contact stresses would have required loads lower than those that could have been supplied accurately by the pneumatic piston. Therefore, a new wear tester would have had to have been built. Similarly, if the geometry was changed to a sphere on flat the loads required for the same contact stress would be too low for the existing wear tester. Another solution to this sample size problem was to clamp together two PE samples so that the direction of the mating faces was perpendicular to the sliding direction, as seen in fig. 3-3.

If two samples were to be clamped together, for this change not to affect the test,

the main contact stresses would have to be along the x and y direction, because the mating surfaces would not transmit any of the tensile component of stress along the z direction. Assuming again that the contact was elastic, from Hertzian analysis, a semi-infinite cylinder on flat (line contact) only has stresses along the x and y direction. The equations for Hertzian analysis for a semi-infinite cylinder on flat, fig. 3-4, are:

$$a = \sqrt{\frac{4WR}{L\pi E^*}} \tag{3.1}$$

$$p_o = \frac{2W}{L\pi a} \tag{3.2}$$

$$E^* = \left(\frac{1-\nu_1^2}{E_1} + \frac{1-\nu_2^2}{E_2} \right)^{-1} \tag{3.3}$$

$2a$=contact width

L=contact length

p_o=maximum contact pressure

E^*=contact modulus

W=load

R= radius of cylinder

ν=Poisson's ratio

$\frac{L}{2a} > 10$ for these equations to hold

If $\frac{L}{2a} \approx 5$ then the equations give a rough approximation

In this case the bulk modulus of Co-Cr is three orders of magnitude larger than that of UHMWPE. Therefore, its contribution to the contact modulus was negligible. Using the equations 3.1, 3.2 and 3.3 in conjunction with the material properties stated in chapter 2 we found that the contact width, $2a$, was 0.00246m. The ratio of the of the contact width and contact length, L=0.015875m, was 6.5. Thus, the assumption of semi-infinite cylinder on flat contact was a reasonable one.

Another factor that needed to be taken into consideration is that the material could undergo plastic deformation in the load range in which the test was carried out; for the analysis to apply the material behavior must be primarily elastic (assuming no viscoelastic behavior), with the main source of surface deformation the elastic

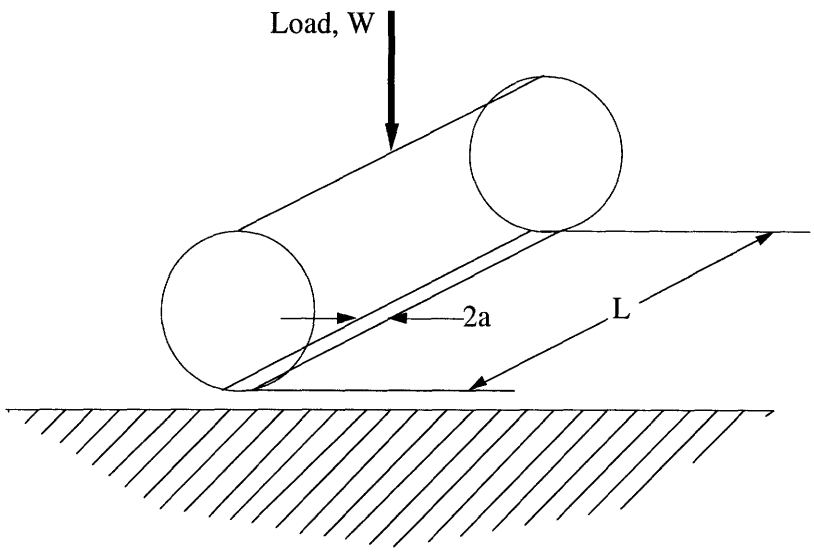

Figure 3-4: Semi-infinite cylinder on flat.

contact. Otherwise, the contact pressure would be underestimated. To determine this we compared the contact width, $2a$, of a purely elastic contact and a purely plastic contact. Plastic contacts could be approximated using equation 3.4, and using the equations 3.1, 3.2, 3.3 for the elastic contact, the effects can be graphed together, fig. 3-5 where it can be observed that at 889.6N. the elastic contact is the dominant one. Therefore, we can assume that clamping the samples together will not change the nature of the wear test. This approach was the one followed.

$$2a \approx \frac{W}{L3\sigma_{max}} \tag{3.4}$$

3.3 Surfaces Tested of the Channel Die and Fiber Oriented UHMWPE

The channel die compressed UHMWPE was anisotropic. There were three different surfaces for testing: the extruded or flow face, the constrained face, and the loaded face, see fig. 3-6. These faces could each be tested in two perpendicular directions for a total of six different directions. Four different directions were tested.

The loaded face was tested with the cylinder sliding in the flow direction, (LD).

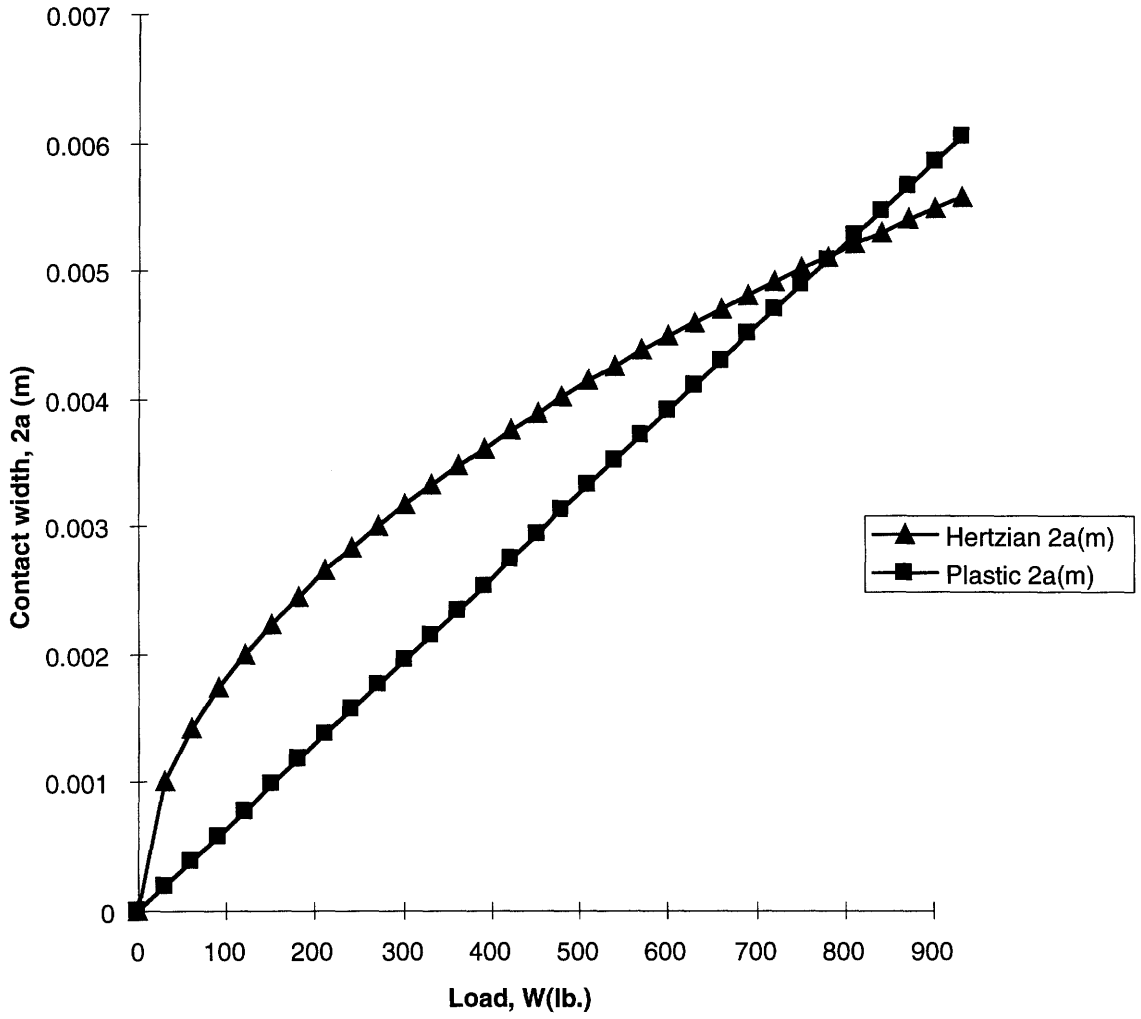

Figure 3-5: Graph of pressure vs. contact width for pure plastic and pure elastic contacts.

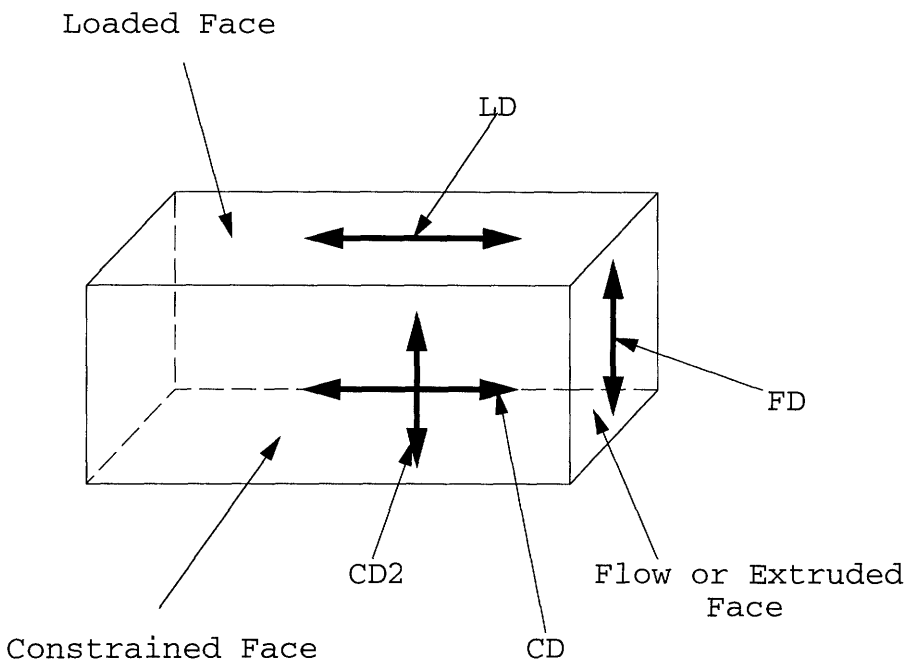

Figure 3-6: Surfaces and directions tested on the compressed samples.

The predominant feature was that the lamella surface and molecules were parallel to the sliding surface. The constrained face was tested on both the flow direction (CD) and on the loaded direction (CD2). In both cases the predominant feature was that the lamella surface were perpendicular to the sliding surface and the molecules were parallel to the sliding surface. When tested in the flow direction (CD) the lamella normal were mainly perpendicular to the sliding direction, and the molecules were oriented along the flow direction. In the loaded direction (CD2) the molecules were oriented perpendicular to the sliding direction and the majority lamella normal were in the sliding direction. The flow face was tested in the loaded direction (FD), both the majority of the lamella normal and surface were perpendicular to the flow surface, and the molecules were perpendicular to the surface. These test directions and surfaces can be seen more readily in fig. 3-6.

The fiber reinforced samples (MP-56, MP-58, MP-60) were only tested in one direction, on the surface parallel to the cloth like layers as shown in fig. 3-7. The texture of the surface tested was not directly the woven layer, but the melted layer that is isotropic standard UHMWPE.

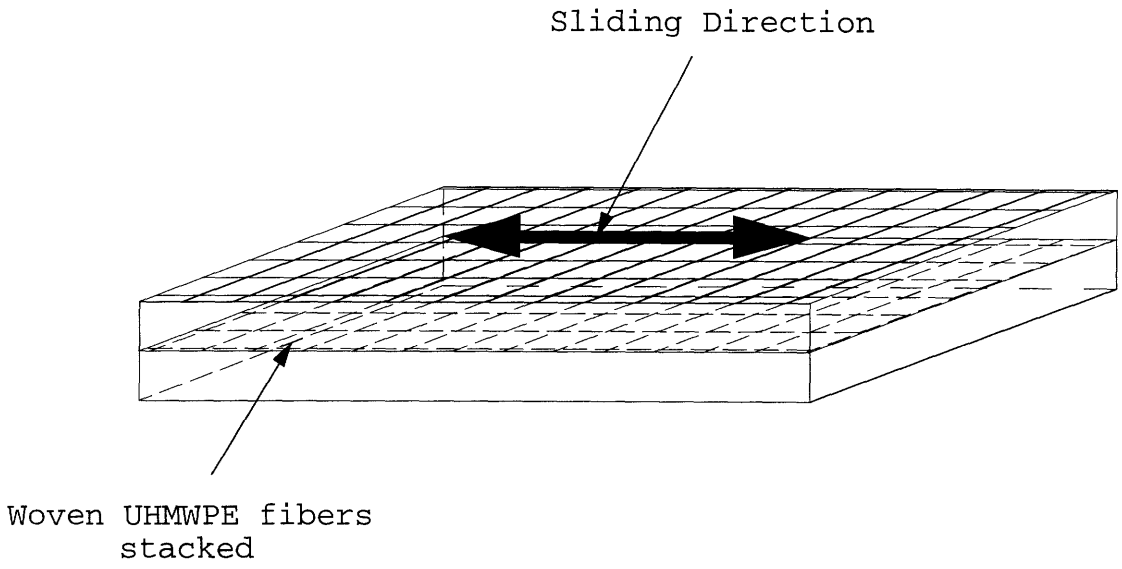

Figure 3-7: Surface and sliding direction tested on the fiber oriented samples.

3.4 Counterface Roughness

The counterface roughness has a strong impact on determining the predominant wear mechanism [16, 17, 18]. The counterface finish used in this experimentation reflected a roughness used in implants and in other *in vitro* wear tests. Cooper, *et al.* [17], found that in general if the starting metal surface was highly polished, its roughness at the end of the test was approximately of Ra of 0.03μm. Several authors [15, 17, 40] have shown that for Ra below 0.03μm the predominant wear mechanism is fatigue. Also, this roughness is comparable to those used in femoral heads. Thus, the counterface roughness chosen was of a Ra equal to approximately 0.027μm measured in the direction with highest roughness, in this case along the length of the cylinder.

The Co-Cr cylinders were polished on a lathe by starting with a 270 grit paper and slowly moving down to the 600 grit silicon carbide polishing compound. For the final polish both the lathe and a dremol tool with a cotton tip dipped into the polishing compound was used. After obtaining a mirror finish the Co-Cr cylinder was cleaned in an ultrasonic acetone bath for ten minutes. The surface finish was then measured with a P-10 Tencor Surface Profiler with a diamond tipped stylus by averaging two traces opposite each other, along the length of the cylinder, fig. 3-8. The trace length was 2mm, with a stylus tip force of 5mg.

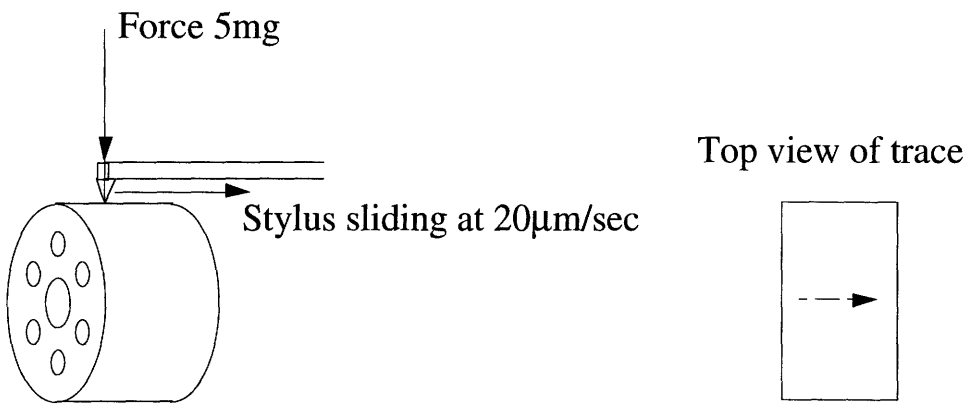

Figure 3-8: Trace path for measurement of Co-Cr roughness.

Samples Tested	Scan	Cylinder A Ra(μm)	Cylinder B Ra(μm)	Cylinder C Ra(μm)	Cylinder D Ra(μm)
Standard and	1	0.0265	0.0275	0.0278	
λ=2.75	2	0.0279	0.0277	0.0275	
λ=2.75 and 1.7	1	0.0262	0.0291	0.0283	0.0270
in FD and CD2	2	0.0254	0.0291	0.0265	0.0249
λ=1.7 in FD, CD2,	1	0.0262	0.0254	0.0247	0.0258
CD, LD, and MP-60	2	0.0267	0.0243	0.0267	0.0249

Table 3.1: Typical roughness values of the Co-Cr cylinder and their sliding pair.

The average Ra of the Co-Cr cylinders was of $0.0265\mu m \pm 0.0015\mu m$. Fig. 3-9 and table 3.1 show a typical scan and the roughness measured.

Some of the counterfaces were also measured at the end of the wear test to have an approximate idea of their roughening. The same trace path as for the initial roughness was used on the worn Co-Cr surface, two measurements were taken and averaged.

3.5 Measurement of the Normal and Friction Force

The normal load and friction force were measured in two of the three channels of the wear tester for the purpose of obtaining the friction coefficient, μ. These measurements were made using a strain gage with an electrical output that was monitored with a chart recorder. A data point was taken with the chart recorder every 24 hours

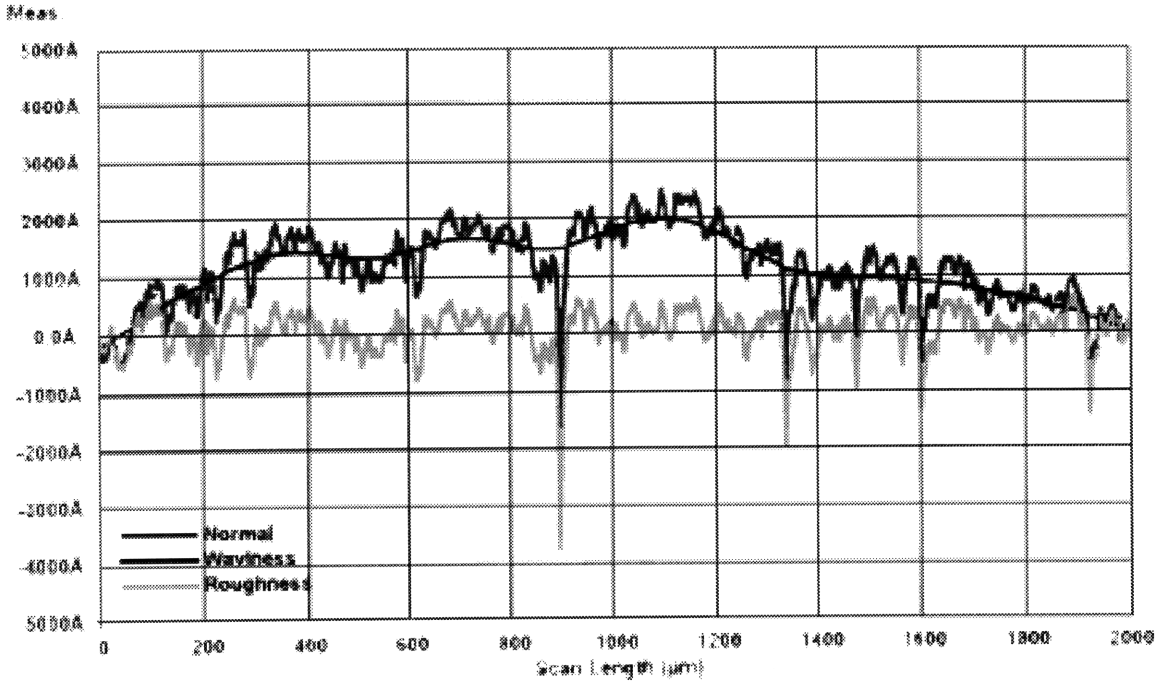

Figure 3-9: Typical scan of initial Co-Cr roughness.

starting at time, t, equal to zero.

3.5.1 The Strain Gage

The strain gages were similar to that described by Cook and Rabinowicz [41]. It was composed of an extended octagonal ring made of aluminum, as shown in fig. 3-10, and fixed contact resistance elements.

The measurements were based on the change of the output voltage due to the changes in the resistance of the fixed contact resistance elements from elastic and plastic deformation. The change in the resistance is based on the principle that as a wire is stretched, its cross sectional area decreases as its length increases because of Poisson's effect; consequently, the resistance increases. The ratio of the strain on the resistor and its change in resistance is called the Gage Factor (GF), which is a reflection of the resistors sensitivity

$$GF = \frac{\left(\frac{\Delta R}{R}\right)}{\epsilon} \tag{3.5}$$

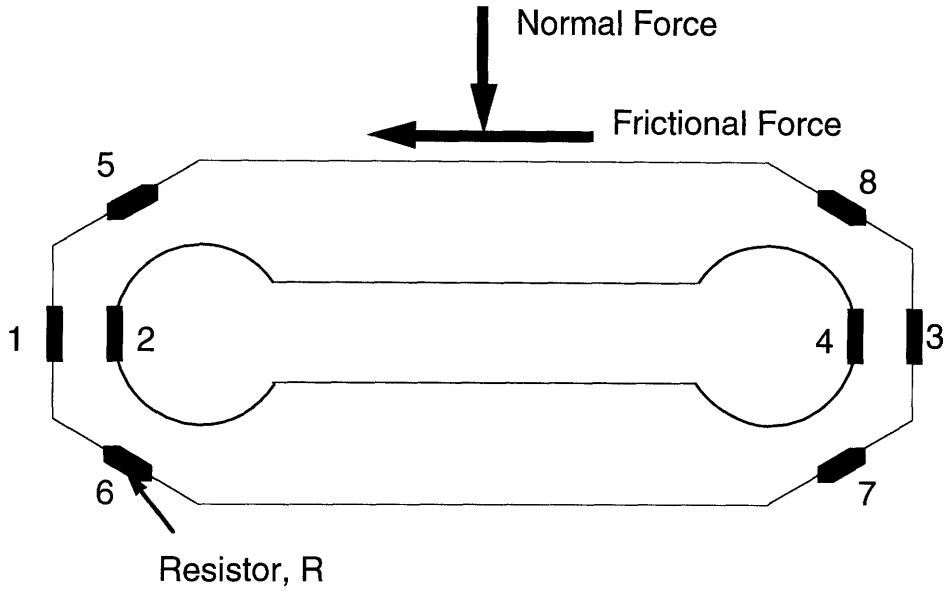

Figure 3-10: Strain Gage, Extended octagonal ring.

$$\epsilon = \frac{\Delta l}{l} \tag{3.6}$$

The resistors are cemented onto the piece where the strain is to be measured, in this case the octagonal ring. Therefore, small deformations on the piece can be measured. Generally these deformations are too small to measure a change in a resistor. Also, the change in resistance includes the changes due to temperature. These problems were solved by using the Wheatstone Bridge, fig. 3-11. Where in this case the following was used:

$V_i = 5V$ dc

$R_1 = R_2 = R_3 = R_4 = R = 262\Omega$

To take into account the effect that temperature has on the resistance of R all four resistors were placed on the piece so that they would change equally and simultaneously with temperature. Consequently, if there was no strain on the resistors, the output voltage, V_o, would be zero, and the current through all the resistors would be the same, $I = V_i/2R$. If there was a small change, ΔR, in one of the resistors the current through it, I, would not be strongly affected; but there would be a measurable voltage drop $V_i \Delta R/4R$. Though if R_1 and R_2 both have an increase ΔR in resistance the output voltage would be zero, but if R_1 increased and R_2 decreased then the volt-

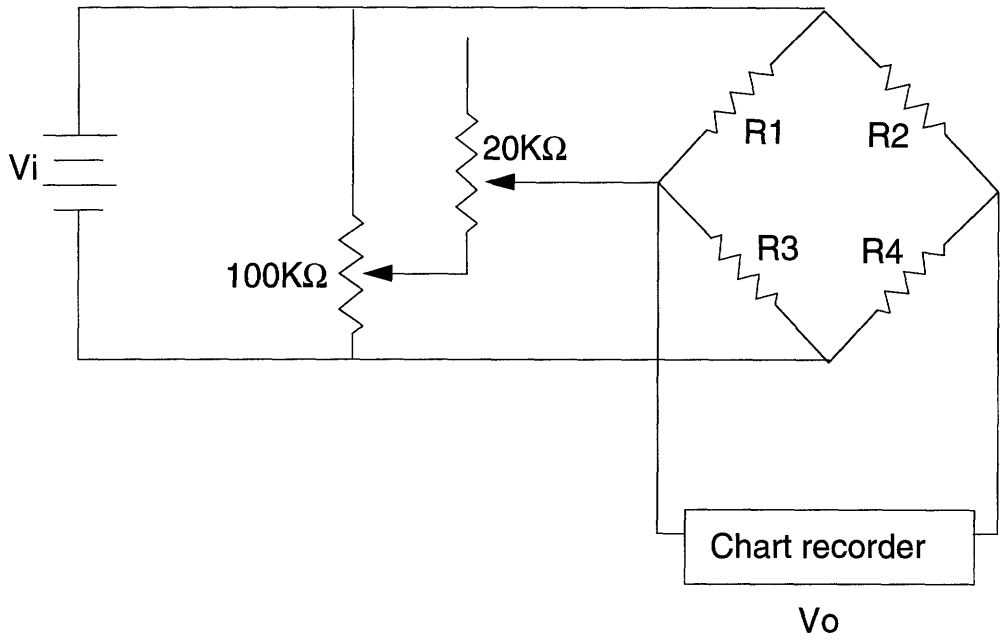

Figure 3-11: Wheatstone Bridge.

age drop of each one would add up, $V_i \Delta R/2R$. Thus, opposite changes in adjacent arms (*i.e.*, R_1 and R_2), or equal changes in opposing arms (*i.e.*, R_1 and R_3) produced double the output. The resistors were then placed on the extended octagonal ring so that the maximum output voltage would be produced in the application of interest.

$$\frac{V_o}{V_i} = \frac{\Delta R}{R} \tag{3.7}$$

For measuring the normal load, the resistors in fig. 3-10 were connected in the Wheatstone bridge in the following fashion: $R_1 = 1$, $R_2 = 2$, $R_3 = 4$, $R_4 = 3$.
For measuring the frictional force: $R_1 = 5$, $R_2 = 6$, $R_3 = 8$, $R_4 = 7$.

3.5.2 Calibration of the Strain Gage

The strain gages were calibrated in both the frictional load and the normal load to obtain the linear equations that relate the load to the voltage output, V_o. For the frictional force the strain gages were removed from the wear tester and dead weights from 0 to 294.68N (66.25lb.) were applied in the tangential direction. The output voltage was then recorded with a voltmeter, and the data were curve fitted to a linear equation. Similarly in the normal force, for one of the strain gages a dead weight from

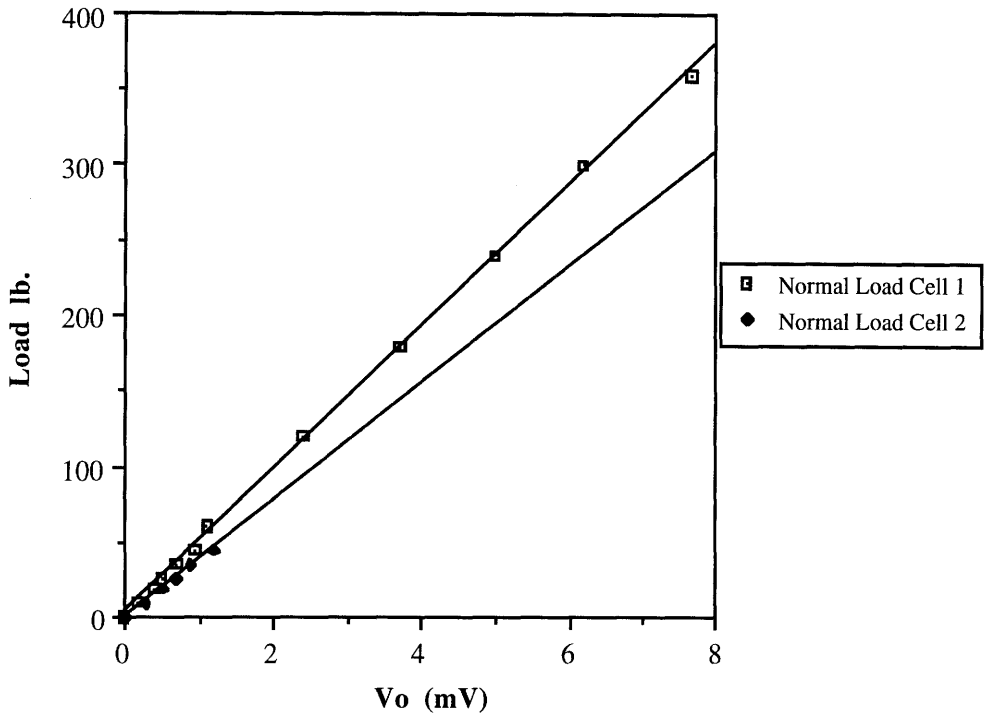

Figure 3-12: Calibration of Strain Gages in the Normal Load (NL).

0 to 202.38N (45.5lb.) was applied in the normal direction, and then using one of the pneumatic pistons loads from 266.88 to 1601.28N (60-360lb.) were applied. Since a linear curve fit was obtained, it was assumed that the pneumatic piston was applying the rated load for the input pressure, and that the strain gages behaved linearly for the load range of 0 to 1601.28N (360lb.). The second load cell was calibrated using only loads from 0 to 202.38N (45.5lb.). This data was then plotted and linearly curve fit as follows in fig. 3-12, 3-13, 3-14. where for Cell 1:

$$NL(lb.) = 2.56 + 47.43(V_o) \quad R^2 = 0.999 \tag{3.8}$$

and for Cell 2:

$$NL(lb.) = -0.40 + 38.59(V_o) \quad R^2 = 0.996 \tag{3.9}$$

where the linear equation is for the frictional force in Cell 1:

$$FF(lb.) = 0.71 + 26.25(V_o) \quad R^2 = 0.999 \tag{3.10}$$

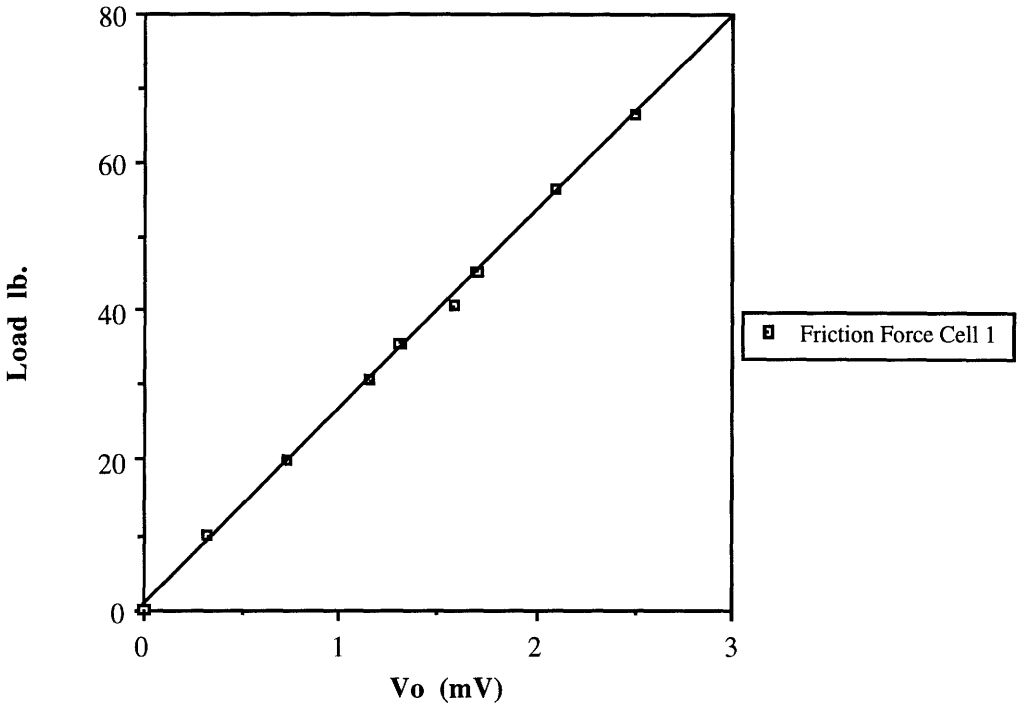

Figure 3-13: Calibration of strain Gage 1 (cell1) in the Frictional Force (FF).

where the linear equation is for the frictional force in Cell 2:

$$FF(lb.) = 1.36 + 26.14(V_o) \quad R^2 = 0.999 \tag{3.11}$$

3.6 Wear Measurement

Two methods for directly determining the wear of the UHMWPE samples from the reciprocating wear test are by measuring the volume lost, and by measuring the mass loss and later converting this to volume. To directly obtain volume lost, the contour of the wear track has to be measured using profilometry. From this information an estimated depth of the track can be obtained. However, this depth is not due exclusively to the wear of the UHMWPE since this material, at the loads that are being applied, exhibits both viscoelastic and plastic deformation. Moreover, the load is not continuously applied on the whole wear track of the specimen because of the nature of the wear tester, instead, the load continuously moves back and forth over it. Therefore, obtaining an estimate of the viscoelastic deformation of the worn

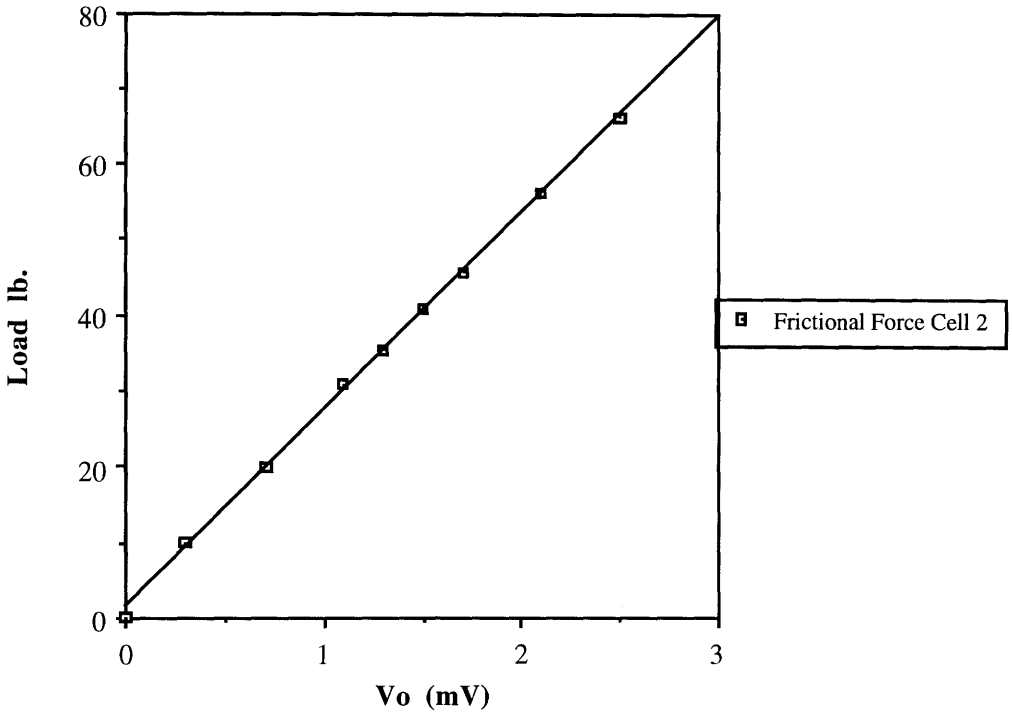

Figure 3-14: Calibration of strain Gage 2 (cell2) in the Frictional Force (FF).

samples by using a load that produces an approximate contact pressure to that used during the wear test, and for a similar duration as the wear test, is an inaccurate simulation of what really occurs. This method most likely overestimates the depth due to viscoelastic deformation. Instead, mass loss in conjunction with the density of the polyethylene was used to obtain the volume loss.

3.6.1 Wear Measurement through Mass Loss

The mass of the UHMWPE samples was measured before and after the wear test with saline solution as a lubricant. In order to obtain an accurate measurement of the mass loss due to wear it was necessary to account for the mass gain from water absorption. Initially the controls and the specimens to be worn were weighed and placed in the saline solution at the same time, and immediately thereafter the wear test was started. Once the test was concluded the samples were taken out of the solution, cleaned with isopropyl alcohol and reweighed. From the controls the average concentration of the saline solution absorbed in the UHMWPE was calculated, $C(t)$.

Sample	Load/length	$M_i - M_f$(g)	Water Abs.(g)	Wear Mass(g)	Wear Vol.(cc)
1	801N/24h	-0.00072	0.00028	-0.00044	-0.00047
2	801N/24h	-0.00044	0.00029	-0.00015	-0.00016
3	1068N/24h	-0.00055	0.00028	-0.00027	-0.00028
4	1068N/24h	-0.00089	0.00029	-0.00060	-0.00064
5	1068N/72h	-0.00107	0.00054	-0.00053	-0.00057

Table 3.2: Wear of samples in saline solution and estimated water absorption.

$$C(t) = \frac{M_i - M(t)}{M_i} \tag{3.12}$$

M_i = initial mass

$M(t)$ = mass at time t

Ten controls were set up and a average $C(t)$ was obtained, $4.4 \times 10^{-5} \pm 1.6 \times 10^{-5}$, $8.2 \times 10^{-5} \pm 0.9 \times 10^{-5}$, $11.5 \times 10^{-5} \pm 3.8 \times 10^{-5}$, for a 1, 2, and 3 day test respectively. The amount of water absorbed was then estimated by multiplying $C(t)$ by the initial mass of the wear sample. The mass gain of the control was then subtracted out from the wear samples to obtain the mass loss due to wear.

From table 3.2 (801N=180lb., 1068N=240lb.) it is obvious that the water absorption is underestimated. This underestimation is probably due to the frictional heating that the wear samples are subjected to, which aides to the diffusion of the solution 3.13 [42], while the controls remain at room temperature.

$$D = D_o e^{\frac{-E}{RT}} \tag{3.13}$$

D= diffusion coefficient (cm^2/sec)

E= activation energy for diffusion

T= temperature (K)

Also, the values of $C(t)$ have a large standard deviation which adds more error to

the wear factor. Since an accurate measurement of the mass absorbed could not be obtained a different approach was found.

The samples were soaked until they were saturated or up to the point where the mass gained was small enough that it would be negligible, ensuring that the small loss measured was an accurate measurement of the mass lost due to wear. An approximate time for the saturation of the samples was calculated from information from the literature and the following mass transfer equations.

For a homogeneous solid the solution of the diffusion through a slab $-L < x < L$ is [43]:

$$\theta(x,t) = \frac{C(x,t) - C_{t=\infty}}{C_{t=0} - C_{t=\infty}} = \sum_{n=0}^{\infty} \frac{2(-1)^n}{(n+1/2)\pi} e^{-(n+1/2)^2\pi^2 \frac{Dt}{L^2}} cos\left[(n+1/2)\frac{\pi x}{L}\right] \quad (3.14)$$

From this the average can be obtained by integrating x:

$$\theta_{ave.}(t) = \frac{1}{2L}\int_{-L}^{L} \theta(x,t)dx \quad (3.15)$$

To obtain a solution of for a parallelepiped is just the multiplication of the different for each of the slabs that would construct the parallelepiped starting at the same time, t [43]. Assuming that the first term is the dominant one and that subsequent terms are negligible, the following equation for the given sample size can be derived:

$$\theta_{ave} = \frac{C_{ave}(t) - C_{t=\infty}}{C_0(t) - C_{t=\infty}} \approx \left(\frac{2}{(1/2)^2\pi^2}\right)^3 e^{-(1/2)^2\pi^2 Dt\left(\frac{2}{L_1^2}+\frac{1}{L_2^2}\right)} \quad (3.16)$$

Assuming that the absorption of water is the dominant factor when soaked in bovine serum, since the protein molecules are considerably larger than the water molecules. For a sample that is approximately 1x1x3.556cm, and with a diffusion coefficient, D, of 1×10^{-7}cm^2/sec [44] to reach the state where $\frac{C_{ave}}{C_{t=\infty}} = 0.95$ would take approximately two weeks. This time agrees with experimental data of Lee and Pienkowski [38]. But due to the variability in the solubility and diffusion data [45], the compressed and standard samples where nevertheless soaked in bovine serum and their weight gain was measured. From this an approximate diffusion coefficient was

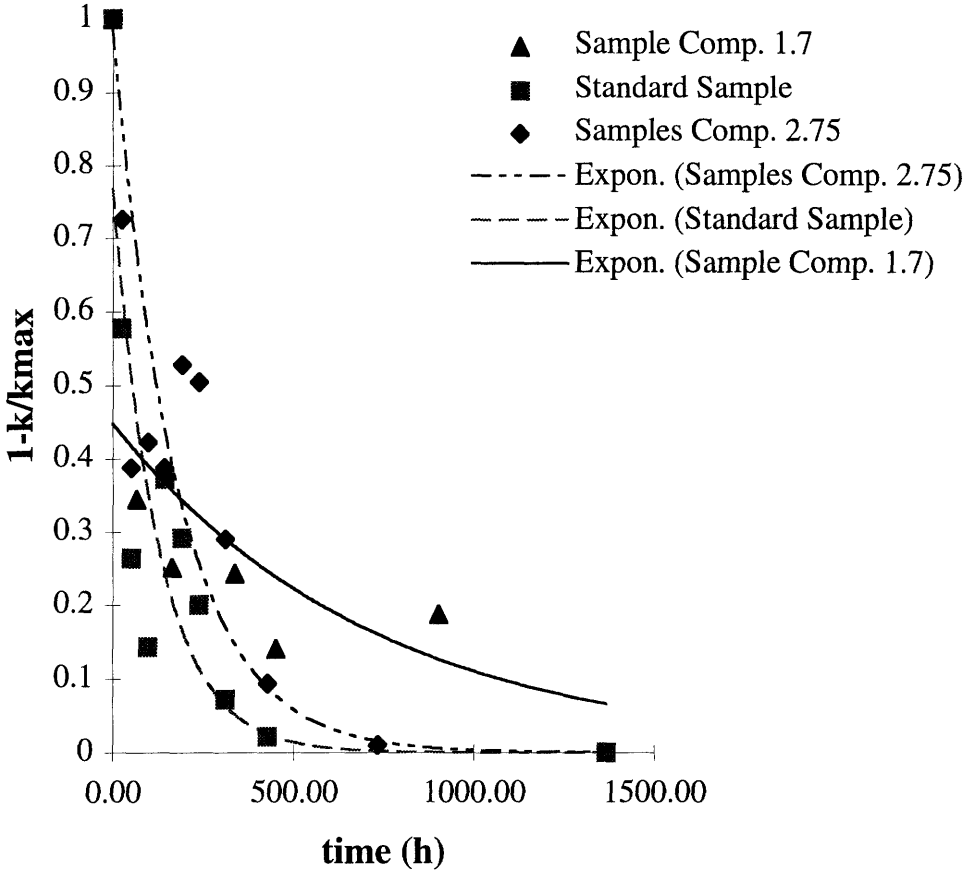

Figure 3-15: Absorption of Bovine Serum by UHMWPE sample.

obtained by curve fitting the data using least squares, fig. 3-15.

$$y = 1 - \frac{k}{k_{max}} \tag{3.17}$$

$$y_{stand.} = 0.77e^{-0.008t} \quad R^2 = 0.977 \tag{3.18}$$

$$y_{\lambda=2.75} = 0.99e^{-0.0056t} \quad R^2 = 0.893 \tag{3.19}$$

$$y_{\lambda=1.7} = 0.45e^{-0.0014t} \quad R^2 = 0.462 \tag{3.20}$$

From the data the following values for the diffusion coefficient can be calculated: 1.083×10^{-7}cm^2/sec, 0.190×10^{-7}cm^2/sec, and 0.758×10^{-7}cm^2/sec for standard samples, and compressed samples with compression ratio of 1.7 and 2.75, respectively. These values are within those estimated by Klute [45] and Stannett [42]. The differences observed between diffusion coefficient values are because the behavior

for polyethylene is strongly dependent on the degree of oxidation, number of polar groups present in the polymer [46], the degree of crystallinity and the distribution of the crystallites [45].

The error between the equation 3.16 and the equations produced from the curve fit of the data was most likely due to the fact that UHMWPE is not a homogeneous material. Only the amorphous fraction of the polyethylene absorbs water [42]. Also the water molecules tend to cluster, which causes a decrease in their mobility; therefore, the effective diffusion coefficient is reduced. This time dependent, or more precisely concentration dependent, diffusion coefficient is not reflected in equation 3.16. Another factor may be that the protein molecules adsorption to the surface of the polyethylene, causing errors in the weight measurements.

The differences between the compressed and standard samples, even though they were made from the same rod stock, are possibly due to the orientation that is imposed upon the UHMWPE as it is compressed, and the difference in the orientation direction of the samples. For water to diffuse through the amorphous regions of the polymer it must circumvent the crystallites since they do not absorb water. Therefore, the crystallite distribution affects the diffusion coefficient [45].

If the wear samples were allowed to equilibrate in the bovine serum for at least two weeks the error that may have been introduced through weight gain of water during the eight day wear test was less than 0.05mg, which is considerably less than the error found between different wear tests (at least an order of magnitude greater).

3.7 Test Protocol for Wear and Friction

Once the wear samples were soaked for at least two to three weeks, they were paired up and machined together with a fly cutter. The same spindle speed, feed rate and fly cutter was used each time. The fly cutter was of 2.54cm in radius, the spindle speed was 1400rpm, and the transverse feed rate was 1.905cm/min (0.75in/min). The surface roughness of three of these samples was measured and it was found that the samples produced in this fashion had an Ra of approximately of 1μm. The fiber

reinforced samples were not fly cut; the melted surface was used as the sliding surface.

After fly cutting, the samples were cleaned with isopropyl alcohol and weighed to 0.01mg of accuracy using a Mettler AT20 scale. Repetitive weighing was made until two measurements with an error of less than 0.03mg were obtained. These measurements were obtained taking care that static electricity was not affecting the measurement of the true weight of the sample, by adding on mass in the form of dust particles. This was achieved by weighing the samples right after they were cleaned and then ten minutes later, if the weight gain was more than 0.1mg it was assumed that the sample was charged. These samples were then discharged with a piece of steel, cleaned and reweighed.

The samples were then placed in the wear tester's holder and the carriage was set in motion. The strain gages were zeroed while unloaded. Using compressed nitrogen from a gas cylinder, 80psi was supplied to the pneumatic pistons, which produced a normal load of 889.6-934.08N (200-210lb.) as measured with the strain gages. The test was conducted at room temperature, 25°C.

The friction was measured with the aid of a chart recorder and the strain gages. A measurement was taken at the beginning of each test and subsequently after every 24 hours. Both the normal load and the frictional force were recorded and the average of these were taken over a period of 30sec. After using the appropriate conversion factors, the coefficient of friction, μ, was calculated by the following equation:

$$\mu = \frac{F}{N} \tag{3.21}$$

F= frictional force

N=normal force (load)

Wear measurements where taken after 2, 4 and 8 days; which corresponded to a sliding distance of 14.81, 29.62, and 59.24km, respectively. These measurements were taken by unloading the samples and stopping the carriage. Samples were then removed and weighed using the same procedure as for the initial weighing. Once weighed, the samples were returned to their original holder and the test was restarted

on the same counterface. The bovine serum that was used as the lubricant was changed every four days because of denaturing. The used bovine serum from the channels with strain gages were stored for later analysis the wear debris. At the end of the test, the UHMWPE samples were stored in bovine serum for future wear test.

3.8 Scanning Electron Microscopy

Scanning Electron Microscopy, SEM, was used to determine the texture of the worn surface and the shape and size of the wear debris particles. This information was later used to aid determining the predominant mode of wear.

3.8.1 Worn Sample Preparation

The worn samples were stirred in a 5N NaOH bath for 1.5 hours at 65°C to remove any bovine serum from the surface of the sample. The samples were then allowed to dry for at least 24 hours before scanning of the worn surface.

3.8.2 Particle Isolation

The wear debris particles were isolated from the bovine serum collected from the second half of a given test wear test. The procedure used was that of Campbell, *et al.* [47], as follows:

-All water used was 0.2μm triple filter distilled water, and all containers, and instruments were triple rinsed with this water. This water was Omnisolve water provided by E. Merk Science.
-The 0.90g/cm^3 solution was 48.48ml of isopropyl alcohol and 60ml of triple filtered water.
-The 0.96g/cm^3 solution was 20.07ml of isopropyl alcohol and 100ml of triple filtered water.
-20ml of the bovine serum with wear debris soup was digested in 15ml of

5N NaOH for two hours at 65°C while being stirred continuously. The protein molecules were digested by this procedure, and at the end of the process the sample was clear.

-The sample was allowed to cool to room temperature. It was then ultrasonicated for ten minutes to break up any clumps that may have formed.

-8ml of the digested soup was placed in a 13.2ml Beckman Polyallomer centrifuge tube.

-A 5% sucrose solution was slowly added on top to create a gradient.

-The sample was ultracentrifuged in a Beckman L8-70 Ultracentrifuge with a SW41Ti swinging bucket rotor at 40000rpm and at 10°C for three hours.

-The UHMWPE was located in the top band. This band was collected taking care that no sucrose was collected.

-Depending on the cloudiness of the sample, water was added to wash of the sucrose until there is between 14-42ml. The cloudier the sample, the more water was necessary.

-Ultrasonicated for 5 minutes to disperse the particles.

-The sample was heated in a tap water bath at 80°C for an hour.

-While the sample was still hot, 7ml of the sample was placed in a 13.2ml Beckman Polyallomer centrifuge tube. 3ml of 0.96g/cm^3 solution was added. On top of this 2ml of 0.90g/cm^3 solution. Care was taken to form a gradient. Then the sample was ultracentrifuged at 40000rpm at 25°C for an hour.

-The white band between the 0.90 and 0.96g/cm^3 interface was collected in a particle free vial. This solution contained the UHMWPE particles. To this 200-300μl solution, 2ml of the triple filtered distilled water was added.

For the SEM analysis, small aliquots of the solution were placed on 0.2μm pore polycarbonate filter paper (Costar No. 111106). This filter paper was placed on a leveled ceramic filter without vacuum and in a low traffic area. It was allowed to dry

completely, and a 1x1cm square was cut from the filter paper for subsequent viewing in the SEM.

3.8.3 The Instrument

The SEM used was a JEOL 6320FV Field Emission Scanning Electron Microscope. It was capable of secondary-electron image resolution of less than 1nm when operating at 15kV, and about 3.5nm when operating at 1kV. For scanning the worn polyethylene surface, a 1kV electron beam and short working distance (6mm) were employed to avoid excessive charging of the sample. For scanning the debris, 0.8kV and a 5mm working distance were used.

3.9 Statistical Analysis

Wear is a process that is dependent on many different factors that cannot always be controlled and specified in a given laboratory test. Therefore a series of tests, conducted under the same operating conditions, may have a high variance. Within a given test series the coefficient of variation can easily be between 20-100%. Particularly for polyethylene, the wear rate is very sensitive to contaminants and roughness of the counterface, and the presence of imperfections in the PE sample. Also, the laboratory wear test is not an accurate representation of what really occurs in the *in vivo* total knee replacement, there considerable variation among patients with respect to the type of contact (*e.g.*, rolling, sliding), and the contact load. Since there are many sources of errors in the laboratory simulation of the wear of UHMWPE in total knee replacements, for the new oriented PE to be considered successful it would need to exhibit a wear rate that is an order of magnitude lower than that of the standard isotropic sample currently used.

Statistical analysis was used to compare the performance of the oriented polyethylene to the standard currently used. Specifically the two tailed Student t-test was used to compare samples with different compression ratios and MP-60, with the same sliding distance.

By using the Student t-test, we made certain assumptions about the population distribution. We assumed that the population distribution for each treatment case was a normal one, *i.e.*, that it has the classic bell shape. The Student t-test also assumed that the samples are independent of one another.

3.9.1 Definitions of Parameters Used

There are different tools used to describe the sample observations. In this thesis we will use the mean, the variance, the standard deviation, the standard error of the mean, and the coefficient of variation as conventionally defined [48].

The mean of a sample, $\bar{X}$, is the average of all the variates, all the observations. If the population mean is normally distributed, then the sample mean estimates the population mean, and the values of the sample will fit in the bell shaped curve. The sample mean has the same units as the variates, and it is defined as follows 3.22.

$$\bar{X} = \sum_{i=1}^{n} \frac{X_i}{n} \tag{3.22}$$

where n is the number of variates.

The variance represents the spread of the data around the sample mean. The higher the variance, the harder it is to get a real close estimate of the mean of the population, or to compare means from different samples because of the increasing likelihood of overlap between the data from different samples. The variance is generally represented in terms of the variate's units squared. It is mathematically defined as in equation 3.23.

$$S^2 = \sum_{i=1}^{n} \frac{(\bar{X} - Xi)^2}{n-1} \approx \sigma^2 \tag{3.23}$$

The standard deviation of the population (σ) is in the same units as the variates. It is the square root of the variance, and it is a good representation of the population spread. Normally $\pm\sigma$ contains 66% of the population, $\pm 2\sigma$ 95% and $\pm 3\sigma$ 99%. If the sample is a good representation of the population, then the standard deviation of the sample ($S \approx \sigma$) will be a good representation of the variability of the original

population.

The Standard Error of the Mean (StEM) represents the variability of the estimated population mean. It represent the level of confidence we have that the mean of our sample represents the population mean. It is expressed mathematically as in equation 3.24.

$$StEM = \frac{\sigma}{\sqrt{n}} \tag{3.24}$$

Generally the σ is given for the control group to give an idea of the population spread, but further comparisons between the treated groups and the control are made with the aide of the StEM.

The Coefficient of Variance (CV) is a representation of the population variation relative to the mean based on a percentile scale, thus making it easier to interpret. It is defined mathematically as in 3.25.

$$CV = \frac{\sigma}{\bar{X}} 100\% \tag{3.25}$$

3.9.2 Types of Error

In our statistical analysis the hypothesis being tested was that there is no difference in the mean wear of the oriented samples and the standard, null hypothesis (Ho). The alternative hypothesis to Ho was that the wear rate was $0.99 \times 10^{-7}\text{mm}^3/\text{Nm}$ lower than the standard ($1.0 \times 10^{-7}\text{mm}^3/\text{Nm}$) [49], *i.e.*,one tenth of the standard.

There were two forms of errors to minimize when using the Student t-test to analyze the data, type I and type II errors. The type I error occurs when the null hypothesis is rejected when it is actually true. The type II error is the accepting the null hypothesis when it is actually false. The probability of committing a type I error, that is finding an effect when there really is none, is termed the significance level, α. The probability of committing a type II error, that is finding no effect when there really is one, is termed the statistical power, β.

It was of interest to reduce as much as possible both these errors. The compressed material and the composite are both materials that if implemented would require

additional processing compared to the current isotropic UHMWPE. Thus, it would be more costly to implement. Consequently, we wanted a low probability of finding a difference when there really was none, we pick an α of 0.05. Also, considering the benefits of finding an improvement in wear of UHMWPE, if no difference was found to the order where it would be considered a significant improvement (an order of magnitude lower wear) we wished the likelihood of committing a type II error low, so we set our β to be equal to 0.05.

From preliminary testing it was found that the coefficient of variance was roughly 30%. This coupled with our specifications stated above we can calculate the sample size required with equation 3.26

$$n = 2\left(\frac{\sigma}{\delta}\right)^2 (t_{\alpha,\nu} + t_{2\beta,\nu})^2 \tag{3.26}$$

σ = population standard deviation

δ = difference desired to detect

α = desired significance level

β = desired statistical power

$t_{\alpha,\nu}$ = t statistic corresponding to significance level α and degrees of freedom ν.

$t_{2\beta,\nu}$ = t statistic corresponding to significance level 2β and degrees of freedom ν

ν = degrees of freedom = a(n-1)

a = number of different samples groups

n = number of independent data points per sample

It is an iterative process to use equation 3.26, but there also exist tables for t-test where equation 3.26 is solved. The table 3.3 from Orthopeadic Basic Science [48] was used. For a $\delta = 0.99 \times 10^{-7}\text{mm}^3/\text{Nm}$, a $\sigma = 0.3 \times 10^{-7}\text{mm}^3/\text{Nm}$, α and β of 0.05 a sample size of roughly four would be sufficient. Also, due to time constraint four test per different sample type would be the maximum possible.

$\frac{\delta}{\sigma}$	$\alpha = 0.01$; $\beta =$					$\alpha = 0.05$; $\beta =$					$\alpha = 0.1$; $\beta =$				
	0.01	0.05	0.1	0.2	0.5	0.01	0.05	0.1	0.2	0.5	0.01	0.05	0.1	0.2	0.5
0.05															
0.1															
0.15															
0.2										99					122
0.25					110				128	64					70
0.3				134	78			119	90	45			139	101	45
0.35			125	99	58		109	88	67	34		122	97	71	32
0.4		115	97	77	45	117	84	68	51	26	101	90	72	52	24
0.45		92	77	62	37	93	67	54	41	21	80	70	55	40	19
0.5	100	75	63	51	30	76	54	44	34	18	65	55	44	33	15
0.55	83	63	53	42	26	63	45	37	28	15	54	45	36	27	13
0.6	71	53	45	36	22	53	38	32	24	13	46	38	30	22	11
0.65	61	46	39	31	20	46	33	27	21	12	39	32	26	19	9
0.7	53	40	34	28	17	40	29	24	19	10	34	28	22	17	8
0.75	47	36	30	25	16	35	26	21	16	9	30	24	19	15	8
0.8	41	32	27	22	14	31	22	19	15	9	27	21	17	13	7
0.85	37	29	24	20	13	28	21	17	13	8	24	19	15	12	6
0.9	34	26	22	18	12	25	19	16	12	7	21	17	14	11	6
0.95	31	24	20	17	11	23	17	14	11	7	19	15	13	10	5
1.0	28	22	19	16	10	21	16	13	10	6	18	14	11	9	5
1.1	24	19	16	14	9	18	13	11	9	6	18	13	11	8	5
1.2	21	16	14	12	8	15	12	10	8	5	15	11	9	7	
1.3	18	15	13	11	8	14	10	9	7		13	10	8	6	
1.4	16	13	12	10	7	12	9	8	7		11	8	7	6	
1.5	15	12	11	9	7	11	8	7	6		10	8	7	5	
1.6	13	11	10	8	6	10	8	7	6		9	7	6		
1.7	12	10	9	8	6	9	7	6	5		8	6	6		
1.8	12	10	9	8	6	8	7	6			8	6	5		
1.9	11	9	8	7	6	8	6	6			7	6			
2.0	10	8	8	7	5	7	6	5			7	5			
2.1	10	8	7	7		7	6				6				
2.2	9	8	7	6		7	6				6				
2.3	9	7	7	6		6	5				6				
2.4	8	7	7	6		6					5				
2.5	8	7	6	6		6									
3.0	7	6	6	5		5									
3.5	6	5	5												
4.0	6														

Table 3.3: Number of observations for t-test of means between two groups.

3.9.3 Student t-test

The Student t-test is generally used to compare the mean of two sample groups of the same size (same n). Generally a control group and a treated group, thus it is used to see if a given treatment had an effect. the null hypothesis, H_o, for this kind of testing is that the means are equal, $\mu_1 = \mu_2$. This simple test can be done with the following mathematical equation 3.27, [48].

$$t = \frac{\bar{X}_1 - \bar{X}_2}{\frac{\sigma}{\sqrt{n}}} = \frac{\bar{X}_1 - \bar{X}_2}{StEM} \tag{3.27}$$

where $\bar{X}_1$ and $\bar{X}_2$ are the sample means of group 1 and 2 and StEM is the average standard error of the mean for both groups.

As shown in [50] equation 3.27 can be modified for the cases where the sample size is unequal. It is necessary to use a pooled estimator of the common variance, σ_p^2 as defined in equation 3.28.

$$\sigma_p^2 = \frac{(m-1)}{m+n-2}S_1^2 + \frac{(n-1)}{m+n-2}S_2^2 \tag{3.28}$$

where n and m are the two different sample sizes. Then for testing the null hypothesis the t-test is modified as in equation 3.29.

$$t = \frac{\bar{X}_1 - \bar{X}_2}{\sigma_p\sqrt{\frac{1}{n} + \frac{1}{m}}} \tag{3.29}$$

Using Microsoft Excel the t-test were conducted between the standard sample and the oriented samples that had undergone the same treatment, and the P values for the two tailed case are reported.

Chapter 4

Results

4.1 Friction and Wear

Following are the results of the eight day (over a million cycles) wear tests in which friction was also monitored. The sample size for the wear test, n, and friction test, m, varied. Initially wear tests were reinitialized after 2, 4, and 8 day. The wear tester was subsequently modified in order to obtain 3 wear measurements in one 8 day run. A sample size of four, as stated in chapter 3, was the desired number of wear tests for each sample type, but due to time and material availability constraint it was not always possible, table 4.1. As stated in chapter 3, the goal sample size of friction measurement was two, which was not always possible because of the limited number of strain gages, table 4.2. The performance of all the sample types was compared to that of the standard UHMWPE, employed as a joined specimen (also referred to as standard).

A complete set of tables with the friction and wear data can be found in appendix A and B.

4.1.1 Solid and Joined Standard Isotropic UHMWPE

The wear values of the solid and joined samples were found to be statistically the same and similar, fig. 4-1, to those reported in the literature [17, 18, 19, 49]. The

Distance Slid (km)	14.81	29.62	59.24
Standard Solid	5	5	
Standard Joined	4	6	4
λ=2.75, CD	4	4	4
λ=2.75, LD	4	6	4
λ=1.7, CD	4	4	4
λ=1.7, LD	4	4	3
λ=1.7, FD	4	4	4
λ=1.7, CD2	4	4	4
MP-60	3	3	3

Table 4.1: Number of wear test, n, conducted on each sample type

Distance Slid (km)	0.00	7.41	14.81	22.22	29.62	37.03	44.43	51.84	59.24
Standard Joined	5	5	5	5	5	3	3	3	3
Standard Solid	4	4	4	4	4	2	2	2	2
λ=2.75, CD	5	5	5	2	2	2	2	2	2
λ=2.75, LD	6	6	6	3	3	3	3	3	3
λ=1.7, CD	3	3	3	3	3	3	3	3	3
λ=1.7, LD	2	2	2	2	2	1	-	1	1
λ=1.7, FD	4	4	4	4	4	4	4	4	4
λ=1.7, CD2	2	2	2	2	2	2	2	2	2
MP-60	2	2	2	2	2	2	2	2	2

Table 4.2: Number of friction measurements, m, conducted on each sample type

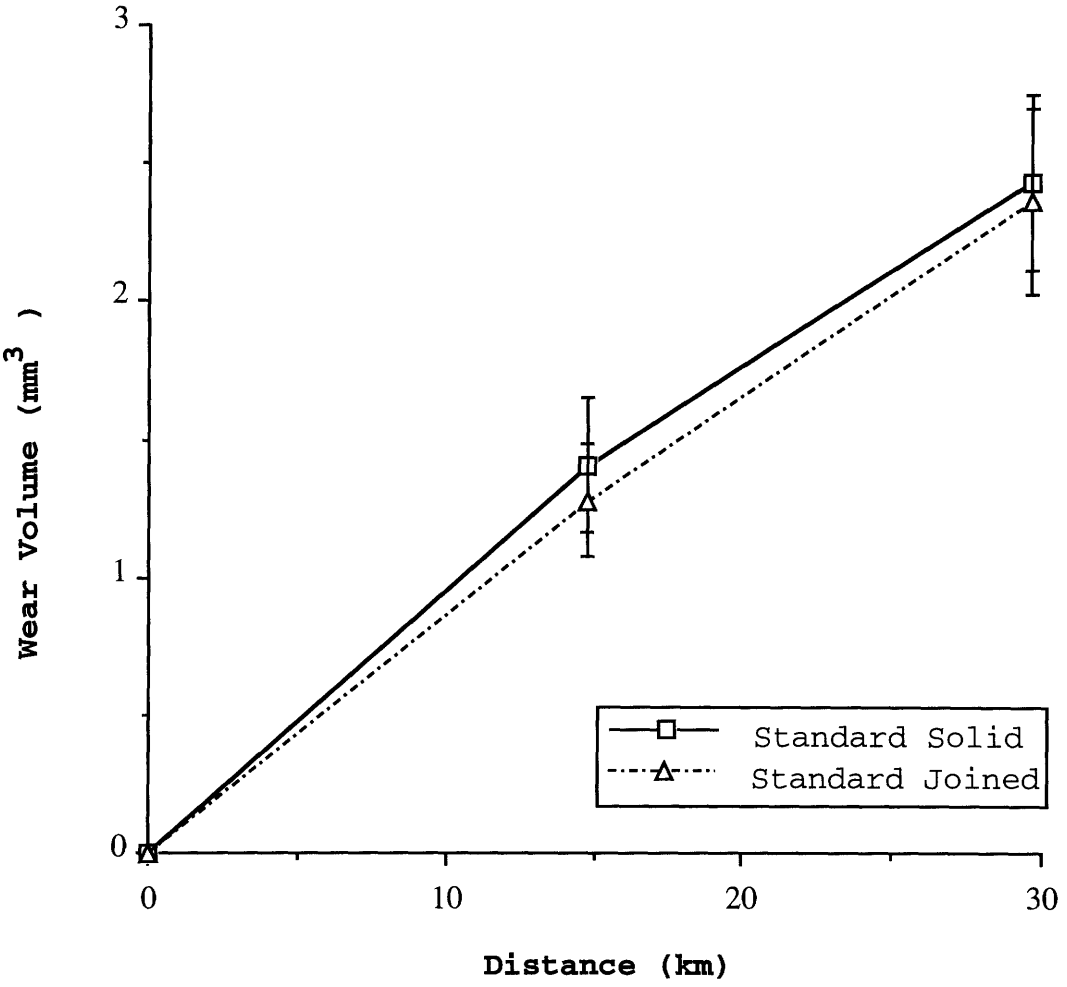

Figure 4-1: Wear of Joined and Solid Standard Isotropic UHMWPE samples.

P values comparing the wear performance of the joined and solid samples after a distance slid of 14.81 and 29.62km, were 0.69 and 0.89 respectively. In both cases the dimensional wear coefficient remained relatively constant within the distance slid, 29.62km. Also, the friction data for both the joined and solid samples had similar values and overlap, fig. 4-2. Both started at average values of μ between 0.05 and 0.06 that leveled out to the final average values between 0.08 and 0.10 at 25-20km of distance slid. Based on these data we concluded that joining two samples for the wear test did not meaningfully affect the results, and thus was a valid test setup.

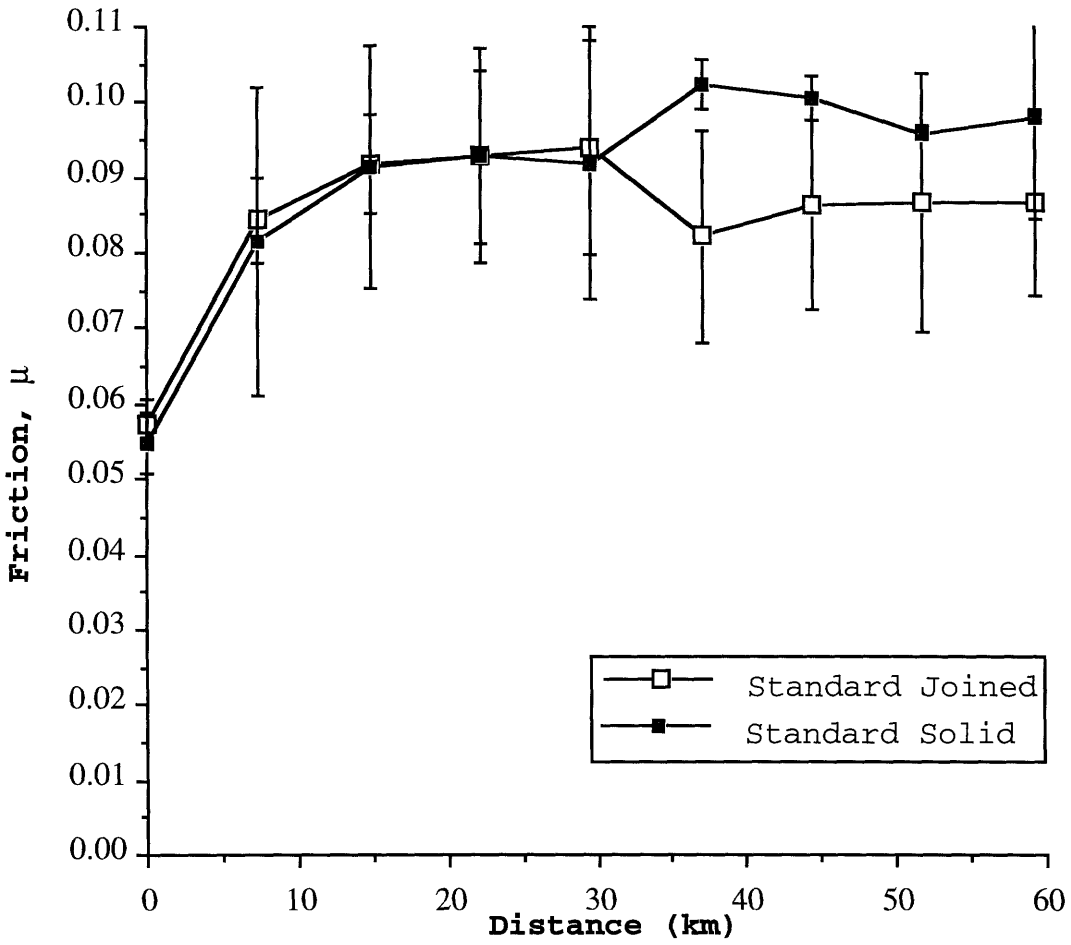

Figure 4-2: Friction of Joined and Solid Standard Isotropic UHMWPE samples.

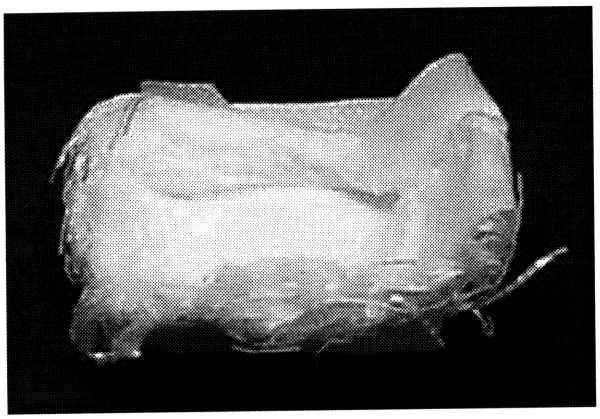

Figure 4-3: Failed sample of MP-56.

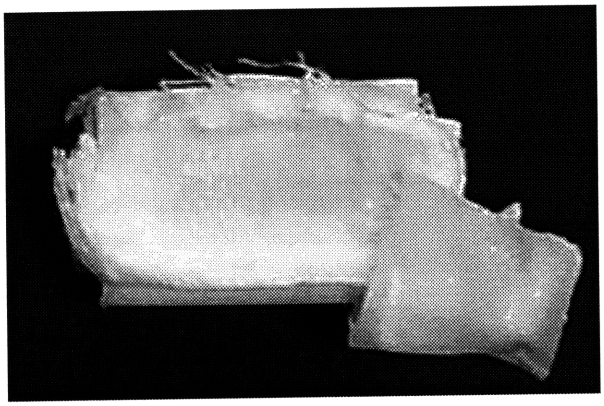

Figure 4-4: Failed sample of MP-58.

4.1.2 Fiber Oriented Samples: MP-60, MP-58, and MP-56

All three sample types were tested. But of the MP-58, and MP-56 only one sample of each was tested. The MP-56 was the least consolidated of the three samples and failed in less than 6 hours of testing, fig. 4-3. The top surface completely sheared off at the interface of different woven layers. Once the melted top surface was removed, the Co-Cr cylinder plowed into the subsequent layers. The MP-58 sample failed similarly but after 4 days, fig. 4-4. For the MP-60 samples, that were more consolidated and had a thicker melted (unoriented) surface layer, catastrophic failure as it occurred in the previous two samples was not reached, and the following data were obtained: figures 4-5, 4-6. In one of the three samples tested there was so much water absorption that negative mass loss was recorded even though there was visible surface damage. This data point was not included in fig. 4-5.

From fig. 4-5 it can be observed that unlike the standard and the channel-die

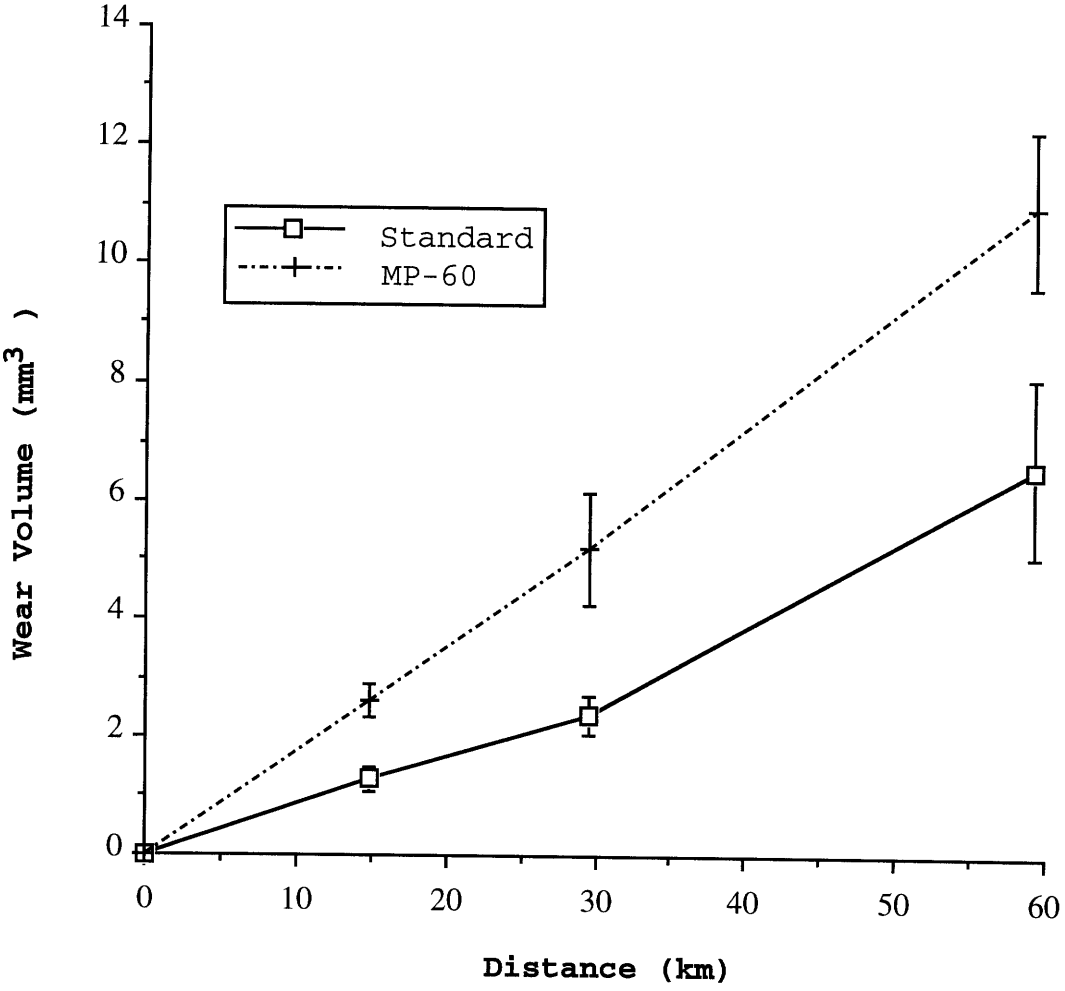

Figure 4-5: Wear of sample MP-60. Only n=2 data points were obtained for MP-60.

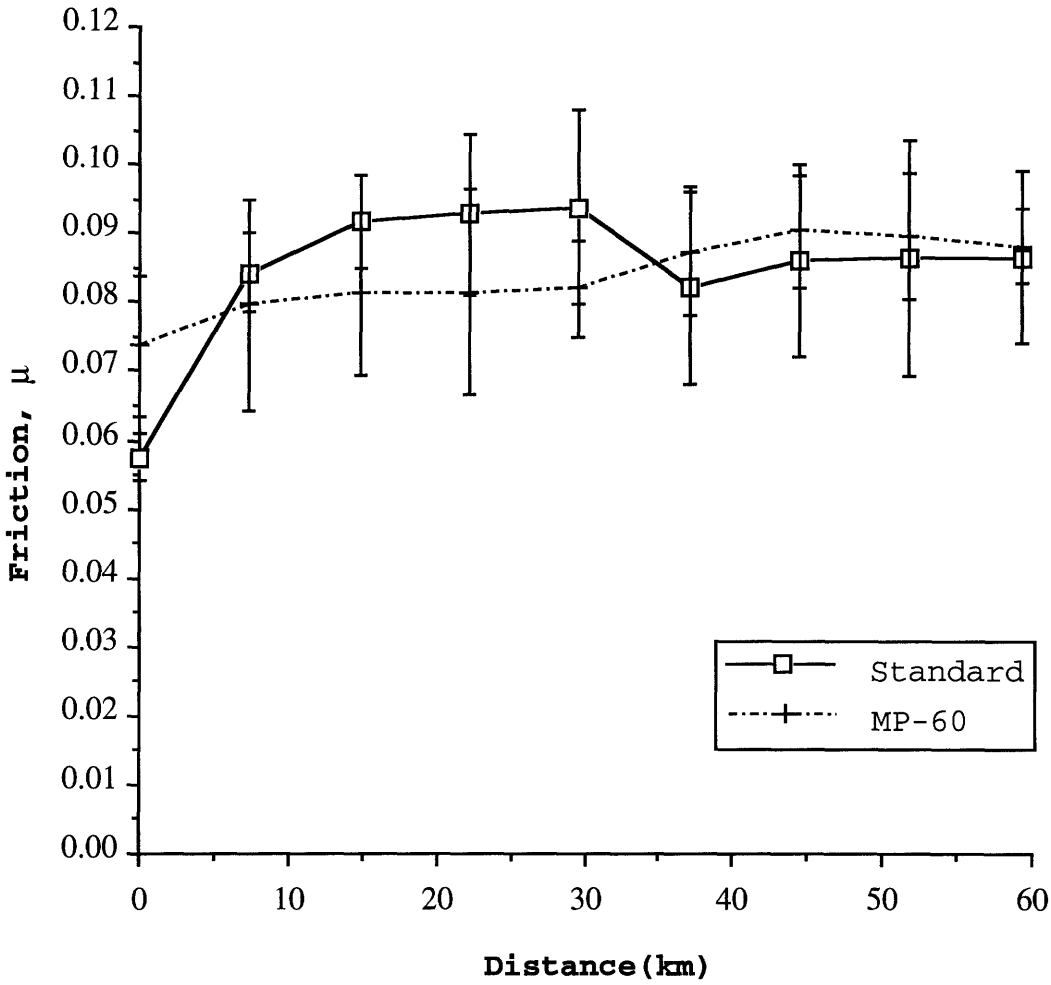

Figure 4-6: Friction of sample MP-60.

compressed samples, discussed later, the dimensional wear rate was relatively constant within the distance slid. The value was on average $2 \times 10^{-7}\text{mm}^3/\text{Nm}$

From fig. 4-6 it can be observed that the average frictional value of MP-60 started out at a higher value, 0.075, than the standard, 0.05-0.06. The average frictional value of MP-60 remained relatively constant through out the test attaining a final value of 0.085. This differed from the standard, whose final value was 50% higher than the initial value.

4.1.3 Samples with a Compression Ratio, λ, of 2.75

The samples with λ of 2.75 could only be tested in the LD and CD configuration. These were some of the first samples tested. Therefore, the values for mass loss at a

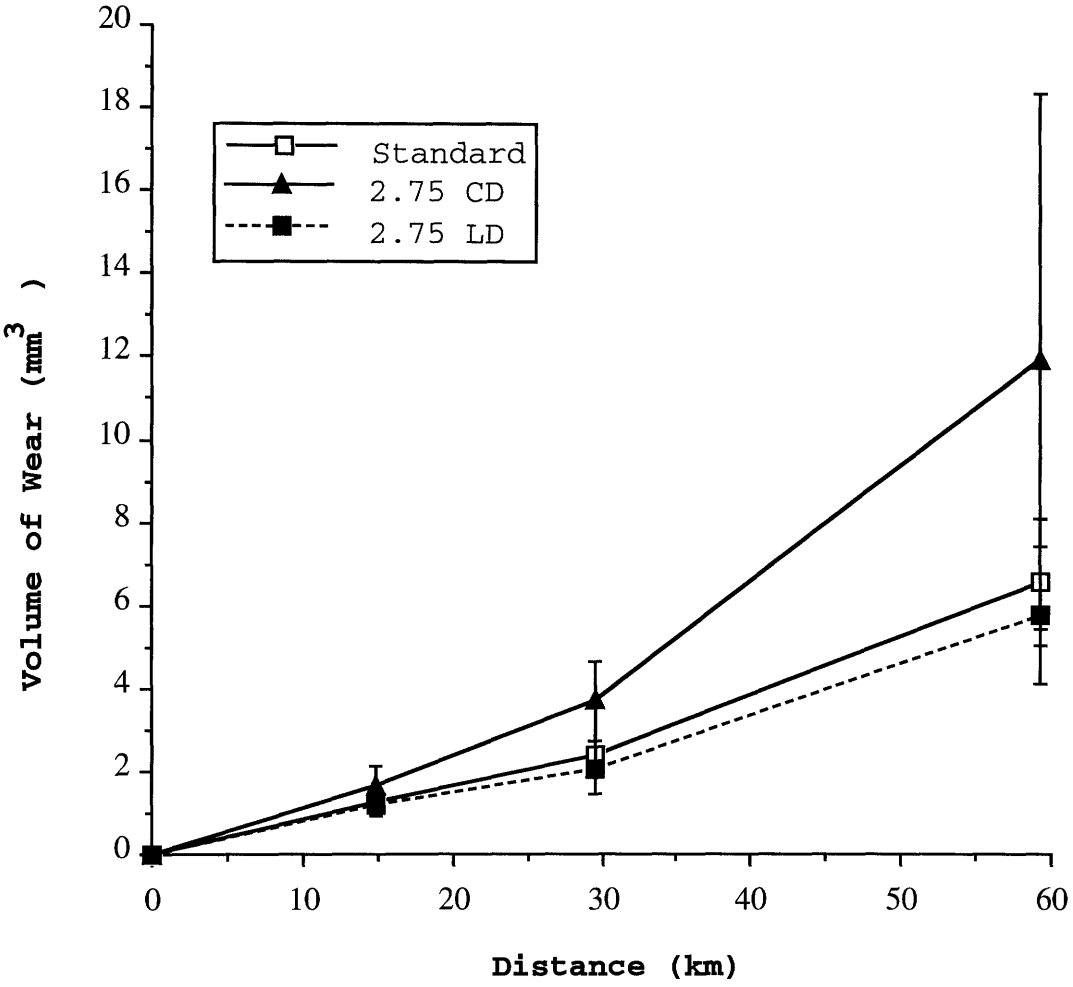

Figure 4-7: Wear of samples with λ of 2.75 in CD and LD.

sliding distance of 14.81km were from a different group than the values reported at 29.62 and 59.24km. The wear volumes reported for the latter two are of the same wear run, data was just collected after 4 and 8 days. The average wear and friction are reported in fig. 4-7 and 4-8.

From fig. 4-7, following the behavior of the standard, the wear of the samples with λ of 2.75 in LD and CD both increase after approximately 30km. The 2.75 LD sample only shows a 20% increase, as the standard, but the 2.75 CD sample shows a 64% increase. The dimensional wear coefficient of 2.75 CD after 59.24km was double that of the standard. Also from fig. 4-8, both the compressed and the standard samples had an average initial frictional value between 0.05-0.06, and level off between 15 and 20km of sliding to values between 0.08 and 0.10.

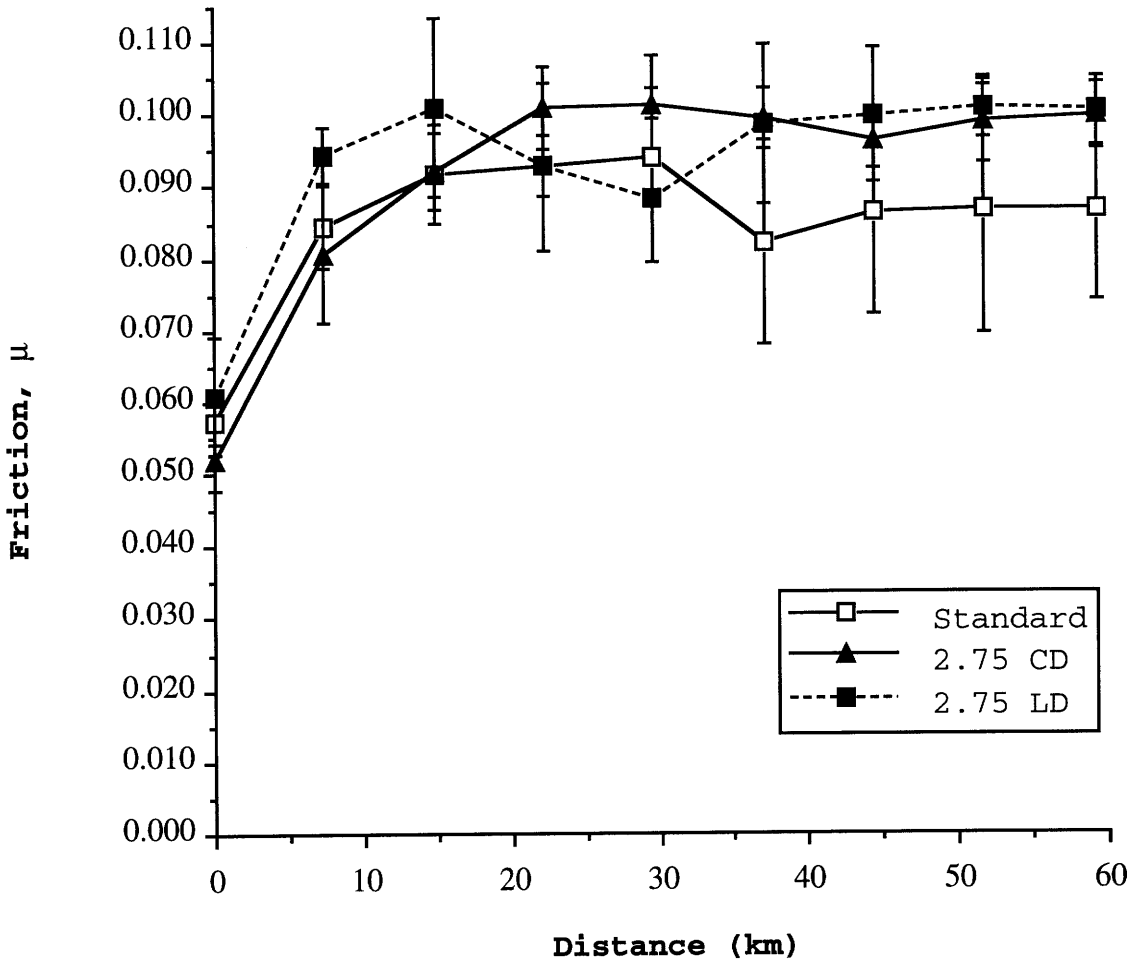

Figure 4-8: Friction of samples with λ of 2.75 in CD and LD.

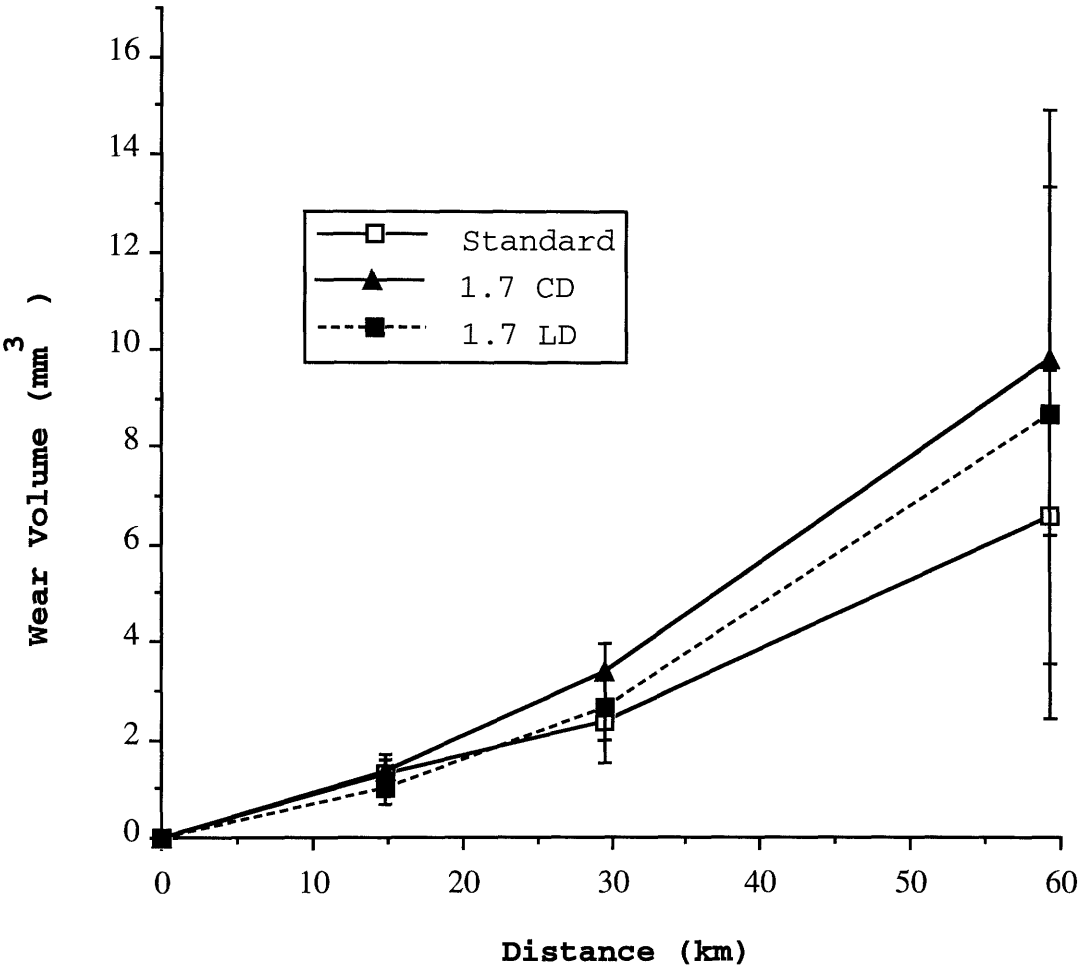

Figure 4-9: Wear of samples with λ of 1.7 in CD and LD.

4.1.4 Samples with a compression ratio, λ, of 1.7

The samples with compression ratio of 1.7 could be tested in CD, LD, CD2 and FD configurations. The results were plotted in two separate groups because of space constraints in the graph. The wear results are plotted in figures 4-9 and 4-10. The friction results are plotted in figures 4-11 and 4-12.

From figures 4-9 and 4-10, the channel-die compressed samples, like the standard, showed an increase in the wear rate after 29.62km. Their increase in wear rate was much higher than the standard's. For samples of λ of 1.7 in the FD, CD2, CD and LD orientations, the values were 178%, 135%, 45% and 65%, respectively. The initial wear rate was slightly higher in the channel-die compressed samples than in the standard, but not statistically significantly different. The final wear rate of 1.7

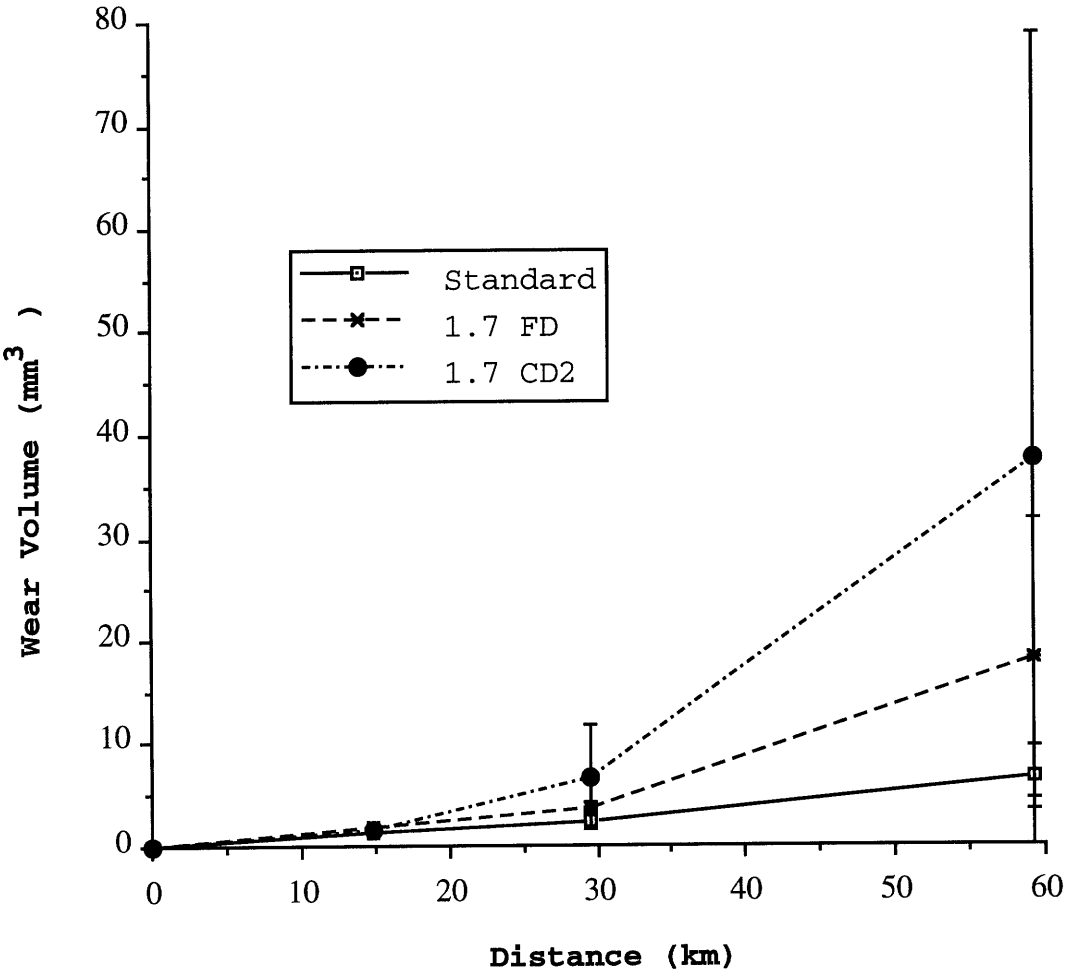

Figure 4-10: Wear of samples with λ of 1.7 in FD and CD2.

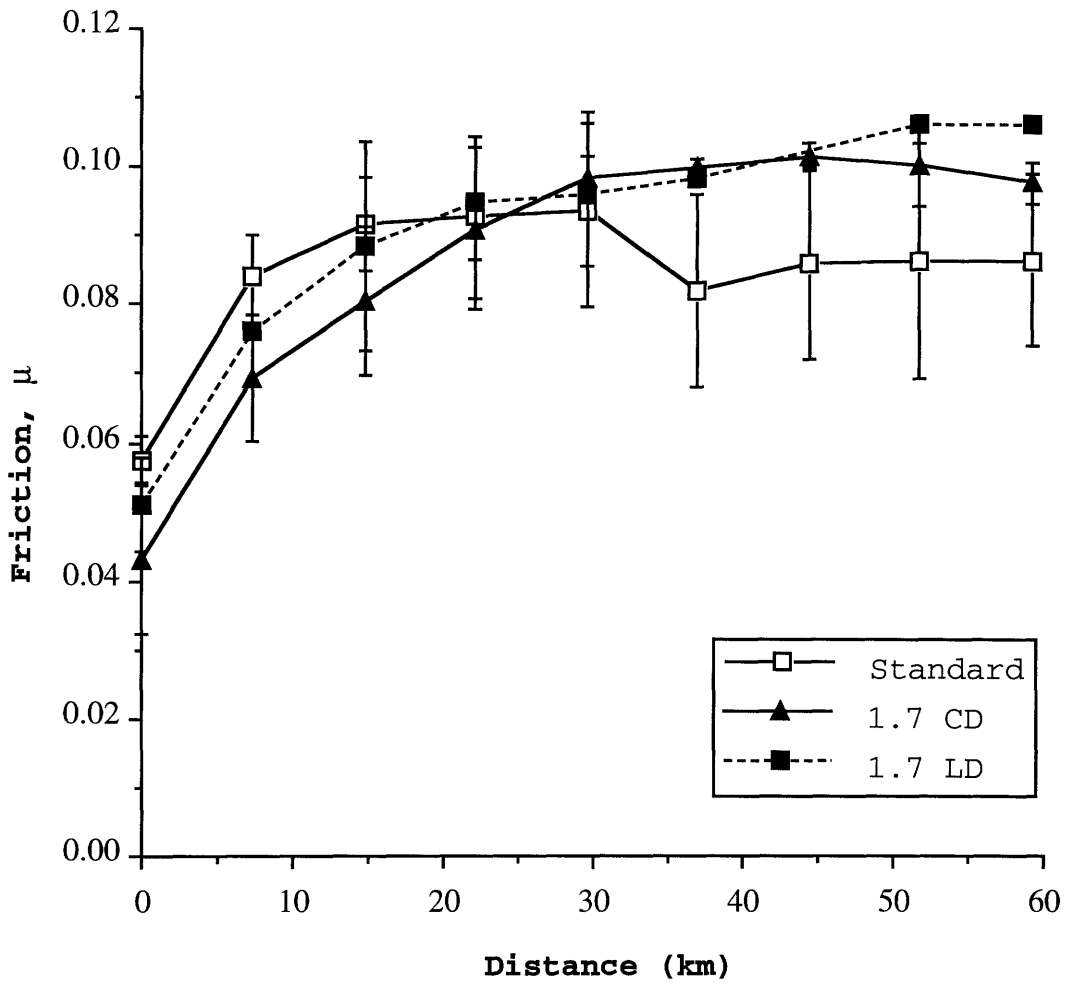

Figure 4-11: Friction of samples with λ of 1.7 in CD and LD.

CD2 and 1.7 FD showed a higher trend than the standard, but again showed did not show a statistically significant difference.

The average frictional values, figures 4-11 and 4-12, all started between 0.05-0.06, except for 1.7 CD which started between 0.04-0.05. In all cases it leveled off after 20km to values between 0.08-0.11.

4.1.5 Average Values of the Dimensional Wear Coefficient

The wear rate of UHMWPE did not behave in a linear fashion as can be seen in figures 4-1, 4-7, 4-9, and 4-10; it varied depending on the distance slid. Archard's

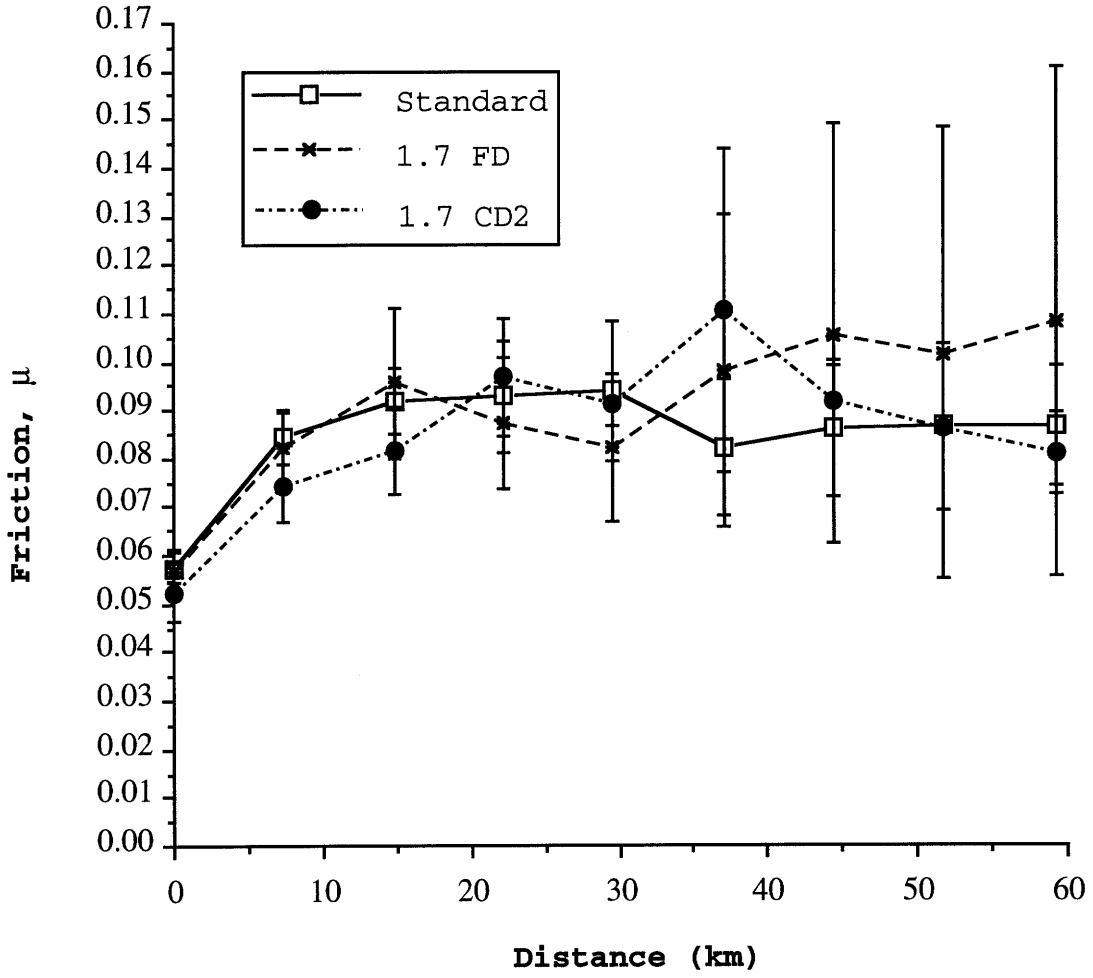

Figure 4-12: Friction of samples with λ of 1.7 in FD and CD2.

Distance Slid	14.81 (km)		29.62 (km)		59.24 (km)	
Sample	$\times 10^{-7}\frac{mm^3}{Nm}$	CV %	$\times 10^{-7}\frac{mm^3}{Nm}$	CV %	$\times 10^{-7}\frac{mm^3}{Nm}$	CV %
Standard Solid	1.07 ± 0.18	17.2	0.93 ± 0.12	13.0		
Standard Joined	0.97 ± 0.15	15.9	0.90 ± 0.13	14.2	1.25 ± 0.29	23.0
λ=2.75, CD	1.26 ± 0.35	27.7	1.40 ± 0.36	25.4	2.27 ± 1.23	54.4
λ=2.75, LD	0.90 ± 0.20	22.6	0.79 ± 0.24	30.7	1.10 ± 0.31	28.3
λ=1.7, CD	1.04 ± 0.15	30.3	1.28 ± 0.22	24.0	1.86 ± 0.68	72.1
λ=1.7, LD	0.77 ± 0.23	14.3	1.00 ± 0.24	16.9	1.65 ± 1.19	36.6
λ=1.7, FD	1.40 ± 0.15	11.0	1.46 ± 0.13	8.8	3.43 ± 2.57	74.9
λ=1.7, CD2	1.26 ± 0.16	13.0	2.56 ± 1.94	75.9	7.11 ± 7.87	110.6
MP-60	1.97 ± 0.21	10.5	1.97 ± 0.36	18.1	2.08 ± 0.26	12.3

Table 4.3: Dimensional wear coefficient and the coefficient of variance of each sample type.

Wear equation 4.1, however, was used for first approximation.

$$w = K\frac{W}{H} \tag{4.1}$$

As explained in chapter 1, the dimensional wear coefficient, k, was used as defined as 4.2.

$$k = \frac{V}{dW} = \frac{K}{H} \tag{4.2}$$

where V is the wear volume (mm^3), d is the distance slid (m), and W is the normal load (N).

The average values of the dimensional wear coefficient and its coefficient of variance are given in table 4.3 for the different sliding distances. The wear data for each individual sample can be found in appendix A. All the samples, except for the fiber oriented (MP-60), showed an increase in the wear rate after 29.62km. Also, from these values one observes that the coefficient of variance, CV, increased dramatically in the samples worn in the CD, FD and CD2 configuration after 29.62km. This was due to certain samples in the group showing a dramatic increase in their wear rate, appendix A, particularly a sample in the 1.7 FD group and a couple of samples in the 1.7 CD2 group. Though the general trend was for a higher wear rate.

Distance Slid	14.81 (km)	29.62 (km)	59.24 (km)
λ=2.75, CD	0.717	0.377	0.668
λ=2.75, LD	0.263	*0.085*	0.209
λ=1.7, CD	0.699	*0.086*	0.221
λ=1.7, LD	0.340	0.751	0.0628
λ=1.7, FD	0.127	*0.008*	0.196
λ=1.7, CD2	0.498	0.198	0.234

Table 4.4: P values comparing the dimensional wear coefficients of the standard with the oriented samples.

4.2 Statistical Analysis of Wear Coefficients

The dimensional wear coefficients of the compressed oriented samples were compared to the standard joined samples using the student t-test. The P values were obtained for a two-tailed test with a level of significance, α, of 0.05 following the procedure outlined in chapter 3. These P values are given in table 4.4. Only three of the P values reported were below 0.10 and they are highlighted in italics. These three cases were for sliding distance of 29.62km, and they are λ of 2.75 LD, 1.7 CD and FD. In all cases the P value took a value of approximately 0.20 at longer sliding distance (59.24km). It was concluded that statistically there was no significant difference.

4.3 The Final State of the Co-Cr Counterface

At the end of the eight days wear test the Co-Cr counterfaces were examined visually. A transfer film of UHMWPE could be observed on the samples worn where saline solution was the lubricant. In the case where bovine serum was the lubricant no transfer film was formed.

The roughness of the counterface at the end of the eight days test was measured in certain samples to observe whether there was significant roughening of the counterface. Two traces were taken of the worn surface. If there is a significant roughening it would have a strong effect on the wear rate of the UHMWPE if the test were prolonged. These measurements are listed in table 4.5, and can be compared with the

Sample	$Ra_1(\mu m)$	$Ra_2(\mu m)$	Average(μm)
MP-60_1	0.600	0.115	0.358
MP-60_2	0.0249	-	0.0249
MP-60_3	0.0412	0.0403	0.0408
MP-58_1	0.101	0.181	0.141
MP-56_1	0.0653	0.0813	0.0733
λ=1.7 LD	0.135	0.0713	0.103
λ=1.7 FD	0.0541	0.180	0.117
λ=1.7 CD	0.0416	0.0403	0.0410
λ=1.7 CD	0.0432	0.0422	0.0427

Table 4.5: Final roughness values of Co-Cr cylinders after 59.24km of sliding.

initial value of $0.0265 \pm 0.0015 \mu m$.

4.4 SEM Images of the Worn Surface

Images of the unworn section (the fly cut surface) were taken as a reference to gage reproducibility. Also, to observe whether the machining marks were eliminated by the wearing action, figures 4-13 and 4-14. As stated in chapter 3, the samples were fly cut at a spindle speed of 1400rpm and a feed rate of 0.01905m/min (0.75in/min). From this information the distance between each groove, l, is calculated as in 4.3.

$$l = \frac{0.01905}{1400} = 13.6 \mu m \tag{4.3}$$

From the SEM pictures of the unworn regions a approximate measurement of the distance between machining marks was between approximately 15-18μm. These values are reasonably close to that calculated in 4.3, and demonstrate the initial topography of the surface of the sample.

The surfaces of the worn samples were first viewed under an optical microscope to look for any salient features. The topography of the surface was mainly scratched along the wear direction, and there were no distinguishing features between the samples. A picture was taken with the SEM at an optical microscope magnification was

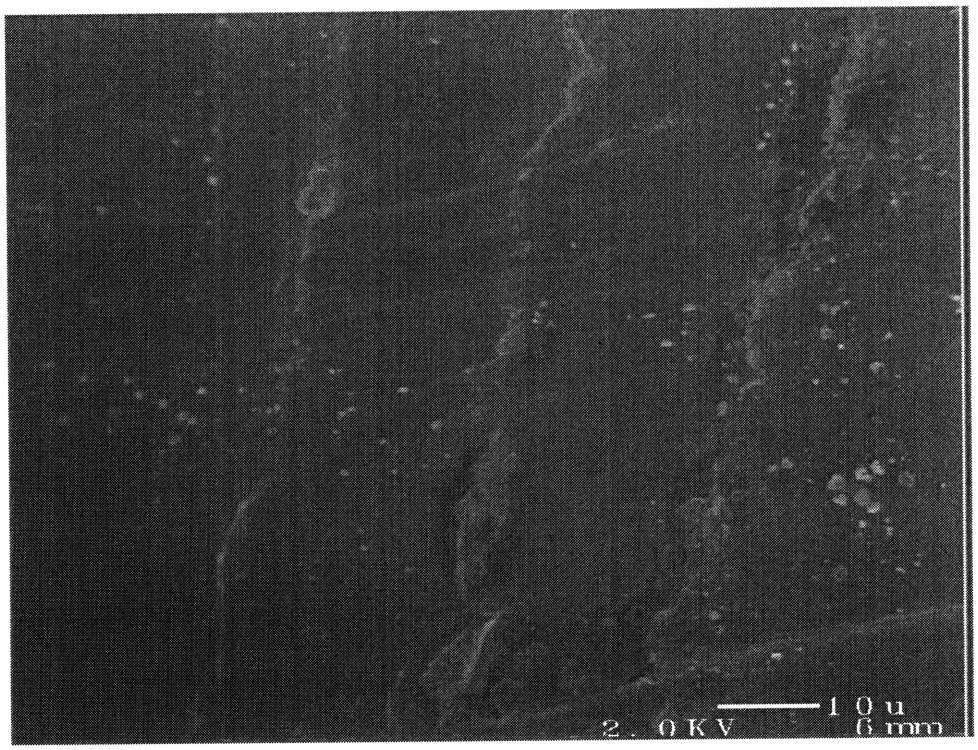

Figure 4-13: Fly cut view at 1000x of unworn section of a standard sample. The sample was coated.

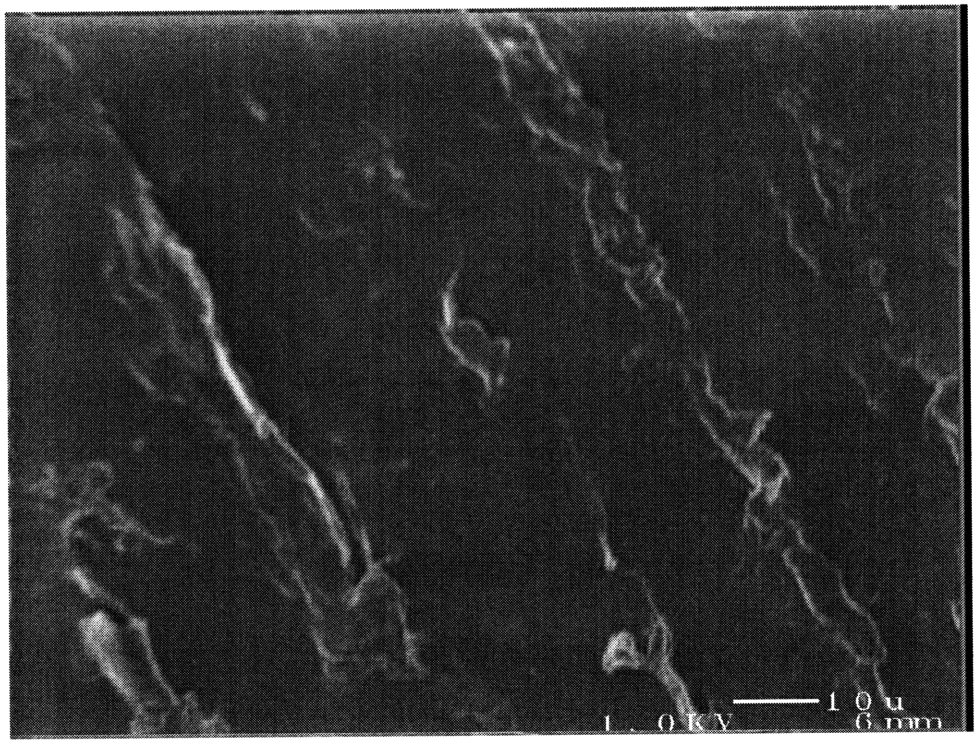

Figure 4-14: Fly cut view of sample with λ=2.75 LD at 1000x.

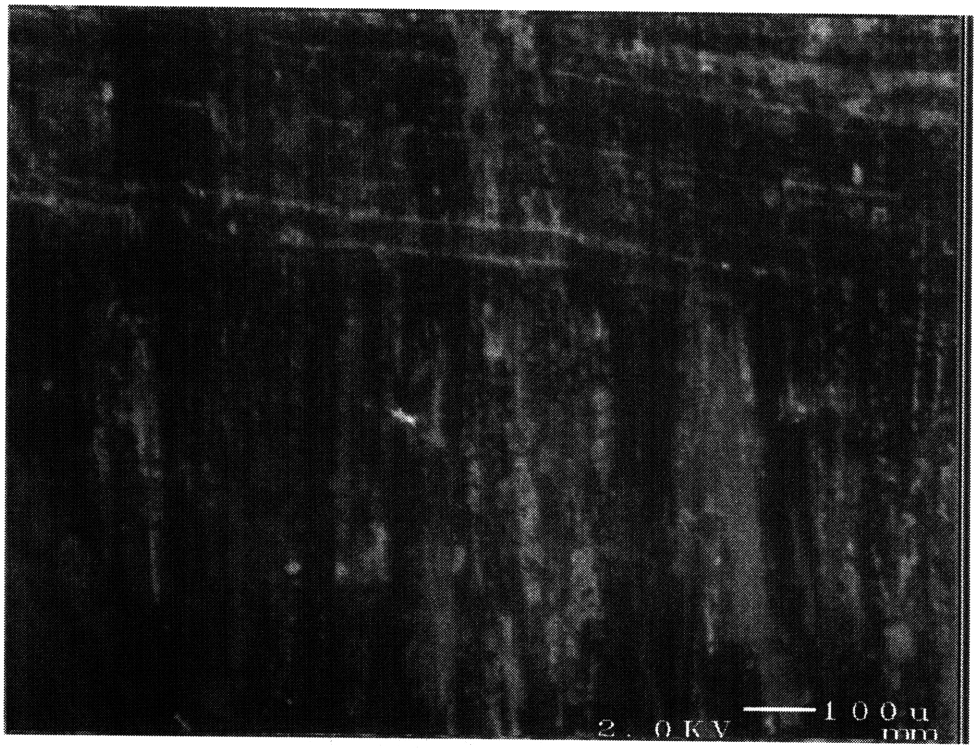

Figure 4-15: Image of the end of the travel of the wear track at 130x of a standard coated sample. The sliding direction is vertical.

take, fig. 4-15. All samples had this topography at the end of the wear test, mainly a scratched surface along the sliding direction. The scratch perpendicular was a remnant from the fly cutting, which was not observed under optical microscope in other samples.

Micrographs of the worn surface of the standard joined samples and the channel-die compressed samples were taken at the middle of the wear travel and at the end of the wear travel. The majority of these images were taken at 2700x and 5000x magnification. The sliding direction in all these images is horizontal. Some of the representative images are in this chapter, the remaining are in appendix C, D, and E.

4.4.1 Images of standard UHMWPE samples

Two different samples of worn standard UHMWPE samples were scanned under the SEM. One of them was gold coated, and scanned at 15kV. The other sample was not coated, and it was scanned at 1kV with a working distance of 6mm. There were no notable differences observed in the quality of the images. The features observed

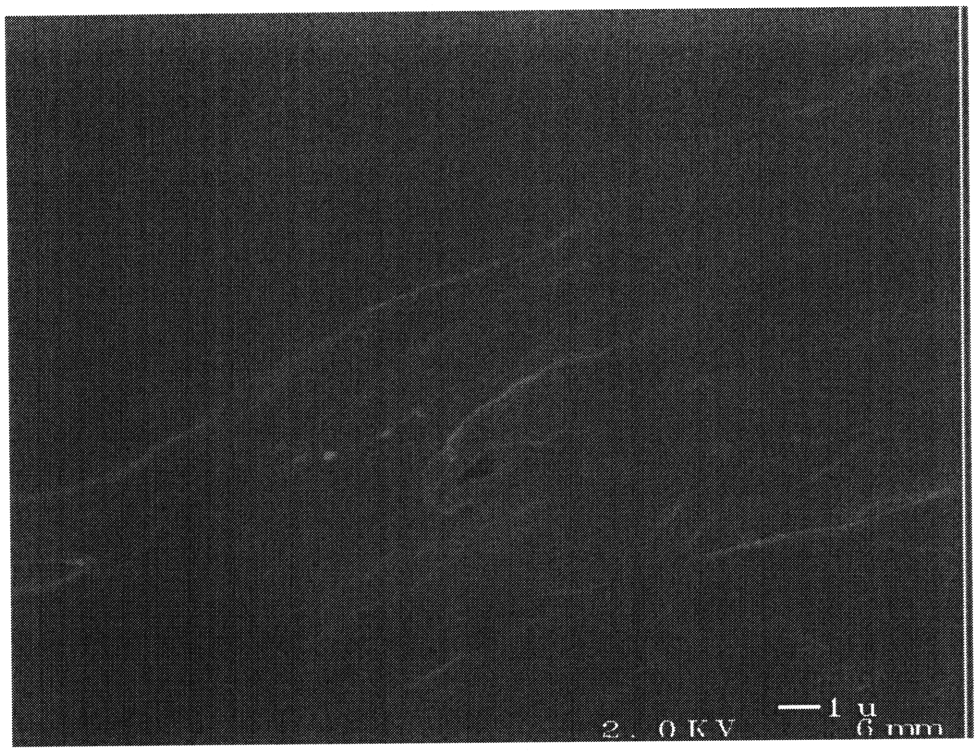

Figure 4-16: Image of the middle of the wear track at 5000x of a standard coated sample.

in both cases were similar. Throughout the whole wear track there were scratches along the sliding direction. The standard sample showed many features toward the end of the wear travel, but in the middle of the wear track the surface was smooth and featureless, fig. 4-16.

At the end of the wear track the most striking feature was a wave like pattern heading toward the end of the travel. The closer toward the end of the wear track the more prominent it became, figures 4-17, 4-18 and 4-19. This wave like pattern was not due to the remnant of the fly cutting because the distance between each was less than 5μm, considerably less than that from the fly cutting.

4.4.2 Images of λ=1.7 FD

Two images are shown in this chapter, figures 4-21 and 4-20. Compared to the other UHMWPE samples scanned, the surface of this sample was featureless (consequently hard to focus). The most salient aspect was the thin scratches that covered the whole wear track, fig. 4-20.

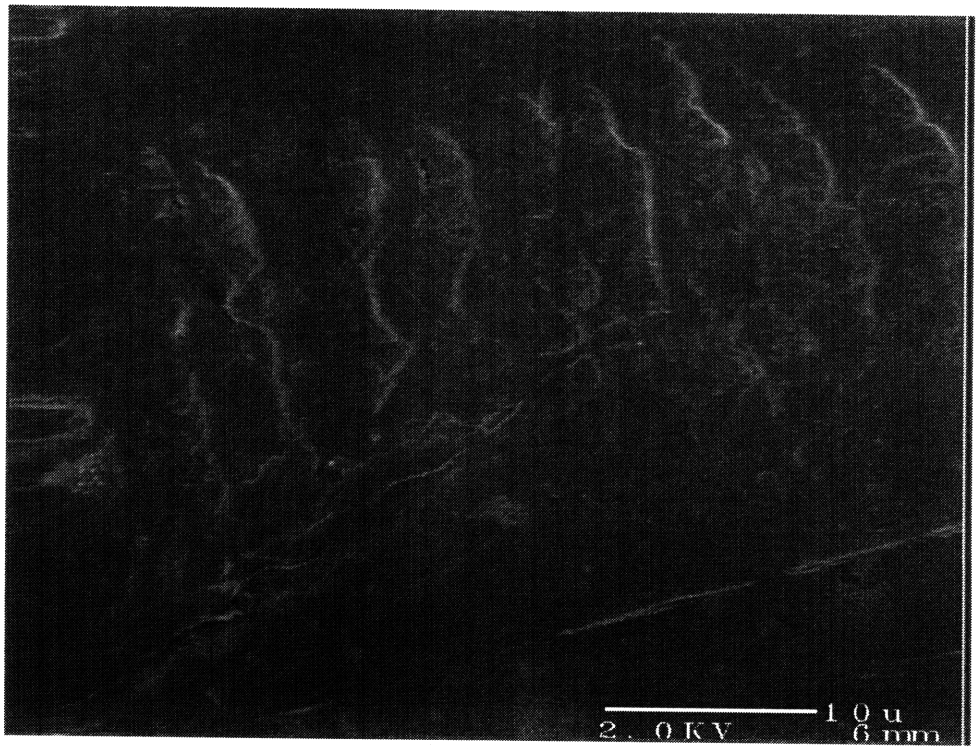

Figure 4-17: Image of the end of the travel of the wear track at 2700x of a standard coated sample.

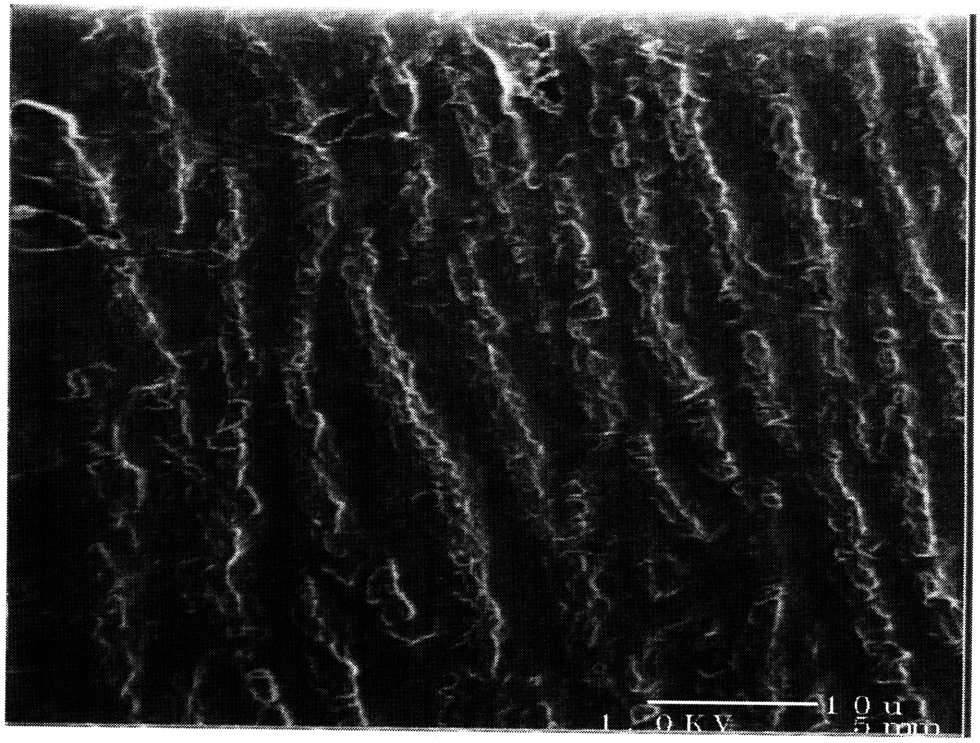

Figure 4-18: Image of the end of the travel of the wear track at 2700x of a standard uncoated sample.

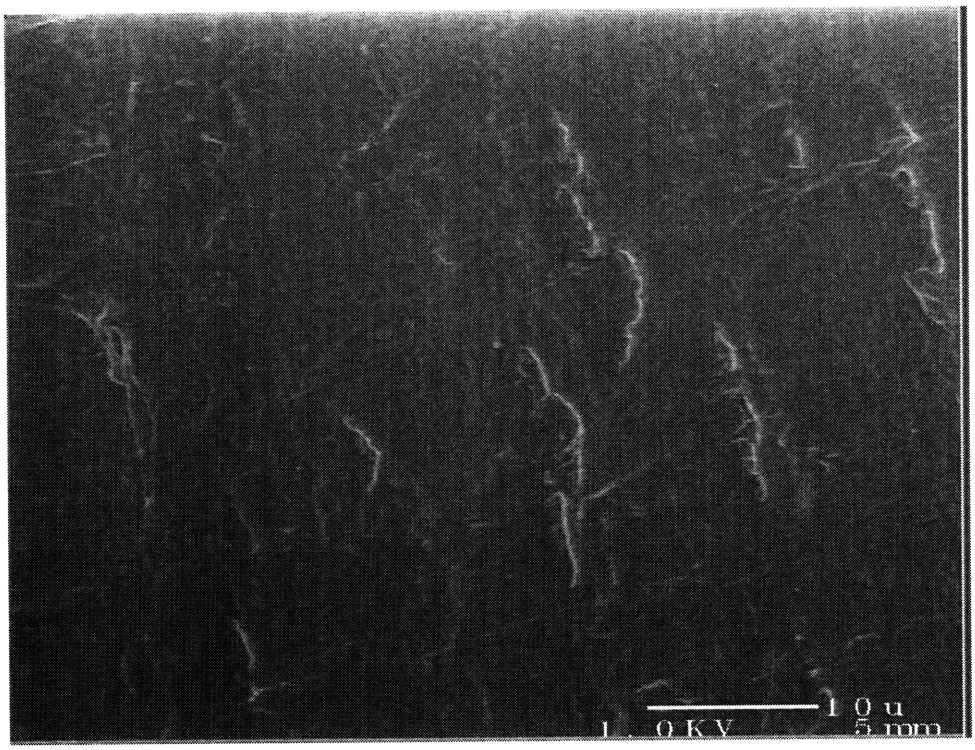

Figure 4-19: Image of near the end of the travel of the wear track at 2700x of a standard uncoated sample.

Figure 4-20: Image of the middle of the wear track at 2700x for λ=1.7 FD.

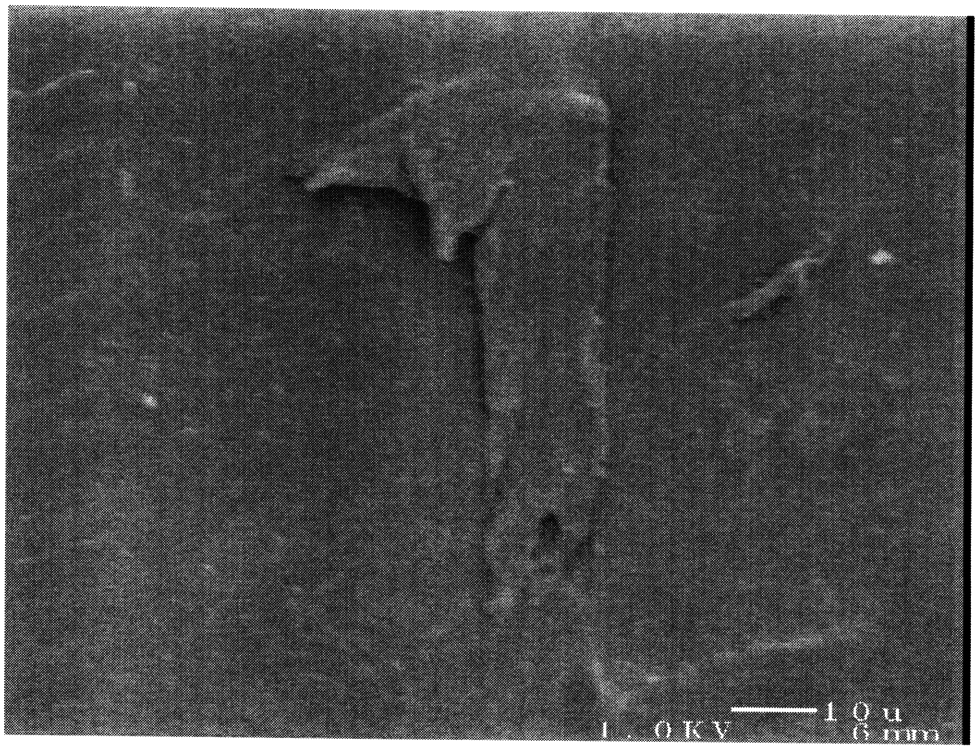

Figure 4-21: Image of the end of the travel of the wear track at 1100x for λ=1.7 FD.

There did not seem to be any accumulation of UHMWPE at the end of the track. There was no formation of a wave like pattern as observed in the standard. There was a chip found that was attached to the surface, but otherwise the surface was featureless, fig. 4-21.

4.4.3 Images of λ=1.7 CD2

The surface of a worn sample of the 1.7 CD2 was scanned. The features observed were similar to the standard's. In the middle of the wear track there were few features, fig. 4-22, and toward the end of the wear track the wave like pattern become prevalent, and had the same pattern as in the standard, fig. 4-23.

4.4.4 Images of λ=2.75 LD

The surface of a worn sample of the 2.75 LD was scanned. In the middle of the wear track there were few features, fig. 4-24. A few large scratches of approximate 4μm in width and micro-scratches of approximately 1μm in width could be seen. Toward the

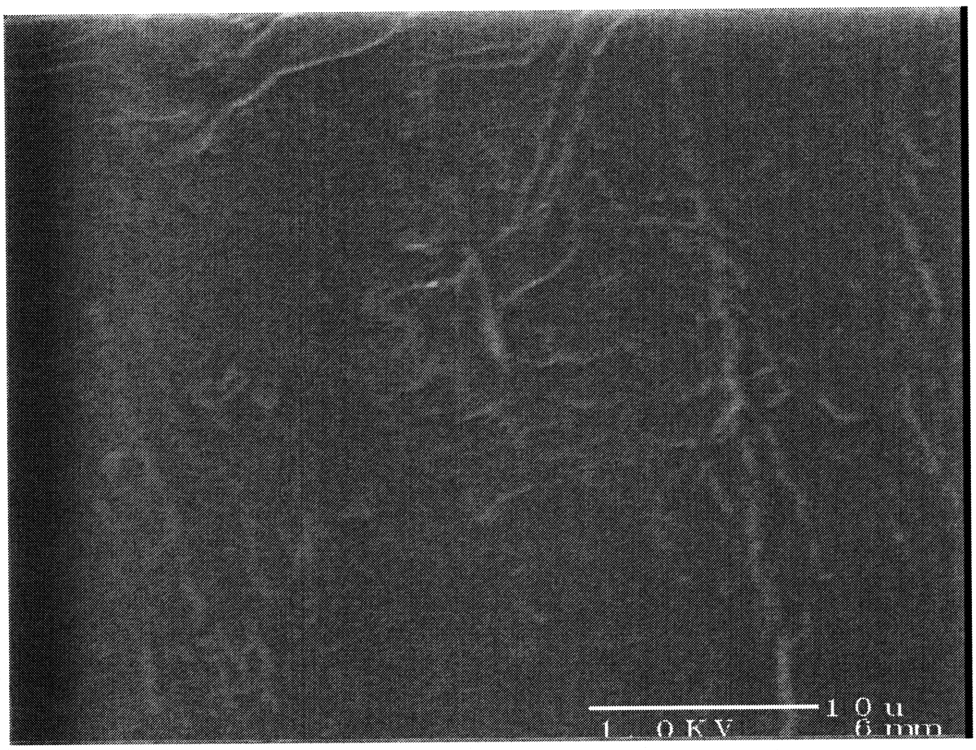

Figure 4-22: Image of the middle of the wear track at 2700x for λ=1.7 CD2.

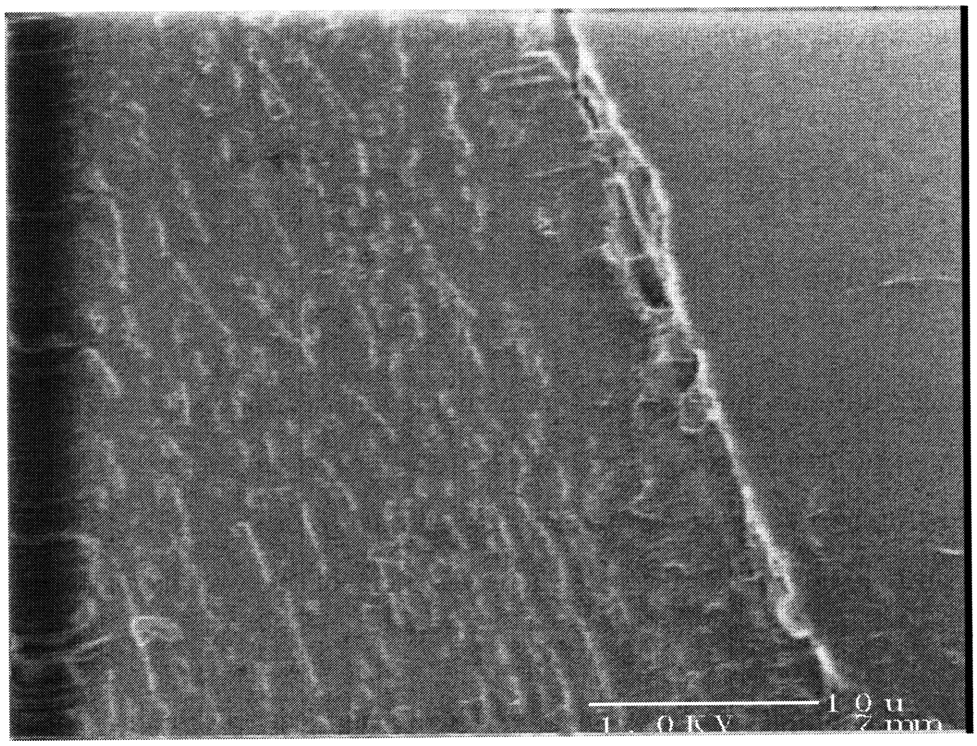

Figure 4-23: Image of the end of the travel of the wear track at 2700x for λ=1.7 CD2.

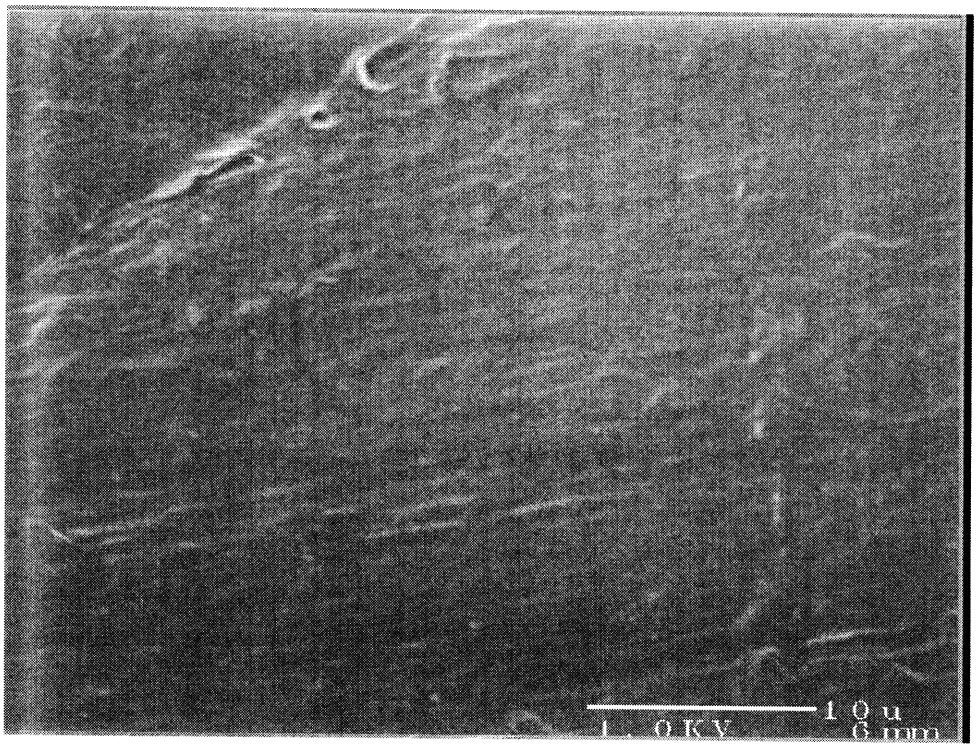

Figure 4-24: Image of the middle of the wear track at 2700x for λ=2.75 LD.

end of the wear track there was what appeared to be a smearing of the UHMWPE, and some wavelike pattern as in the standard, fig. 4-25.

4.4.5 Images of λ=2.75 CD

Two images are shown in this chapter. As in previous samples, the middle of the worn region was featureless, except for some scratches or plowing from the Co-Cr cylinder, fig. 4-26. At the end of the wear track there seemed to be smearing of the UHMWPE on the surface and some scratches. There were none of the wavelike patterns observed in the standard, fig. 4-27.

One of the samples being worn cracked along the wear track and perpendicular to the wear surface. The crack length was of 15mm and the crack depth of approximately 1mm. A SEM image of the crack was taken, fig. 4-28.

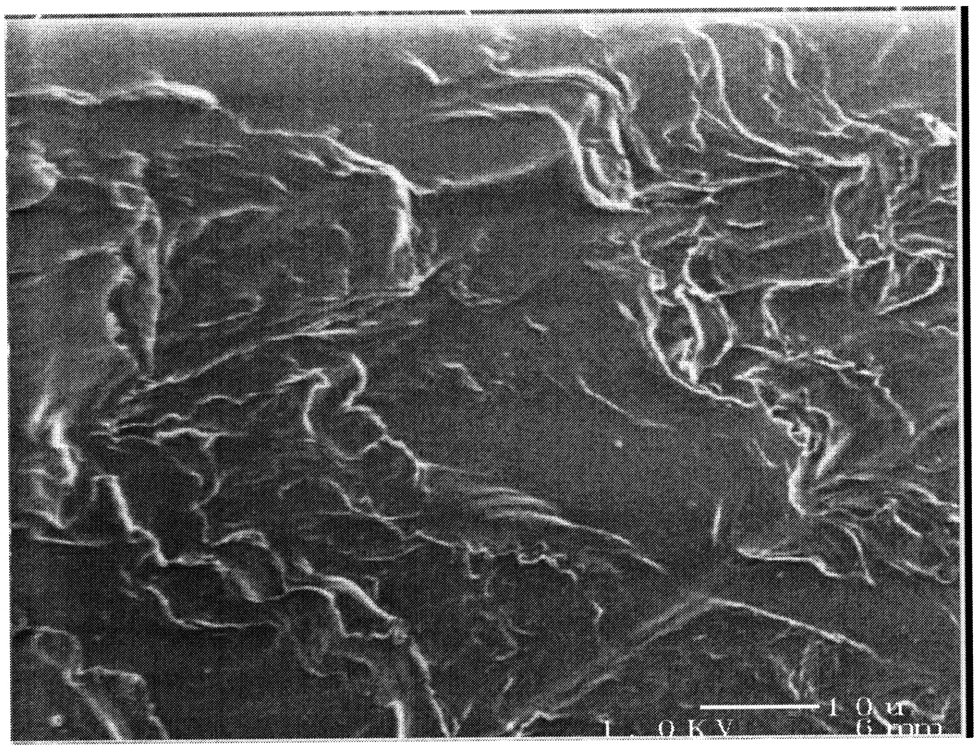

Figure 4-25: Image of the interface at the end of the travel of the wear track and the unworn surface. The magnification is of 1400x for a sample λ=2.75 LD.

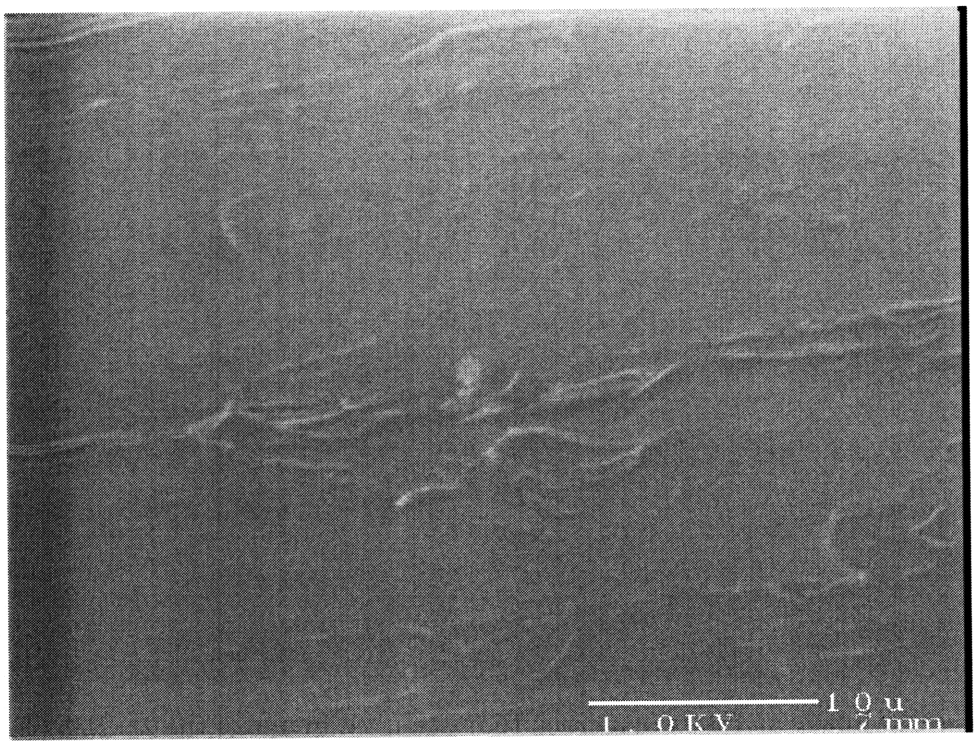

Figure 4-26: Image of the middle of the wear track at 2700x for λ=2.75 CD.

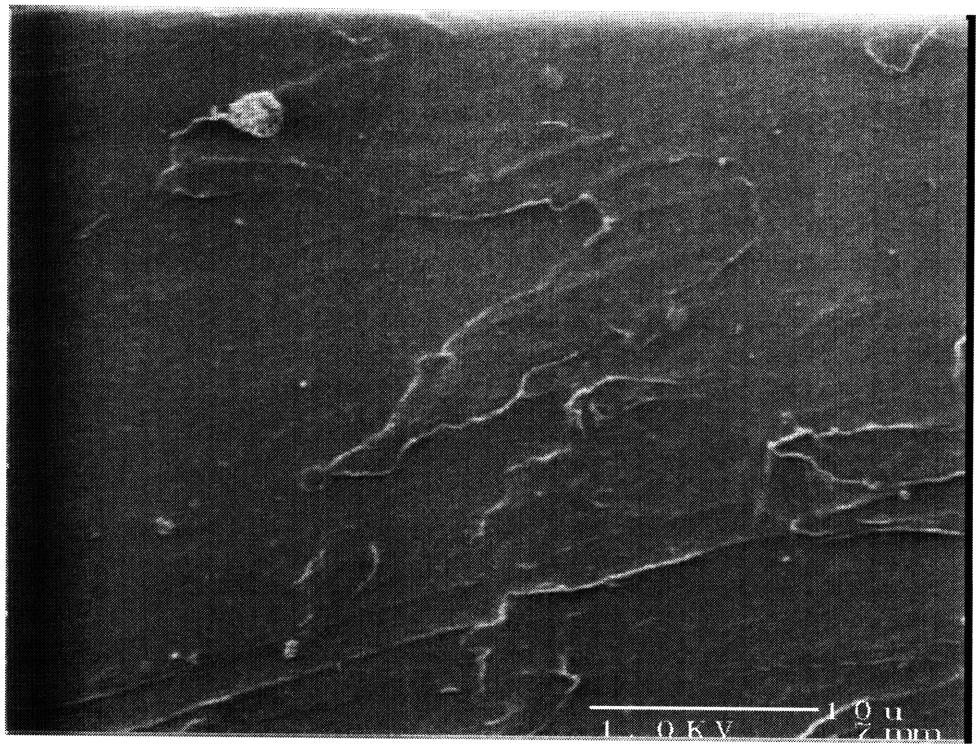

Figure 4-27: Image of the end of the travel of the wear track at 2700x for λ=2.75 CD.

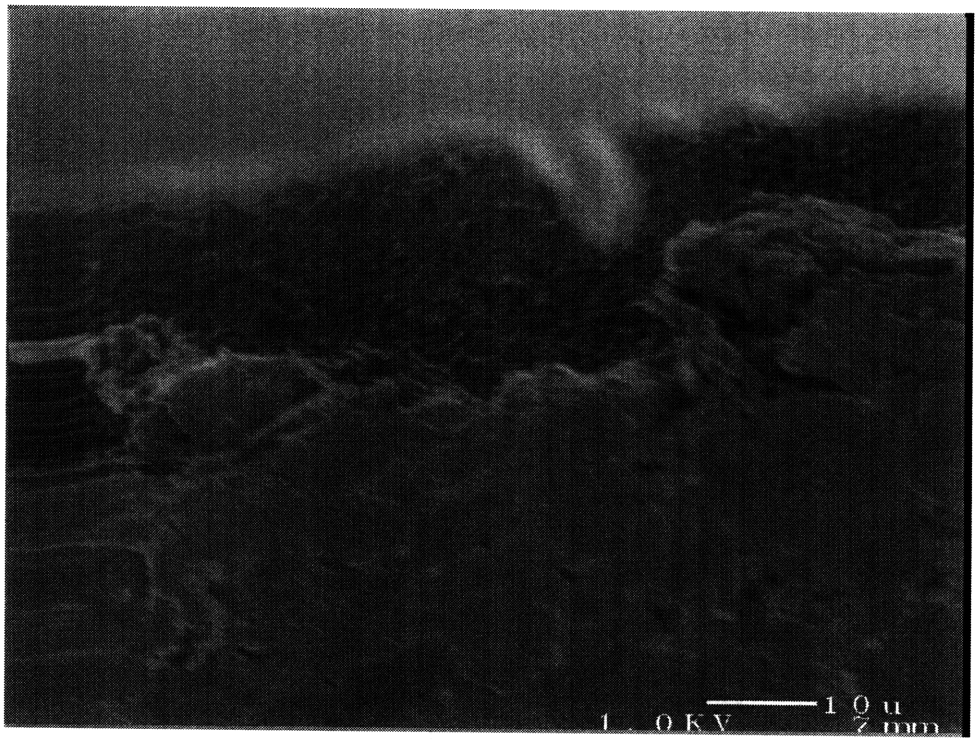

Figure 4-28: Image at 1300x of a crack that occurred in one of the λ=2.75 CD sample. The crack is normal to the surface and along the wear track. Its located at the edge of the wear track.

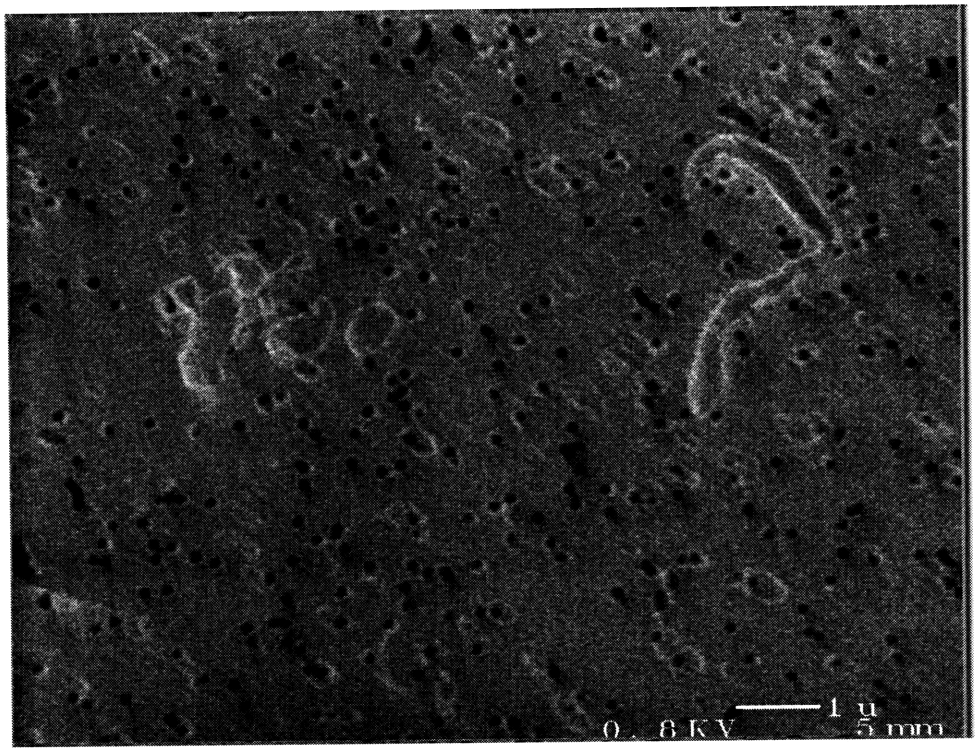

Figure 4-29: Wear debris from sample with λ of 2.75 CD, at 10000x.

4.5 SEM Images of the Wear Debris

SEM images were taken of the debris from the bovine serum collected at the end of the wear for each of the channel-die compressed samples and the standard. The wear debris of all the samples looked similar in size and shape. They were either fibrillar or spheroid in shape. Their size ranged approximately from 3 microns to 0.5 microns. The following figures show some representative images, figures 4-29, 4-30 and 4-31. The remaining images are in appendix F.

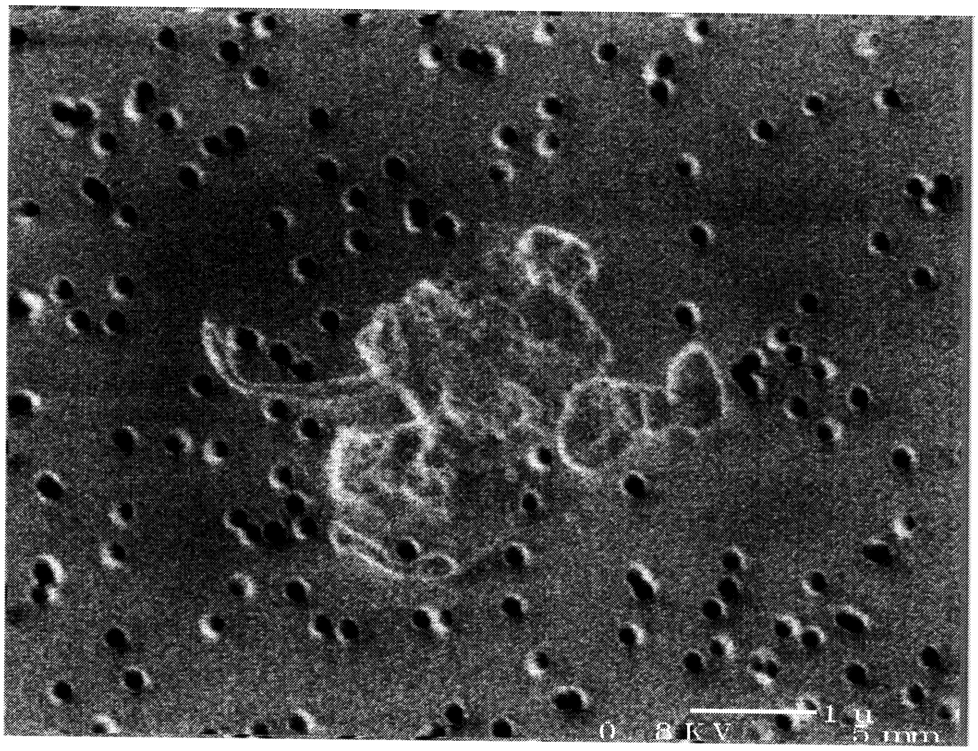

Figure 4-30: Wear debris from sample with λ of 1.7 FD, at 15000x.

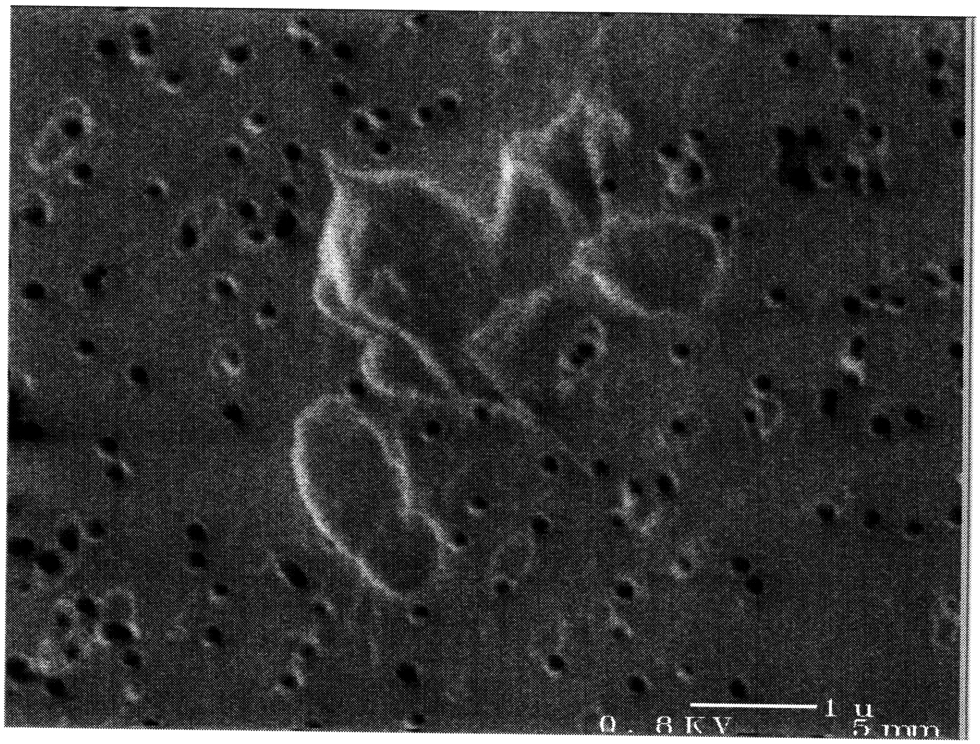

Figure 4-31: Wear debris from sample with λ of 1.7 CD2, at 15000x.

Chapter 5

Discussion

As stated in section 4.1.1, the wear rate of the standard in a solid block and the standard joined were found to be statistically the same, approximately $1.0 \times 10^{-7} mm^3/Nm$. The frictional values were also similar, leveling off at values between 0.08-0.10. These values are similar to those reported in the literature, [17, 18, 19, 49]. Based on this data it was concluded that joining the samples for the wear test did not strongly affect its wear properties. Thus, validating the experimental setup.

There was no evidence from the SEM micrographs and optical microscopy of delamination wear and subsurface cracking taking place in the standard UHMWPE. Also, the wear debris collected and viewed under the SEM was similar in size and morphology to those reported in other studies, [37, 47, 51].

5.1 Fiber Oriented Samples

The premature failure of MP-56 and MP-58 precluded their extensive evaluation. The wear of this material in the orientation tested, and conditions tested was significantly higher than the standard. Examination of the failed samples revealed what appeared to be debonding of the fiber from the bulk polyethylene, indicating that failure took place at the interface. The woven material was in the form of layers parallel to the worn surface. The plastic strain most likely accumulated at a certain depth, between plies of the material, causing the eventual shearing of the top layer. The MP-60

samples were able to complete the wear test without undergoing catastrophic failure, but other problems were encountered in measuring the mass loss.

The fiber oriented samples had a relatively high void content, approximately 10%. This high void content made it difficult to obtain a reliable measurement of mass loss, even though the samples were soaked for more than a month. The fibers of the woven material had a crystallinity of 99-98% which made them impermeable to water, thus, the woven layer would not allow the water to reach the inner voids and pockets of amorphous polyethylene of the sample easily. But once the wear test was begun the fibers were rearranged and the water could reach these areas. This unaccounted water absorption caused an underestimation of the mass loss. In one of the three samples tested there was so much water absorption that negative mass loss was recorded, even though, there was visible surface damage. This data point was not included in fig. 4-5.

From visual examination of the worn MP-60 samples it was concluded that the material being removed was only the melted unoriented UHMWPE, and that the Co-Cr cylinder had not worn into the woven layers. Thus it was no surprise that the wear rate was of the same order of magnitude as the standard, though slightly higher in value. The mass loss was later converted to volume loss using the density of the standard UHMWPE.

For this material friction and wear appeared to increase concurrently. The friction data were within the range of that reported for UHMWPE sliding against Co-Cr, [49, 25]. The average frictional values remained constant throughout the duration of the test, unlike the standard and channel die compressed samples. This behavior was reflected in the approximately constant wear rate. However, it is likely that once the melted surface layer has been worn off, the sample will fail in a similar fashion as the MP-56 and MP-58 samples.

The higher wear rate for samples with fibers oriented parallel to the surface, likely due to poor bonding of the fibers and the bulk matrix, has been reported previously by Sung and Suh [24] for fibers and matrix of different materials. Based on the data provided by the supplier of this homocomposite it was hypothesized that the bonding

was stronger, but the wear test disproved this.

The fiber oriented material was not tested on the surface with the fibers normal to it. A recent publication has shown a lower wear rate in a homocomposite tested on the surface with the fibers normal to it, [25]. It was not possible to test this configuration in this thesis because of the lack of samples with the appropriate dimensions for the wear test.

The potential risk for catastrophic failure of the MP-60 coupled with the fact that the wear rate was found to be of the same order of magnitude as the standard sample, leads the author to believe that it would be a poor choice as a tibial bearing material if used at the orientation tested.

5.2 Channel Die Oriented Samples

The length of the wear test was such that enough debris was produced to be consider detrimental in the body. The average wear after 14.81km was of at least $1mm^3$. From the particle size observed in the SEM images, and from the literature [37], it was a conservative estimate to assume that the average wear particle size was of $1\mu m$ in diameter. Therefore, the average volume was of approximately $4 \times 10^{-18}m^3$. From this information we could estimate the number of particles produced as 250 million, which could cause adverse reaction from the body.

The surface tested of all the channel die compressed samples and the standard sample were fly cut prior to testing. The material removed through fly cutting was enough that to ensure that the surface being tested was the one that possessed the properties of the bulk material. The effect that the fly cutting may have on the texture of the UHMWPE on the surface was not known. Another reason for fly cutting all the samples uniformly was because the initial roughness is generally removed during the run-in period. Generally this removal occurs through abrasive wear and plastic deformation of the surface, and the length of the run-in period depends mainly on the initial topography of the surface. Therefore, the surfaces were fly cut to the smoothest possible surface, Ra of $1\mu m$.

The samples were visually inspected each time they were removed from the wear tester for mass loss measurement. On the worn surface after 14.81km of sliding some remnants of the machining marks could be observed. After 29.62km machining marks were no longer found. Therefore, the end of the run-in period when the worn surface had become conformal, probably occurred between these two sliding distances.

The average initial frictional value for the compressed and the standard UHMWPE sample was 0.05-0.06, except for 1.7 CD which had an average initial value 0.043. Average frictional values for all the compressed and standard samples leveled off between the 15-20km of sliding to an that ranged from 0.08 to 0.11. These values were similar to others reported in the literature, [25, 49]. The sliding distance at which the frictional values plateau was consistent with the estimated point at which the end of the run in period occurred, where there would be a larger contact surface and other wear mechanisms, such as adhesive and delamination wear, may have begun to play a greater role.

The average wear rate of the standard and the compressed samples changed after 29.62km of sliding. There was an increase in the wear rate by at least 20%. Again the change in wear rate was consistent with the earlier leveling off of the frictional value and removal of the machining marks. Most likely, the run-in period which was generally characterized by abrasive wear, had a lower wear and friction because there was less contact area. But once the run in period ended and the contacting surfaces became more conformal, the wear rate and friction increased.

The particles comprising the wear debris obtained between 29.62 and 59.42km of sliding were similar in size and shape to those reported in the literature [37, 47]. This type of particle was generally attributed to abrasive wear. The SEM images of the worn surfaces of the samples did not reveal any evidence of cracking or surface fatigue that could induce delamination wear. Therefore, we could conclude that the main wear mechanism within the sliding distance tested was abrasive wear.

There was no statistical significant difference in the wear rate of the compressed samples and the standard within the distance tested. Polyethylene is a considerably softer material than Co-Cr, and any change in surface hardness of the oriented

UHMWPE would be minimal compared to the difference in hardness between the UHMWPE and the Co-Cr. Therefore, regardless of the orientation of the UHMWPE the asperities of the Co-Cr could easily plow through the material. Evidence of this could be found in the SEM images of the worn surface, all had similar grooves in the middle of the wear track, and the wear debris was similar in morphology. It could be concluded from this data that within the abrasive wear regime, the channel die molecular orientation does not affect the wear rate.

The wear rate and debris morphology suggest that, within the distance tested, the primary wear mechanism was abrasive wear, and this evidence could suggest that all the samples regardless of treatment would continue to behave similarly with longer sliding distance. But from the SEM images of the worn surface, differences could be found in the surface topography at the end of the travel in the wear track. It is in this area where the majority of the plastic strain would accumulate and folds of the surface of the sample might get smeared. Therefore, it is an indication of whether the materials were undergoing the same degree of plastic strain and surface deformation that could, in longer sliding distances, develop into delamination wear.

The surface of the standard sample was similar to that reported by others [10, 18], a wavy pattern which was probably due to the accumulation of plastic strain, and the middle of the wear track the main surface feature were the scratches from the Co-Cr. The topography of the middle of the sample was similar in all the samples scanned, the main surface feature were the scratches from the Co-Cr cylinder. But at the end of the wear travel the topography was different depending on the sample. The 2.75 LD and 1.7 CD2 showed a similar behavior as the standard with a wavy pattern that is probably due to the accumulation of plastic strain and UHMWPE particles that had still not broken off the bulk. The 1.7 FD and 2.75 CD had a different surface topography. For the 1.7 FD the topography of the end of the wear track was similar to that of the middle of the worn region, there did not seem to be any accumulation of plastic deformation or chips smeared onto the surface. For the 2.75 CD sample the end of the wear travel seem to have some smeared UHMWPE on it, but no wavy pattern that would indicate large accumulation of plastic strain.

The roughness of the Co-Cr cylinder was measured at the end of wear test for some samples. It reveal that there was a wide variability of the final Ra, ranged from approximately 0.03 to 0.35μm. There was not enough data collected to determine whether there were material factors the Co-Cr roughening was dependent on, but there was a general trend toward the roughening of the counterface.

The progressive roughening of the counterface would have an impact on the wear rate as the sliding distance is lengthen. If the Co-Cr cylinder become considerably rougher (over 0.05μm) the primary mode of wear could continue on being abrasive wear. If the Co-Cr cylinder remains smooth (Ra of 0.03μm) the difference in surface topography may indicate that if the wear test were prolonged there might be differences in wear found that could not be revealed in the sliding distance used in this thesis.

Chapter 6

Shortcomings of the Experimental Procedure

6.1 The Specimen

The specimens produced through the channel die compression were not ideal for the size required in the wear tester. The degree of molecular orientation varied throughout the specimen [31]. This was particularly true for the samples with low compression ratio (*i.e.*, λ=1.7). By visual inspection the isotropic UHMWPE was white and opaque in appearance, while the anisotropic UHMWPE was more translucent. The larger samples (1.05x4x7.65cm), from which the FD, CD, and CD2 samples were taken, demonstrated that the samples molecular orientation was not uniform. In these larger samples there were areas that were translucent and others that were opaque as in fig. 6-1. The samples for wear testing were generally taken from the middle of one of the halves of the compressed sample.

In the current study it was not possible to achieve as high a compression ratio as desired because of constraints of the channel die apparatus. Therefore, the effect of texturization of UHMWPE on its wear performance could not definitively be determined.

Another factor to be taken into account was that the samples had to be clamped together so that they could be mounted in the wear tester. By clamping the samples,

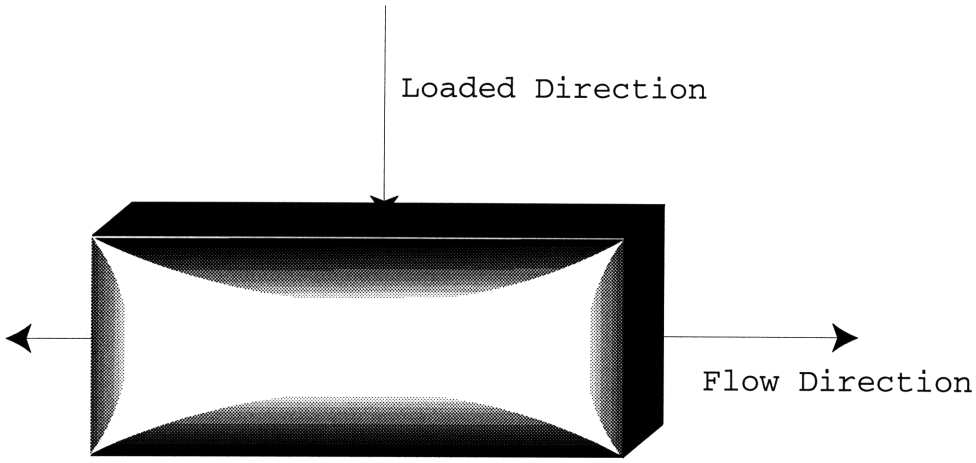

Figure 6-1: UHMWPE sample compressed to λ=1.7.

stresses were created parallel to the surface to be tested. The effect of these stresses on the wear behavior could not be assessed. Also, the smaller size sample made it impossible to maintain a zero strain condition on the surface that was clamped. This impossibility could either enhance or arrest cold flow of the sample; in either case it would not accurately reflect the deformation the surface of the sample could undergo and its effect on the wear rate.

The specimen, after over a million cycles in the wear tester, only wore off approximately 0.02mm in depth. It has not been determined how deep an effect, if any, the fly cutting process had on the orientation of the molecules and crystallites on the surface. Therefore, we could not be certain whether the results we were observing were due to the texturing of the sample or some effect brought about from the fly cutting.

6.2 The Wear Tester

There were several shortcomings of the wear tester. Some have an impact on the accuracy of the wear test, others are related to user ease. The wear tester had accurate strain gages, but the data acquisition system was suboptimal. For purposes of this thesis a chart recorder was used to collect the normal and tangential load acting

on the cylinder. From directly measuring this data on the chart recorder, the friction coefficient, μ was calculated. These data could not be collected continuously with a computer and μ calculated directly without room for human error. With continuos friction measurements comparison of the behavior of the different samples could have been performed more readily.

From the data obtained from the chart recorder it was also obvious that the normal load that was rated as being applied was not the true normal load. The load that was rated was of 1067.52N (240lb.), but if all three pneumatic pistons were used simultaneously, as in a typical wear test, the output load was approximately 889.6N (200lb.). Also, the pneumatic pistons were not very accurate and the applied load generally fluctuated by $\pm$88.96N (20lb.).

The components of the wear tester were not sufficiently robust for extended testing. The component that produces the reciprocating motion, the ball reverser, given the loads its subjected to, has an approximate life of 41,472,000 cycles. Polyethylene has different wear regimes depending on the length scale of the test [1, 21]. For delamination wear, the higher the number of cycles the more dominant it would be. If the ideal 10 million cycle test were made the ball reverser would fail after 4 tests. Another factor limiting the test protocol was time; a 10 million cycle test would have taken approximately 80 days. For the number of tests that were conducted it would have been beyond the time given for thesis work.

To circumvent the time scale problem, the wear test could be accelerated. A study by Barret, *et al.* [16], in dry sliding against stainless steel, showed that the wear rate was not strongly affected by sliding speeds up to 5m/sec, about 60 times faster than the sliding speed used in this thesis. A similar study conducted by Fisher, *et al.* [15], with a tri-pin on disc apparatus in bovine serum, showed that sliding velocity had little effect on wear. Their tests were carried out using speeds of 0.035m/sec and 0.240m/sec. The wear test might then be accelerated without loosing its experimental value. It would, however, be necessary to consider how the frictional heating at these higher speeds affects the denaturing of the bovine serum.

The receptacle for the sample and lubricant was such that it would not allow for

replenishment of the lubricant without stopping and dismantling the wear test apparatus. Also, the receptacle was not large enough to allow for re-circulation of the lubricant to dissipate frictional heating and maintain the lubricant at room temperature. Another issue was that because the reservoir for bovine serum was so small, after 4 days when it was renewed, the majority of the bovine serum was denatured. Water evaporation was also taking place. In order to solve this problem, a drip mechanism was used to replenish the lost water, using a intra-venous drip controller. Unfortunately, it is not a very precise mechanism, and therefore a constant bovine serum concentration could not be maintained.

The receptacles that contained the samples and bovine serum were exposed to several components of the wear test apparatus from which particulate debris might have been released. Hard metallic particles from components of the wear tester could have contaminated the wear test. These particles could have roughened the Co-Cr counterface, and this would have increased the wear rate.

In the interest of time, the wear tests were run such that wear data could be collected after 2, 4 and 8 days. This meant that the samples were removed, weighed, and replaced at those given days. Due to the play of the system the samples were not always reloaded in the same manner at which they were previously set. Also, each time the samples needed to be removed, the wear tester had to be dismantled, increasing the likelihood of contamination of the bovine serum. The play of the system also made it difficult to align the samples such that the end of the travel of the Co-Cr cylinder would not be at the edge of the sample.

The wear tester was intended to simulate the wear in the total knee prosthesis where there is fluctuations in the load, sliding speed and wear track length. These variations are observed in normal knees, and have a range of several hundred Newtons, [13, 14]. These variations were not built into the wear tester, and would probably increase the wear rate and surface damage to the point that it could be characterized without the need of a very extended test. This would also be a more realistic test.

Chapter 7

Conclusion

The dominant wear mechanism that was observed, under given wear test conditions, is abrasive wear. The steady state frictional values of the oriented UHMWPE did not vary from the standard. Their values ranged from 0.08 to 0.11.

The less consolidated fiber oriented samples fail in a plane parallel to the woven UHMWPE fibers. These poor wear properties are due primarily to the poor bonding between the UHMWPE fibers and the bulk matrix. If the bonding problem is improved the wear properties of the material will most likely improve.

The more consolidated fiber oriented sample with thicker melted surface was able to withstand the wear test conducted in this thesis without failing. The wear properties were not better than the standard, and there is still the risk of the material failing in the same fashion due to poor bonding as the less consolidated samples once the enough of the standard UHMWPE is worn off.

Both the added cost of producing the fiber oriented sample and the risk of catastrophic failure of the bearing would make this material a poor choice as a tibeofemoral bearing material.

Molecular orientation of UHMWPE through channel die compression does not improve the abrasive wear performance of the polymer in the conditions employed in this thesis. Though, from the SEM images of the worn surfaces of the standard and oriented sample the wear properties for a more prolonged test maybe different. Particularly, if the primary mode of wear becomes delamination wear.

Chapter 8

Future Work

8.1 Wear Test

The experimental work carried out in this thesis was meant to simulate the wear of the UHMWPE bearing in the principally unidirectional tibiofemoral contact. The channel die used to produce the samples for the wear test was originally made to produce samples just for the microstructure characterization of the compressed specimens. Thus, why the samples were too small for the wear testing. To continue this wear study it would be better to use larger sample that are more appropriate to the dimensions of the wear tester. This would also have the added benefit that samples with higher compression ratios could be tested.

The wear tester that was used for the experimental work in this thesis had been previously used in several other projects, and modified extensively. These extensive modifications and usage have rendered the wear tester unsuitable for extended testing, and are a possible source of experimental errors. In light of on what was stated in the previous chapter on the shortcomings of the wear tester, the easiest and most effective course of action would be to design and construct a new wear tester. This new wear tester should be run faster, for a more extended period of time, make the samples more accessible to the user (for easier measuring of the wear values). Run more concurrent test, and most importantly produce a detectable amount of delamination wear.

There could also be some added benefit to run some wear test with a roughened Co-Cr counterface with higher Rp. The roughened counterface might cause a different form of abrasive wear that might show up greater differences in wear performance of the standard and the channel die oriented PE.

8.2 Mechanical Properties

A thorough characterization of the microstructure of the channel-die oriented polyethylene has been done at different compression ratios [23, 31], but the mechanical properties have not been studied yet. It is of interest to know the mechanical properties of these materials, particularly, fracture toughness, creep, compressive and tensile properties. This information would give some insight on how the anisotropy of the compressed UHMWPE affects its properties.

From the experimental data no strong effect was observed in the time scale studied on the wear and friction UHMWPE due to molecular orientation. The information from the mechanical properties would give some insight whether there are really differences to be found, and how to make these differences manifest themselves in the wear test.

Appendix A

Tables of Wear Data

Following are the wear data of each of the individual samples tested. The averages and standard deviation can be found in chapter 4. In this appendix the dimensional wear coefficient, k, is referred to as W.

Sample	48h			96h		
	ΔM	cc	W mm^3/Nm x10^(-7)	ΔM	cc	W mm^3/Nm x10^(-7)
1	0.00097	0.00091	0.689	0.00133	0.00124	0.470
2	0.00169	0.00158	1.197	0.00318	0.00296	1.213
3	0.00123	0.00115	0.871	0.00305	0.00284	1.079
1	0.00244	0.00228	1.727	0.00301	0.00280	1.064
2	0.00122	0.00114	0.863	0.00252	0.00235	0.891

Table A.1: Wear of the standard solid samples.

Sample	48h			96h			192h		
	ΔM	cc	W mm^3/Nm x10^(-7)	ΔM	cc	W mm^3/Nm x10^(-7)	ΔM	cc	W mm^3/Nm x10^(-7)
7,10	0.00165	0.00154	1.343						
2,3	0.00109	0.00102	0.822	0.00184	0.00171	0.694			
18,24	0.00133	0.00124	1.083	0.00172	0.00160	0.700			
9,17	0.00078	0.00073	0.635						
2,3				0.00257	0.00240	0.969	0.00612	0.00570	1.154
18,24				0.00346	0.00322	1.409	0.00926	0.00863	1.885
1,23				0.00264	0.00246	1.075	0.00705	0.00657	1.435
4, 14				0.00148	0.00138	0.558	0.00274	0.00255	0.516

Table A.2: Wear of the standard joined samples.

Sample	48h			96h			192h		
	ΔM	cc	W mm^3/Nm x10^(-7)	ΔM	cc	W mm^3/Nm x10^(-7)	ΔM	cc	W mm^3/Nm x10^(-7)
A,C	0.0012	0.00112	0.905						
N,O	0.00084	0.00078	0.684	0.00184	0.00171	0.694			
P,R	0.00103	0.00096	0.839	0.00172	0.00160	0.700			
E,F	0.00144	0.00134	1.172						
N,O				0.00143	0.00133	0.539	0.00474	0.00442	0.893
E,F				0.00193	0.00180	0.786	0.00451	0.00420	0.918
A,C				0.00183	0.00171	0.745	0.00505	0.00471	1.028
E,F				0.00306	0.00285	1.246	0.00765	0.00713	1.557

Table A.3: Wear of samples with λ=2.75 LD.

Sample	48h			96h			192h		
	ΔM	cc	W mm^3/Nm x10^(-7)	ΔM	cc	W mm^3/Nm x10^(-7)	ΔM	cc	W mm^3/Nm x10^(-7)
B,D	0.00107	0.00100	0.807						
P,R	0.00153	0.00143	1.246						
N,O	0.00203	0.00189	1.653						
B,D	0.00176	0.00164	1.326						
P,R				0.00454	0.00423	1.848	0.02017	0.01880	4.106
F,R				0.00402	0.00375	1.515	0.00952	0.00887	1.794
A,B				0.00263	0.00245	1.071	0.00772	0.00720	1.571
C,D				0.00286	0.00267	1.164	0.00780	0.00727	1.588

Table A.4: Wear of samples with λ=2.75 CD.

Sample	48h			96h			192h		
	ΔM	cc	W mm^3/Nm x10^(-7)	ΔM	cc	W mm^3/Nm x10^(-7)	ΔM	cc	W mm^3/Nm x10^(-7)
18,19	0.00067	0.00062	0.546	0.00235	0.00219	0.957	0.00529	0.00493	1.077
20, 17	0.00083	0.00077	0.626	0.00199	0.00185	0.750			
18, 19	0.00104	0.00097	0.847	0.00237	0.00221	0.965	0.00471	0.00439	0.852
18, 19	0.00141	0.00131	1.063	0.00365	0.00340	1.328	0.00800	0.00746	3.016

Table A.5: Wear of samples with λ=1.7 LD.

Sample	48h			96h			192h		
	ΔM	cc	W mm^3/Nm x10^(-7)	ΔM	cc	W mm^3/Nm x10^(-7)	ΔM	cc	W mm^3/Nm x10^(-7)
21	0.00144	0.00134	1.086	0.0039	0.00363	1.470	0.00820	0.00764	1.546
22	0.00102	0.00095	0.831	0.00238	0.00222	0.969	0.00857	0.00799	1.745
22	0.00142	0.00132	1.071	0.0036	0.00336	1.357	0.00686	0.00639	1.293
21	0.00145	0.00135	1.181	0.00325	0.00303	1.323	0.00697	0.00650	2.838

Table A.6: Wear of samples with λ=1.7 CD.

Sample	48h			96h			192h		
	ΔM	cc	W mm^3/Nm x10^(-7)	ΔM	cc	W mm^3/Nm x10^(-7)	ΔM	cc	W mm^3/Nm x10^(-7)
7,8	0.00089	0.00083	0.725	0.00428	0.00399	1.742	0.01146	0.01068	2.333
7,8	0.00219	0.00204	1.433	0.01336	0.01245	5.439	0.04594	0.04282	18.700
3,4	0.00176	0.00164	1.107	0.00297	0.00277	1.209	0.01311	0.01222	5.337
7,8	0.00152	0.00142	1.238	0.00451	0.00420	1.836	0.01145	0.01067	2.072

Table A.7: Wear of samples with λ=1.7 CD2.

Sample	48h			96h			192h		
	ΔM	cc	W mm^3/Nm x10^(-7)	ΔM	cc	W mm^3/Nm x10^(-7)	ΔM	cc	W mm^3/Nm x10^(-7)
1,2	0.00146	0.00136	1.101	0.00342	0.00319	1.289	0.00852	0.00794	1.606
5,6	0.00173	0.00161	1.409	0.00359	0.00335	1.462	0.00873	0.00814	1.777
1,2	0.00219	0.00204	1.165	0.00466	0.00434	1.757	0.01894	0.01765	7.139
5,6	0.00235	0.00219	1.913	0.00431	0.00402	1.755	0.00789	0.00735	3.212

Table A.8: Wear of samples with λ=1.7 FD.

Appendix B

Tables of Friction Data

Sample	0	7.41	14.81	22.50	29.62	37.03	44.44	51.85	59.24
2,3	0.053	0.081	0.087	0.094	0.097				
18,24	0.056	0.085	0.092	0.106	0.108				
2,3	0.057	0.088	0.097	0.101	0.101	0.097	0.101	0.101	0.099
18,24	0.062	0.091	0.099	0.087	0.092	0.080	0.084	0.091	0.088
4,14	0.059	0.077	0.084	0.076	0.071	0.069	0.074	0.068	0.074
Average	0.058	0.084	0.092	0.093	0.094	0.082	0.086	0.087	0.087
σ	0.003	0.006	0.007	0.012	0.014	0.014	0.014	0.017	0.012
C.V.	0.057	0.067	0.073	0.125	0.151	0.172	0.162	0.199	0.143

Table B.1: Frictional values of the standard joined samples.

Sample	0	7.41	14.81	22.50	29.62	37.03	44.44	51.85	59.24
B,D	0.047	0.080	0.083						
P,R	0.056	0.089	0.092						
B,D	0.052	0.088	0.096						
F,R	0.049	0.065	0.094	0.105	0.100	0.096	0.094	0.095	0.096
A,B	0.057	0.083	0.095	0.097	0.103	0.102	0.099	0.103	0.103
Average	0.052	0.081	0.092	0.101	0.101	0.099	0.096	0.099	0.100
σ	0.004	0.010	0.005	0.006	0.002	0.004	0.004	0.006	0.005
C.V.	0.080	0.122	0.059	0.056	0.021	0.041	0.040	0.058	0.046

Table B.2: Frictional values of the samples at λ of 2.75 in CD.

Sample	0	7.41	14.81	22.50	29.62	37.03	44.44	51.85	59.24
B,D	0.057	0.089	0.110						
P,R	0.071	0.098	0.115						
E,F	0.059	0.098	0.107						
N,O	0.048	0.095	0.102	0.097	0.089	0.107	0.104	0.103	0.100
E,F	0.064	0.096	0.086	0.093	0.087	0.103	0.106	0.104	0.096
E,F	0.067	0.091	0.086	0.089	0.088	0.086	0.089	0.096	0.105
Average	0.061	0.094	0.101	0.093	0.088	0.099	0.100	0.101	0.100
σ	0.008	0.004	0.012	0.004	0.001	0.011	0.009	0.004	0.005
C.V.	0.133	0.039	0.123	0.044	0.010	0.113	0.094	0.042	0.048

Table B.3: Frictional values of the samples at λ of 2.75 in LD.

Sample	0	7.41	14.81	22.50	29.62	37.03	44.44	51.85	59.24
1,2	0.059	0.077	0.084	0.076	0.071	0.069	0.074	0.068	0.074
5,6	0.060	0.079	0.090	0.084	0.076	0.092	0.088	0.083	0.083
1,2	0.051	0.091	0.113	0.102	0.099	0.133	0.155	0.155	0.169
5,6	0.066	0.060	0.099	0.107	0.104	0.104		0.107	0.107
Average	0.057	0.082	0.095	0.087	0.082	0.098	0.106	0.102	0.108
σ	0.005	0.007	0.015	0.013	0.015	0.032	0.043	0.047	0.053
C.V.	0.082	0.091	0.162	0.154	0.183	0.330	0.411	0.459	0.485

Table B.4: Frictional values of the samples at λ of 1.7 in FD.

Sample	0	7.41	14.81	22.50	29.62	37.03	44.44	51.85	59.24
7,8	0.048	0.080	0.075	0.105	0.095	0.134	0.097	0.085	0.075
7,8	0.057	0.069	0.088	0.088	0.088	0.087	0.087	0.087	0.087
Average	0.052	0.075	0.082	0.097	0.091	0.110	0.092	0.086	0.081
σ	0.006	0.008	0.009	0.012	0.005	0.033	0.007	0.001	0.008
C.V.	0.111	0.104	0.110	0.127	0.050	0.303	0.080	0.013	0.104

Table B.5: Frictional values of the samples at λ of 1.7 in CD2.

Sample	0	7.41	14.81	22.50	29.62	37.03	44.44	51.85	59.24
21	0.038	0.062	0.077	0.082	0.096	0.099	0.099	0.094	0.096
22	0.036	0.067	0.072	0.087	0.097	0.100	0.103	0.106	0.096
22	0.055	0.080	0.093	0.104	0.102	0.101	0.103	0.101	0.101
Average	0.043	0.069	0.080	0.091	0.098	0.100	0.102	0.100	0.098
σ	0.011	0.009	0.011	0.012	0.003	0.001	0.002	0.006	0.003
C.V.	0.251	0.134	0.134	0.129	0.035	0.015	0.021	0.059	0.031

Table B.6: Frictional values of the samples at λ of 1.7 in CD.

Sample	0	7.41	14.81	22.50	29.62	37.03	44.44	51.85	59.24
20,17	0.056	0.077	0.078	0.089	0.089				
18, 19	0.046	0.076	0.099	0.101	0.104	0.099		0.107	0.107
Average	0.051	0.076	0.088	0.095	0.096	0.099		0.107	0.107
σ	0.007	0.000	0.015	0.008	0.010				
C.V.	0.132	0.005	0.172	0.088	0.108				

Table B.7: Frictional values of the samples at λ of 1.7 in LD.

Sample	0	7.41	14.81	22.50	29.62	37.03	44.44	51.85	59.24
sample1	0.054	0.064	0.075	0.075	0.071				
sample2	0.054	0.088	0.104	0.103	0.109				
sample2	0.051	0.067	0.081	0.089	0.083	0.100	0.099	0.095	0.088
sample1	0.061	0.108	0.107	0.105	0.105	0.105	0.103	0.097	0.107
Average	0.055	0.082	0.091	0.093	0.092	0.102	0.101	0.096	0.098
σ	0.004	0.021	0.016	0.014	0.018	0.003	0.003	0.001	0.014
C.V.	0.074	0.252	0.175	0.152	0.196	0.033	0.028	0.010	0.138

Table B.8: Frictional values of the standard solid samples.

Sample	0	7.41	14.81	22.50	29.62	37.03	44.44	51.85	59.24
MP-60_1	0.067	0.069	0.073	0.071	0.077	0.081	0.085	0.083	0.085
MP-60_2	0.081	0.090	0.089	0.092	0.087	0.094	0.096	0.096	0.092
Average	0.074	0.080	0.081	0.081	0.082	0.087	0.090	0.090	0.088
σ	0.010	0.015	0.012	0.015	0.007	0.009	0.008	0.009	0.005
C.V.	0.138	0.193	0.144	0.184	0.084	0.108	0.090	0.101	0.060

Table B.9: Frictional values of the fiber oriented sample, MP-60.

Appendix C

SEM Images of Worn Standard Samples

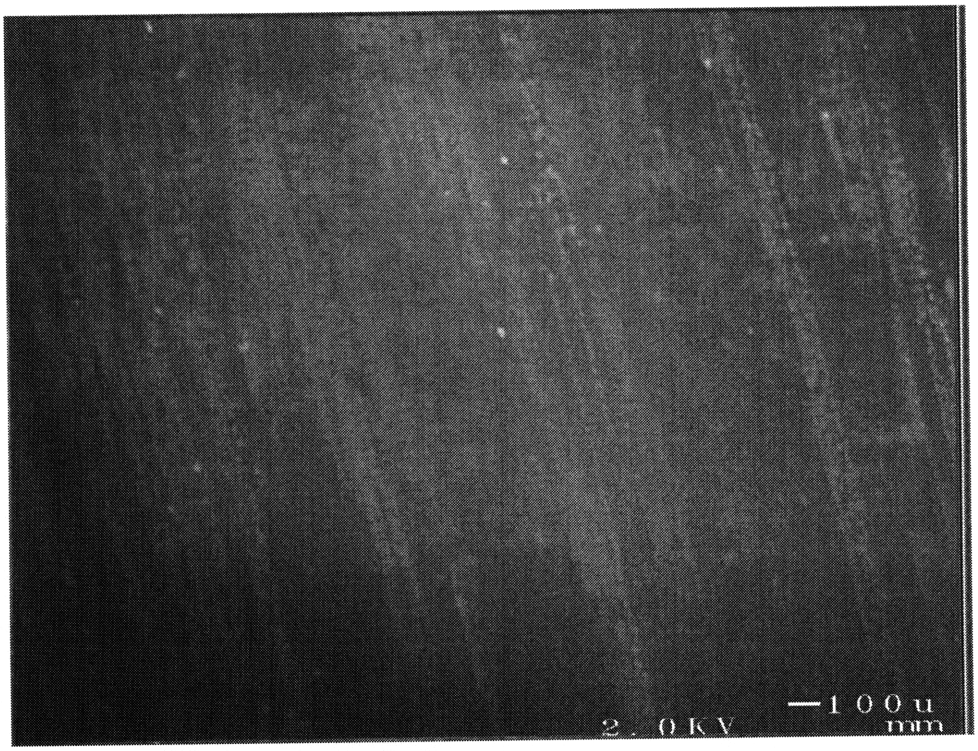

Figure C-1: Image of the middle of the wear track at 600x of a standard coated sample.

Figure C-2: Image of the middle of the wear track at 2700x of a standard coated sample.

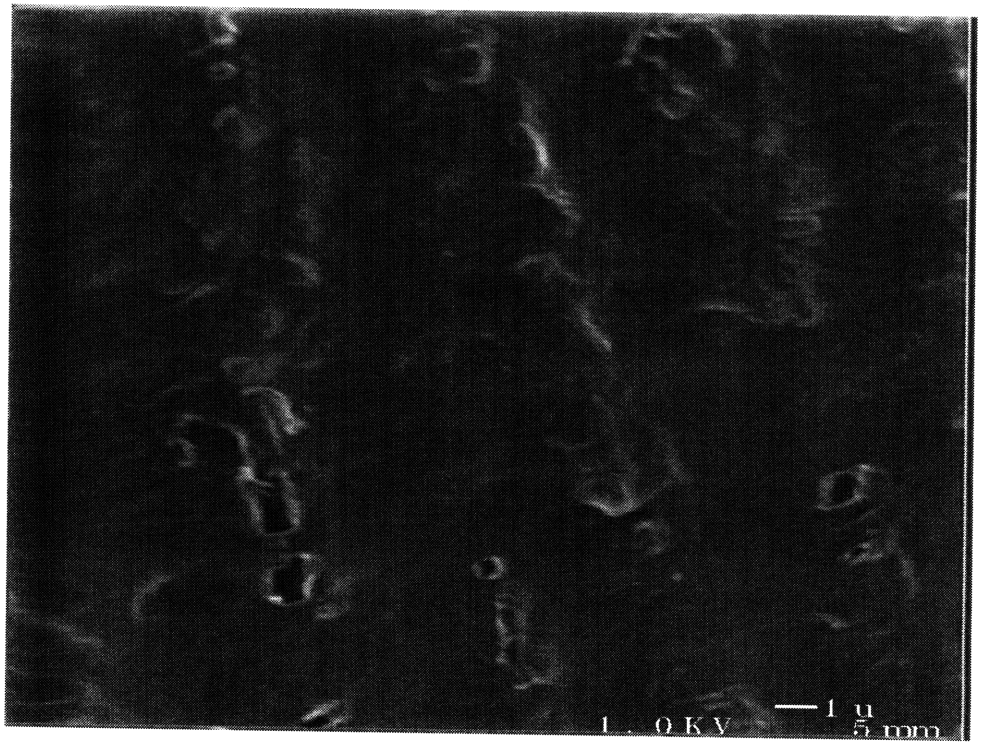

Figure C-3: Image of the end of the travel of the wear track at 5000x of a standard uncoated sample.

Appendix D

SEM Images of Worn λ=1.7 CD2 Samples

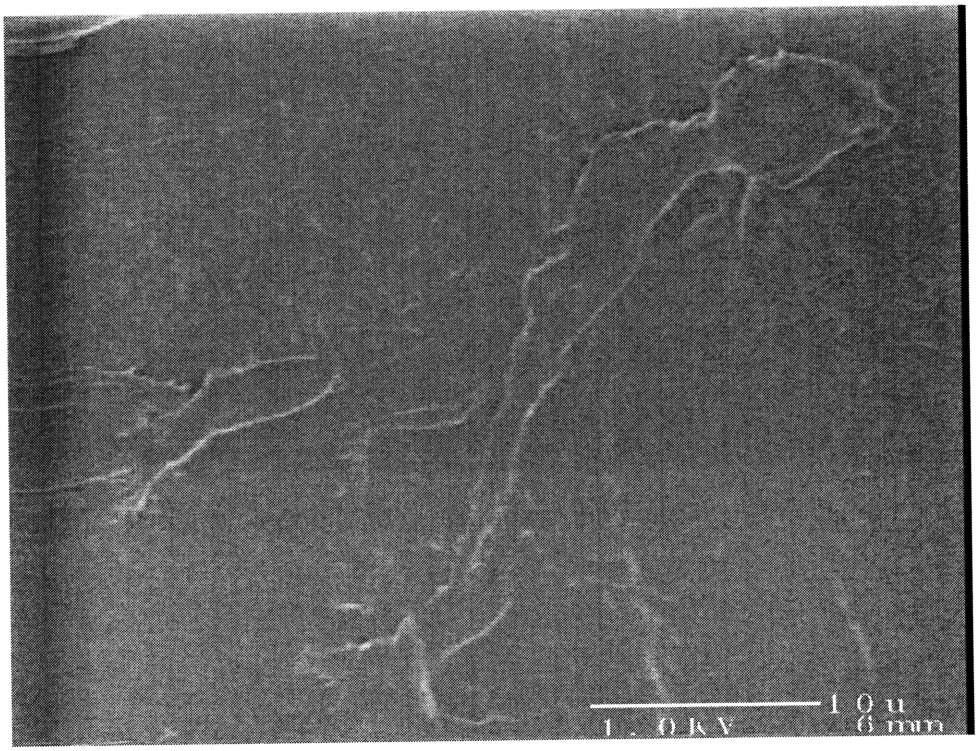

Figure D-1: Image of the middle of the wear track at 2700x for λ=1.7 CD2.

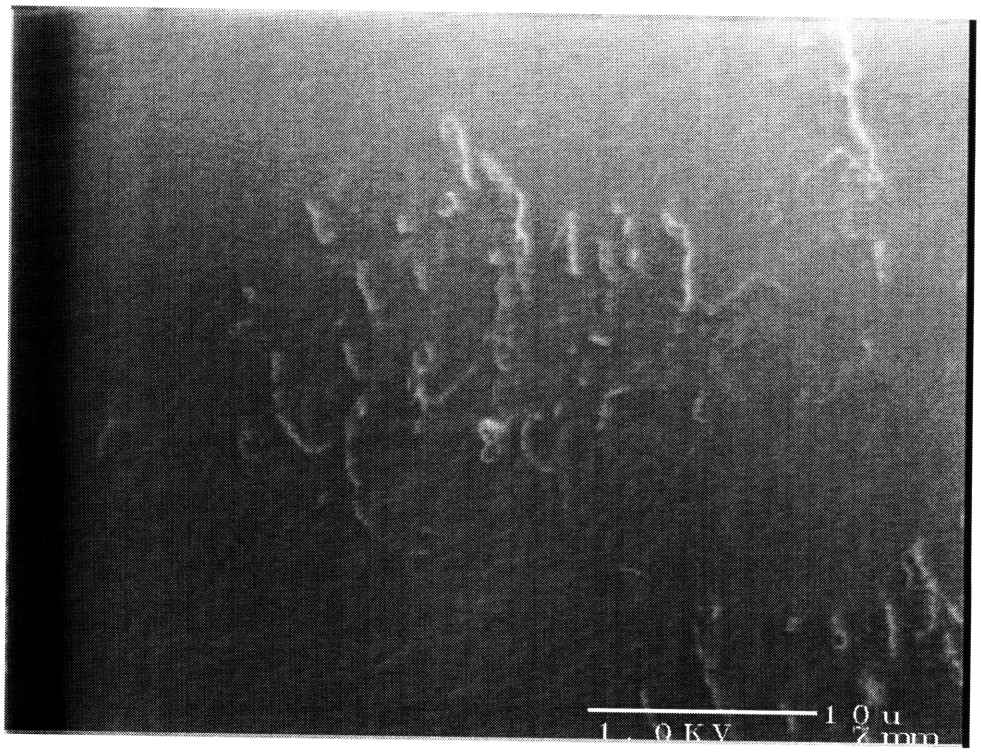

Figure D-2: Image of near the end of the travel of the wear track at 2700x for λ=1.7 CD2.

Appendix E

SEM Images of Worn λ=2.75 LD Samples

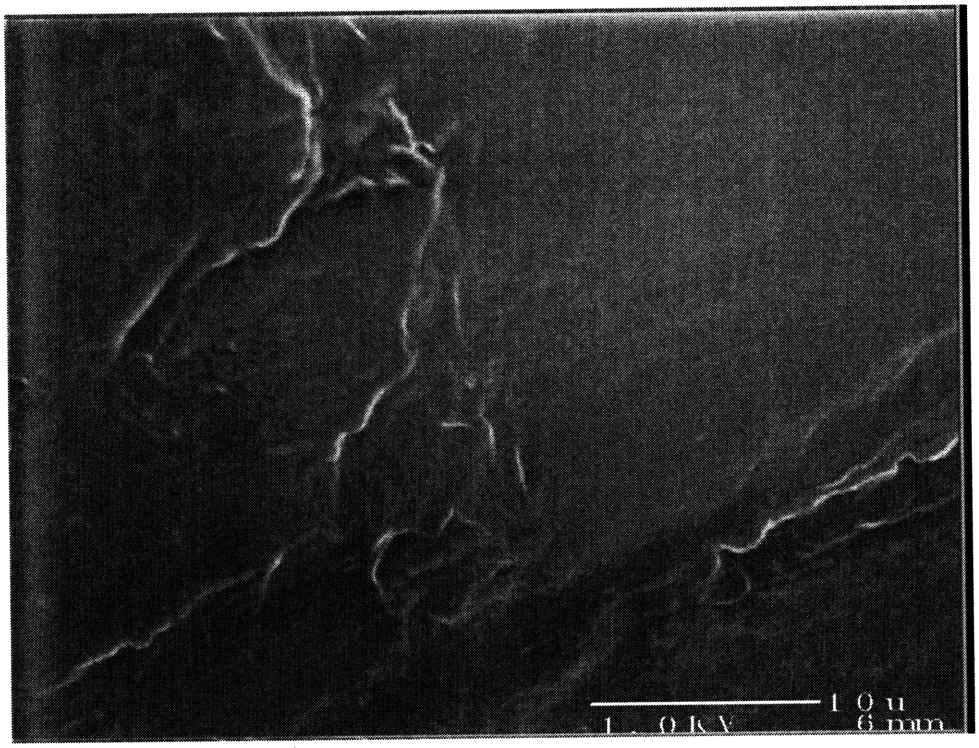

Figure E-1: Image of the end of the travel of the wear track at 2700x for λ=2.75 LD.

Appendix F

SEM Images of Wear Debris

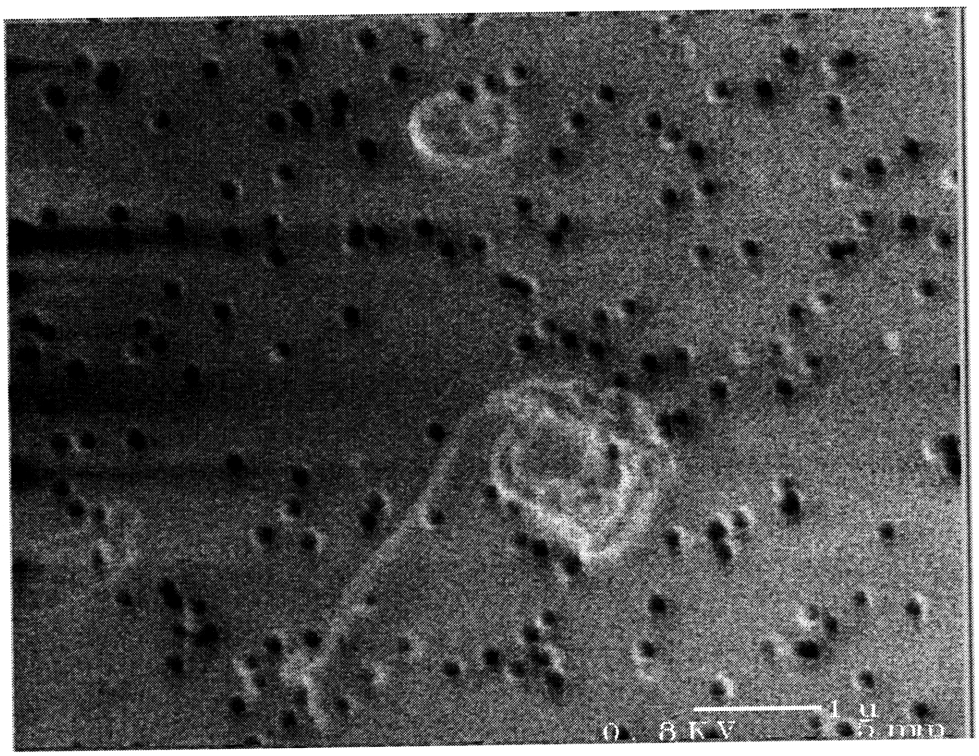

Figure F-1: Wear debris from sample with λ of 1.7 FD, at 15000x.

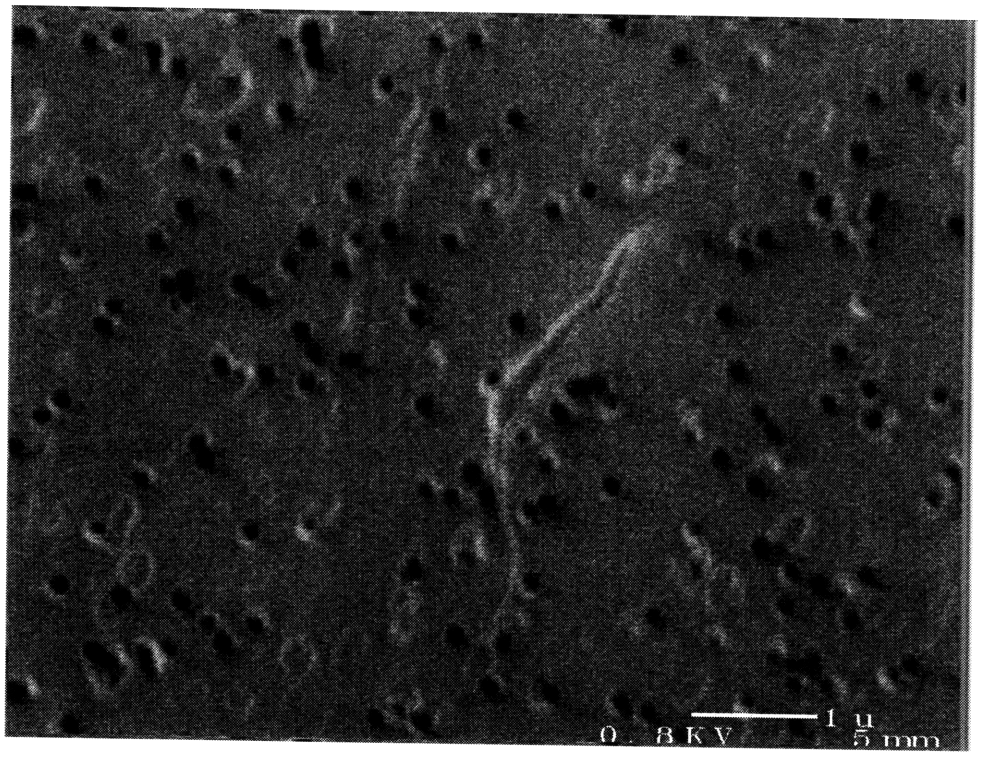

Figure F-2: Wear debris from sample with λ of 2.75 CD, at 15000x.

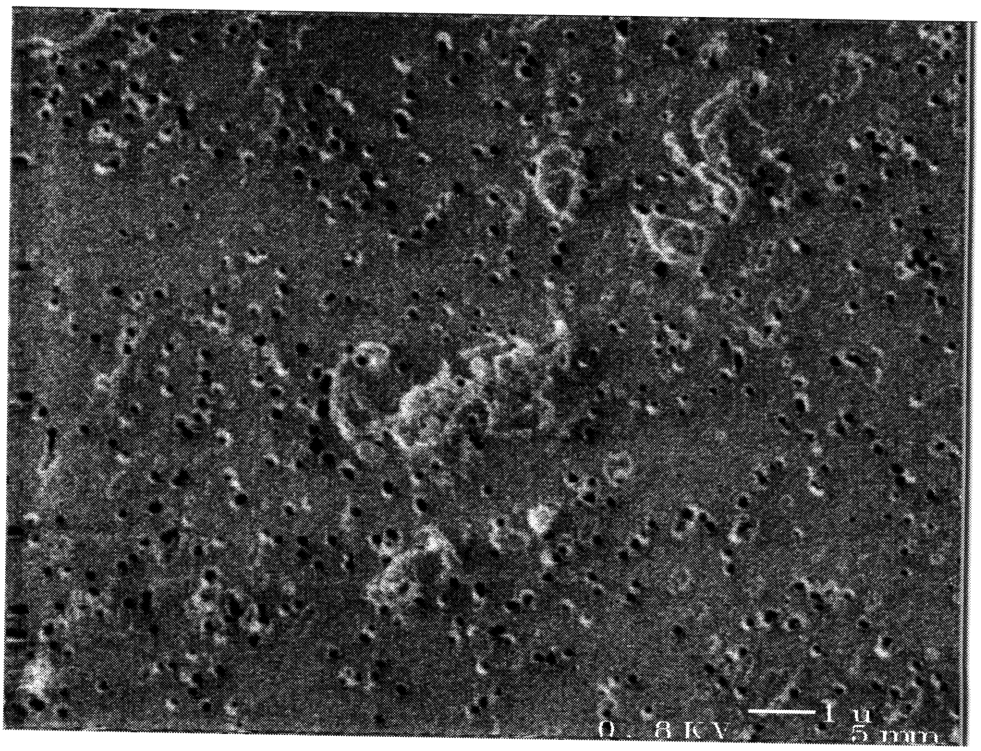

Figure F-3: Wear debris from sample with λ of 2.75 CD, at 8000x.

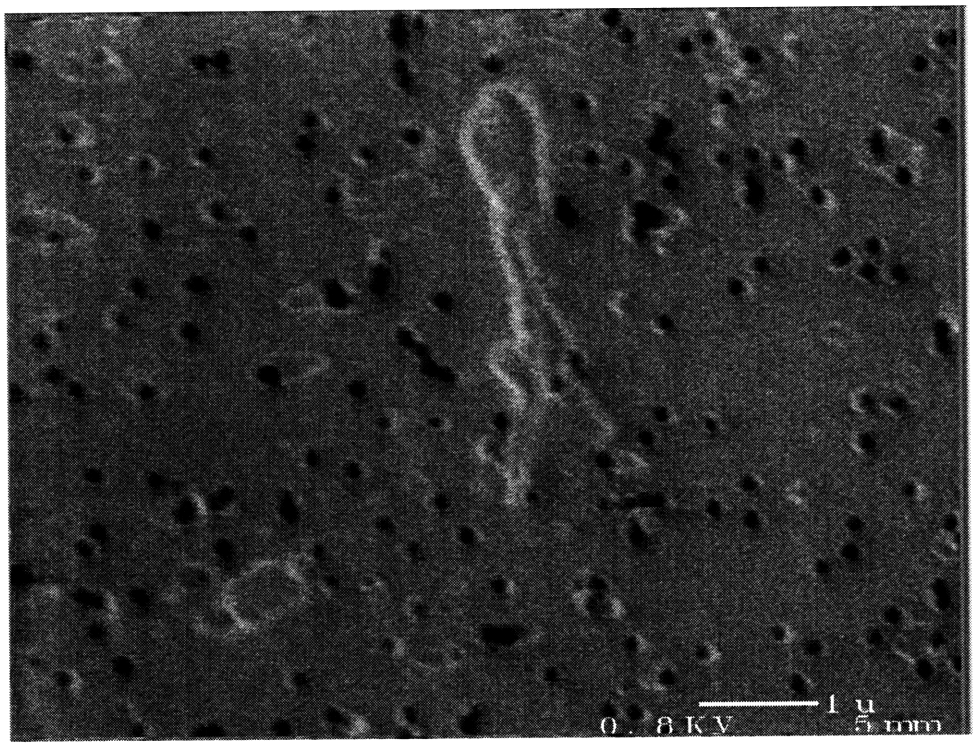

Figure F-4: Wear debris from sample with λ of 2.75 LD, at 14000x.

Bibliography

[1] G.W. Blunn, A.B. Joshi, P.A. Lilley, E. Engelbrecht, L. Ryd, L. Lidgren, K. Hardinge, E. Nieder, and Walker P. Polyethylene wear in unicondylar knee prostheses. *Acta Orthop Scand*, 63(3):247–255, 1992.

[2] P.C. Peters, G.A. Engh, K.A. Dwyer, and T.A. Vinh. Osteolysis after total knee anthroplasty without cement. *Journal of Bone and Joint Surgery*, 74–A(6):864–876, July 1992.

[3] D.W. Howie, B. Vernon-Roberts, R. Oakeshott, and B. Manthey. A rat model of resorption of bone at the cement-bone interface in the presence of polyethylene wear particles. *Journal of Bone and Joint Surgery*, 70–A(2):257–263, February 1988.

[4] H. Willert and M. Semlitsch. Reaction to the articular capsule to wear products of artificial joint prothesis. *Journal of Biomedical Material Research*, 11:157–164, 1977.

[5] J.A. Williams. *Engineering Tribology.* Oxford University Press, New York, 1994.

[6] N.P. Suh. An overview of the delamination theory of wear. *Wear*, 44:1–16, 1977.

[7] N.P. Suh. The delamination theory of wear. *Wear*, 25:111–124, 1973.

[8] J.P. Collier, M.B Mayor, J.L. McNamara, V.A. Surprenant, and R.E. Jensen. Analysis of the failure of 122 polyethylene inserts from uncemented tibial knee components. *Clinical Orthopeadics and Related Research*, 273:232–242, December 1991.

[9] R. Rose, A. Crugnola, S.B. Ries, W.R. Cimino, I. Paul, and E.L. Radin. On the origins of high in vivo wear rates in polyethylene components of total joint protheses. *Clinical Orthopeadics and Related Research*, 145(6):277–286, 1979.

[10] W. Rostoker, E.Y.S. Chao, and J.O Galante. The appearence of wear on polyethylene-a comparison of in vivo and in vitro wear surfaces. *Journal of Biomedial Materials Research*, 12:317–335, 1978.

[11] M. Mosleh, J. Eisenberg, and N.P. Suh. Influence of sterilization technique on wear of polyethylene. Fifth World Biomaterials Congress, Toronto, Canada, May 1996. Orthopeadic Research Society.

[12] M. Mosleh, J. Arinez, and N.P. Suh. Delamination wear of polyethylene enhanced by gamma irradiation. 42rd Annual Meeting, Atlanta, Georgia, February 1996. Orthopeadic Research Society.

[13] P.J. Atkinson and R.C Haut. A method for determining regions of diarthroidal joint contact during dynamic loading of the human knee. 43rd. Annual Meeting, pages 133–139, San Francisco, February 1997. Orthopeadic Research Society.

[14] D.L. Churchill, S.J. Incavo, R.P. Jewell, and B.D. Beynnon. A comparison of patello-femoral sontac loads in the normal knee and total knee arthroplasty. 43rd. Annual Meeting, pages 133–139, San Francisco, February 1997. Orthopeadic Research Society.

[15] J. Fisher, D. Dowson, H. Hamdzah, and H.L. Lee. The effect of sliding velocity on the friction and wear of uhmwpe for use in total artificial joints. *Wear*, 175:219–225, 1995.

[16] T.S. Barret, G.W. Stanchowiak, and A.W. Batchelor. Effect of roughness and sliding speed on the wear and friction of ultra-high molecular weight polyethylene. *Wear*, 153:331–390, 1992.

[17] J.R. Cooper, D. Dowson, and J. Fisher. Macroscopic and microscopic wear mechanisms in ultra-high molecular weight polyethylene. *Wear*, 162–164:378–384, 1993.

[18] A. Wang, D.C. Sun, C. Stark, and J.H. Dumbleton. Wear mechanisms of uhmwpe in total joint replacements. *Wear*, 181–183:241–249, 1995.

[19] J.R. Cooper, D. Dowson, and J. Fisher. Birefringent studies of polyethylene wear specimens and acetabular cups. *Wear*, 151:391–402, 1991.

[20] W. Rostoker and J.O Galante. Contact pressure dependence of wear rates of ultra high molecular weight polyethylene. *Journal of Biomedial Materials Research*, 13:957–964, 1979.

[21] G.W. Blunn, Walker P., A.B. Joshi, and K. Hardinge. The dominance of cyclic sliding in producing wear in total knee replacements. *Clinical Orthopaedics and Related Research*, 273(3):255–260, December 1991.

[22] D.C.M. Chang, J.C. Goh, S.H. Teoh, and K. Bose. Cold extrusion deformation of uhmwpe in total knee replacement prothesis. *Biomaterials*, 16(3):219–223, 1995.

[23] Y. Boontongkong. Orientation of channel-die compressed ultra-high molecular weight polyethylene. Master's thesis, Massachusetts Institute of Technology, Department of Material Science and Engineering, June 1997.

[24] N. Sung and N.P. Suh. Effect of fiber orientation on friction and wear of fiber reinforced polymeric composites. *Wear*, 53:129–141, 1979.

[25] N.P. Suh, M. Mosleh, and J.. Arinez. Tribology of polyethylene homocomposites. *Wear*, 214:231–236, 1998.

[26] J.A. Brandrup and E.H. Immergut. *Polymer Handbook*. Wiley Interscience Publication, New York, 3rd. edition, 1989.

[27] E.A. Grulke. *Polymer Process Engineering*. Prentice Hall, U.S.A., 1994.

[28] Y. Cohen, D.M. Rein, and L. Vaykhansky. A novel composite based on utra-high-molecular-weight polyethylene. *Composites Science and Technology*, 57:1149–1154, 1997.

[29] In M.B. Bever, editor, *Encyclopeadia of Material Science and Engineering*, volume 1, page 1057. MIT Press, Cambridge, 1986.

[30] L. Lin and A.S. Argon. *Macromolecules*, 25:4011, 1992.

[31] Y. Boontongkong, R.E. Cohen, M. Spector, and A. Bellare. Orientation of plane strain-compressed uhmwpe. October 1997.

[32] H.H. Song, A.S. Argon, and R.E. Cohen. Contact pressure dependence of wear rates of ultra high molecular weight polyethylene. *Macromolecules*, 23:870, 1990.

[33] T.A. Blanchet and Kennedy F.E. The development of transfer flims in uhmwpe/stainless steel oscillatory sliding. *Tribology Transactions*, 32(3):371–379, 1989.

[34] J.R. Atkinson, K.J. Brown, and D. Dowson. The wear of high molecular weight polyethylene part i. *Journal of Lubrication Technology*, 100:208–218, April 1978.

[35] B. Derbyshire, J. Fisher, D. Dowson, C.S. Hardaker, and K. Brummitt. Wear of uhmwpe sliding against untreated, titanium nitride-coated and 'hardcor'-treated stainless steel counterfaces. *Wear*, 181–183:258–262, 1995.

[36] M. Kernick and C. Allen. The sliding wear of uhmwpe against zirconia in saline containing proteins. *Wear*, 203–204:537–543, 1997.

[37] A. Wang, A. Essner, C. Stark, and J.H. Dumbleton. Comparison of the size and morphology of uhmwpe wear debris produced by a hip joint simulator under serum and water lubricated conditions. *Biomaterials*, 17:865–871, 1996.

[38] K.Y. Lee and D. Pienkowski. Reduction in the initial wear of ultrahigh molecular weight polyethylene after compressive creep deformation. *Wear*, 203–204:375–379, 1997.

[39] William Sauer. Private communication, 1997.

[40] J.C. Anderson. High density and ultra-high molecular weight polyethenes: their wear properties and bearing applications. *Tribology International*, pages 43–47, February 1982.

[41] N. Cook and E. Rabinowicz. *Physical Measurement and Analysis.* Addison-Wesley, Massachusetts, 1963.

[42] V. Stannett and H.. Yasuda. Permeability. In R. Raff and K. Doak, editors, *Cristalline Oleofin Polymers, Part II*, page 138. Wiley and Sons, New York, 1965.

[43] A.F. Mills. *Heat and Mass Transfer.* Irwin, Boston, 1995.

[44] D.W. McCall, J.F. Ambrose, and V.L. Lanza. Diffusion in ethylene polymers. *Journal of Polymer Science*, 26:168.

[45] C.H. Klute. Diffusion of small molecules in semicrystalline polymers: water in polyethylene. *Journal of Applied Polymer Science*, 1(3):340–350.

[46] J.A. Barrie. Water in polymers. In J Crank and G.S Park, editors, *Diffusion in Polymers*, pages 264–265. Academic Press, New York, 1968.

[47] P. Campbell, S. Ma, B. Yeom, H. McKellop, T.P. Schmalzried, and H.C. Amstutz. Isolation of predominantly submicron-sized uhmwpe wear particles from periprothestic tissue. *Journal of Materials Research*, 29:127–131, 1995.

[48] R.L. Lieber. Experimental design and statistical analysis. In S.R. Simon, editor, *Orthopaedic Basic Science*, pages 623–665. Amer. Acad. Orthop. Surg., 1994.

[49] V. Saikko. Wear and friction properties of prosthetic joint materials evaluated on a reciprocating pi-on-flat apparatus. *Wear*, 166:169–178, 1993.

[50] J.L. Devore. *Probability and Statistics for Engineering and the Sciences.* Brooks/Cole Publishing Company, Pacific Grove, California, 3rd. edition, 1991.

[51] H.A. McKellop, P. Campbell, S.H. Park, T.P. Schmalzried, P. Grigoris, H.C. Amstutz, and A. Sarmiento. The origin of submicron polyethylene wear debris in total hip arthroplasty. *Clinical Orthopaedics and Related Research*, 311:3–20, 1995.